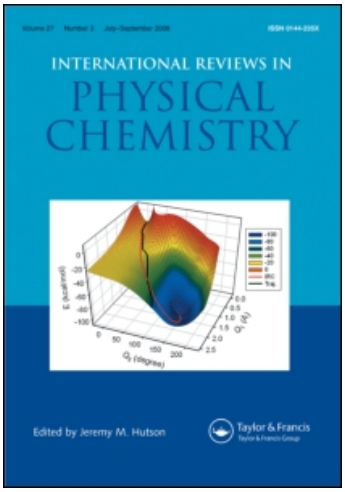

International Reviews in Physical Chemistry
Publication details, including instructions for authors and subscription information:
http://www.informaworld.com/smpp/title~content=t713724383

Magnetic exchange between metal ions with unquenched orbital angular momenta: basic concepts and relevance to molecular magnetism

Andrei Palii[a]; Boris Tsukerblat[b]; Juan Modesto Clemente-Juan[cd]; Eugenio Coronado[c]
[a] Institute of Applied Physics, Academy of Sciences of Moldova, MD 2028 Kishinev, Moldova [b] Department of Chemistry, Ben-Gurion University of the Negev, Beer-Sheva 84105, Israel [c] Instituto de Ciencia Molecular, Universidad de València, s/n 46980 Paterna, Spain [d] Fundació General de la Universitat de València (FGUV), 46002 València, Spain

Online publication date: 29 January 2010

To cite this Article Palii, Andrei , Tsukerblat, Boris , Clemente-Juan, Juan Modesto and Coronado, Eugenio(2010) 'Magnetic exchange between metal ions with unquenched orbital angular momenta: basic concepts and relevance to molecular magnetism', International Reviews in Physical Chemistry, 29: 1, 135 — 230
To link to this Article: DOI: 10.1080/01442350903435256
URL: http://dx.doi.org/10.1080/01442350903435256

International Reviews in Physical Chemistry
Vol. 29, No. 1, January–March 2010, 135–230

Taylor & Francis
Taylor & Francis Group

Magnetic exchange between metal ions with unquenched orbital angular momenta: basic concepts and relevance to molecular magnetism

Andrei Palii[a], Boris Tsukerblat[b]*, Juan Modesto Clemente-Juan[cd] and Eugenio Coronado[c]

[a]*Institute of Applied Physics, Academy of Sciences of Moldova, Academy Str. 5, MD 2028 Kishinev, Moldova;* [b]*Department of Chemistry, Ben-Gurion University of the Negev, P.O. Box 653, Beer-Sheva 84105, Israel;* [c]*Instituto de Ciencia Molecular, Universidad de València, Polígono de la Coma, s/n 46980 Paterna, Spain;* [d]*Fundació General de la Universitat de València (FGUV), Placa del Patriarca, 4–1, 46002 València, Spain*

(*Received 1 October 2009; final version received 22 October 2009*)

This review article is a first attempt to give a systematic and comprehensive description (in the framework of the unified theoretical approach) of the exchange interactions in polynuclear systems based on orbitally degenerate metal ions in the context of their relevance to the modern molecular magnetism. Interest in these systems is related to the fundamental problems of magnetism and at the same time steered by a number of impressive potential applications of molecular magnets, like high-density memory storage units, nanoscale qubits, spintronics and photoswitchable devices. In the presence of orbital degeneracy, the conventional spin Hamiltonian (Heisenberg–Dirac–van Vleck model) becomes inapplicable even as an approximation. The central component of this review article constitutes the concept of orbitally-dependent exchange interaction between metal ions possessing unquenched orbital angular momenta. We present a rigorous procedure of derivation of the kinetic exchange Hamiltonian for a pair of orbitally degenerate transition metal ions that is expressed in terms of the orbital matrices and spin operators. The microscopic background reveals the interrelations between the parameters of the Hamiltonian and the internal parameters of the system including all relevant transfer integrals and fundamental intracenter interactions. The developed formalism integrated with the irreducible tensor operator (ITO) technique makes it possible to describe the exchange coupling and all relevant interactions (crystal fields, spin–orbit (SO) and Zeeman couplings) in terms of the ITOs of the full spherical group, and in this way to develop anunified and efficient computational tool. The orbitally-dependent exchange was shown to lead to an anomalously strong magnetic anisotropy that can be considered as a main physical manifestation of the unquenched orbital angular momentum in metal clusters of orbitally-degenerate ions. The theoretical background is illustrated by the following applications. The magnetic properties of the binuclear face-shared unit $[Ti_2Cl_9]^{3-}$ in $Cs_3Ti_2Cl_9$ are discussed with the emphasis on the observed magnetic anisotropy and on the non-trivial symmetry properties of the exchange Hamiltonian. The major electronic factors controlling the magnetic anisotropy in Co(II) pairs are discussed. The degree of the exchange anisotropy was shown to depend on the strength of the cubic crystal field, on the relative efficiency of the electron transfer pathways between unfilled d-shells and

*Corresponding author. Email: tsuker@bgu.ac.il

ISSN 0144–235X print/ISSN 1366–591X online

DOI: 10.1080/01442350903435256
http://www.informaworld.com

SO coupling. Provided strong SO coupling, the effective Hamiltonian was projected onto the subspace of low-lying Kramers doublets and similarly a pseudo-spin-1/2 Hamiltonian was derived. The described procedure allows to establish the interrelation between idem parameters of the system and the parameters of the pseudo-spin-1/2 Hamiltonian. Pseudo-spin-1/2 approach is illustrated by the study of the inelastic neutron scattering spectra and magnetic susceptibility of polyoxometalates encapsulating Co(II) clusters: Keggin derivative $K_8[Co_2(D_2O)(W_{11}O_{39})]\cdot nD_2O$, $[Co_4(H_2O)_2(PW_9O_{34})_2]^{10-}$ and $[Co_3W(D_2O)_2(CoW_9O_{34})_2]^{12-}$ clusters. In the consideration of the cyanide-bridged Mn(III)–CN–Mn(II) pair, it was demonstrated that under certain conditions the orbitally-dependent exchange is able to produce a barrier for the reversal of magnetisation. This seems to be instructive for the controlled design of cyano-based single molecule magnets with high-blocking temperatures.

Keywords: molecular magnetism; metal clusters; exchange interactions; magnetic anisotropy; single-molecule magnets; polyoxometalates; cyanides; orbital degeneracy; orbitally-dependent exchange; spin-orbit interaction

Contents

Abbreviations

HDVV model	Heisenberg-Dirac-Van Vleck model
SO	spin-orbit
ZFS	zero-field splitting
ITO	irreducible tensor operator
INS	inelastic neutron scattering
EPR	electron paramagnetic resonance
TIP	temperature independent paramagnetism
CT	charge transfer
SMM	single molecule magnet
SCM	Single chain magnet
JT	Jahn-Teller
JTE	Jahn-Teller effect

1. Introduction

Contemporary molecular magnetism originates from classical magnetochemistry and represents a fascinating interdisciplinary field of science that incorporates basic concepts of physics, chemistry and materials science. The evolution and the state-of-art in this field is given in several papers and books [1–12] and summarised in the latest book '*Molecular Nanomagnets*' by Gatteschi *et al*. [1]. The main objects of molecular magnetism are either magnetic molecules consisting of a finite number of exchange coupled spin sites (molecular magnetic clusters and molecular magnets), or the extended materials based on magnetic molecules exhibiting cooperative interactions (molecule-based magnets) [1–23]. A third class of magnetic molecular systems are the so-called spin-crossover materials, coordination compounds in which the spin state of the metal ion changes from low spin to high spin upon the application of an external stimulus (temperature, light or pressure) [2b]. Some of these magnetic systems exhibit interesting material properties and applications. Thus, they behave as single molecule magnets (SMMs) and single chain magnets (SCMs) [23–32], room temperature molecule-based ferromagnets [33–41], multifunctional nanomaterials for molecular spintronics [42] or photoswitchable magnetic materials [43–51]. As it was demonstrated, coexistence of ferromagnetism and metallic conductivity can be reached in one molecular material [42,52]. Organic molecules of increasing sizes and large numbers of unpaired electrons are also being explored as building blocks for molecular-based magnets [53–59]. Molecular magnetic clusters are not only ideal model systems for the study of exchange interactions between metal ions, they are also of current interest in many areas of research, like material science, biophysics, biochemistry (e.g. ferredoxins, photosystems II and the storage protein ferritin [60–63]).

As far as the molecular magnets are concerned, one can assess that, presently, the fundamentals of the field are established (at least the main concepts) [3b] and SMMs are expected to provide impressive nano-technological applications as the memory storage units of molecular size [1–3] and as carriers of quantum bits of information. In solid state these molecules have been shown to behave as magnets of nanometer size, exhibiting magnetic bistability and quantum tunnelling of magnetisation at low temperatures. As SMMs can be placed on the border between the objects of quantum and classical physics, they show, from one side, slow relaxation of magnetisation and magnetic hysteresis as a bulk magnet, and, on the other side, they are still small enough to show important quantum effects. The use of molecular magnets in quantum computing as *nanoscale qubits* is one of the fascinating possibilities provided by these quantum objects [64–71]. The observation of Rabi oscillations in molecular nanomagnets [71,73,82] is expected to provide an impact on the development of this area of research and applications [71–82].

The properties of molecular spin clusters, including those which are explored in the so far mentioned applications, are strongly dependent on the magnetic exchange interactions between constituent ions. In this respect, these systems can be quite conventionally divided into two classes according to the orbital nature of the ground ligand field term of the constituent metal ions. If the clusters are composed of the ions with half-filled orbitals that give rise to orbitally non-degenerate ground states, the leading term in the exchange interaction can be represented by the usually accepted Heisenberg–Dirac–van Vleck (HDVV) Hamiltonian that is expressed in terms of spin operators only. For this reason

the systems of such kind can be referred to as *spin clusters*. The key physical peculiarity of the HDVV interaction is that it is magnetically isotropic. This property follows from the fact that the HDVV Hamiltonian is invariant with respect to all kinds of rotations. The anisotropy of spin clusters is relatively small in the sense that the parameters of the anisotropic interactions are much smaller as compared to those involoved in the HDVV coupling. The second type of the systems involves clusters comprising magnetic ions with orbitally degenerate ground crystal field terms that, for the sake of brevity, will be termed as *degenerate clusters*. As distinguished from the exchange interaction in spin clusters, the magnetic coupling in degenerate clusters cannot be described in terms of spin operators only and has much more complicated form that also includes orbital variables along with spin operators. In general, the orbital degeneracy is directly related to an unquenched orbital angular momentum in the electronic shell that will be shown to manifest itself in a strong magnetic anisotropy. It is to be noted preliminarly that the anisotropic interactions in systems composed of ions with unquenched orbital angular momenta are of the same order of magnitude as the isotropic ones.

The theoretical background of molecular magnetism dealing with spin-clusters is higly developed and has been described in detail in many reviews and books [1–7,14–20]. On the contrary, the problem of orbital degeneracy has not received much attention in the field of molecular magnetism in spite of its conceptual and practical importance. Although the ability of the orbitally-dependent magnetic interactions to create strong magnetic anisotropy was mentioned (in general terms) by van Vleck [83] many years ago, this phenomenon has not been understood to the full extent till last decade, and consequently has not been studied and reviewed. To the best of our knowledge, the present review article is the first attempt to give a systematic and comprehensive description (in the framework of the unified theoretical approach) of this kind of phenomenon in the context of its relevance to the modern problems of molecular magnetism. This review is mainly devoted to the conceptual aspects of the problem rather than to the detailed description of particular applications, the last section is given in order to illustrate the approaches and methodology. Along with the general ideas, we also wanted to provide the reader with the computational tools and working formulae for the notable cases that would avoid (at least in many cases) the necessity to read numerous original papers.

This review article is organised as follows. After this section, in Section 2 we give a brief description of the very basic concepts used throughout this article. These include the kinetic and potential mechanisms of the magnetic exchange and the definition of the HDVV spin-Hamiltonian. Then the notions of the local (single-ion) and anisotropic exchange interactions are introduced. Finally, the comparison of the anisotropy in spin-clusters with that arising in degenerate clusters is made. Since a simultaneous consideration of both local and pairwise interactions would mask their consequences, it seems to be reasonable to treat them separately.

Section 3 contains a preliminary discussion of the exchange interaction in context of orbital degeneracy. It is shown how the orbital angular momentum of a free ion is quenched by the crystal fields of different symmetries and an important concept of T–P isomorphism is introduced. Then a single-ion anisotropy in degenerate systems is discussed. The key concept of the orbitally-dependent exchange is introduced through a simple illustration that is aimed to give an explanation of the generalised Hamiltonian adapted to the case of degeneracy.

In Section 4, a simplified theory of degenerate systems that takes into account only the single-ion anisotropy is presented. Within this framework, the effects of the orbital angular momentum are included by taking into account spin–orbit (SO) coupling and low-symmetry components of the crystal field. At the same time, the exchange interaction between the metal ions is still assumed to be of the isotropic HDVV form that was adopted in the so-called Lines model. Within this approach, we consider a phenomenological pseudo-spin-1/2 Hamiltonian widely used for the description of the clusters containing high-spin Co(II) ions. The pseudo-spin-1/2 approach is illustrated by the studies of inelastic neutron scattering (INS) and magnetic susceptibility of polyoxometalates encapsulating Co(II) clusters: Keggin derivative $K_8[Co_2(D_2O)(W_{11}O_{39})]\cdot nD_2O$, $[Co_4(D_2O)_2(PW_9O_{34})_2]^{10-}$ and $[Co_3W(D_2O)_2(CoW_9O_{34})_2]^{12-}$ clusters. Finally, the microscopic background of the pseudo-spin-1/2 Hamiltonian is derived.

In Section 5, we go beyond the assumption about the isotropic character of the exchange and present a more comprehensive theory of the magnetic exchange in degenerate clusters that take into account the orbitally-dependent terms in the Hamiltonian. We derive a general form of the orbitally-dependent kinetic exchange Hamiltonian and show how this Hamiltonian supplemented by a set of relevant interactions (crystal field, SO coupling, etc.) can be treated with the use of the powerful technique of the irreducible tensor operators (ITO).

Section 6 illustrates selected applications of the theory. The developed formalism is applied to the study of the magnetic anisotropy of the corner shared and face-shared bioctahedral $^2T_2(t_2^1) - {}^2T_2(t_2^1)$ pairs with D_{4h} and D_{3h} overall symmetries. The last case is exemplified by the $[Ti_2Cl_9]^{3-}$ unit in $Cs_3Ti_2Cl_9$ crystals whose magnetic behaviour is discussed in detail. We also elucidate the major electronic factors controlling the magnetic anisotropy in the Co(II) pairs and discuss the applicability of the conventional isotropic Lines model. In the case of strong SO coupling, the effective Hamiltonian is projected onto the subspace of low-lying Kramers doublets and similarly a pseudo-spin-1/2 Hamiltonian is derived. The described procedure allows to establish the interrelation between the physical parameters of the system and the parameters of the pseudo-spin-1/2 Hamiltonian. Then the orbitally-dependent magnetic exchange in the Mn(III)–CN–Mn(II) pair and its relevance to the SMM behaviour of cyanide bridged systems are analysed.

Finally, in Section 7 we summarise the results also paying attention to the problems remaining out of this scope of the review, in particular, the Jahn–Teller (JT) coupling and unresolved questions. We conclude with some brief perspectives of the field, for instance, hints for a meaningful serch of new SMMs.

2. Exchange interaction: basic definitions

2.1. *Kinetic exchange*

The basic concepts of the microscopic theory of magnetic exchange can be illustrated by considering spin-clusters for which the ground terms of the constituent ions are orbitally non-degenerate. It is conventional to distinguish two main mechanisms of the exchange interaction according to the dominating interatomic interaction responsible for the exchange, namely the *kinetic and potential exchange*. We start with the concept of the kinetic exchange in the simplest case of exchange-coupled pair of transition metal ions

A and B, when each ion possesses one unpaired electron in a non-degenerate orbital φ_i ($i = A, B$) whereas the first excited orbital ϕ_i is unoccupied. Usually, the magnetic exchange between the metal ions is mediated by the bridging diamagnetic atoms (ligands) and for this reason such coupling was called superexchange. The theoretical framework for treating the kinetic superexchange was developed by Anderson [84,85]. The basic idea was that the unpaired electrons are not fully localised on the metal ions and some non-zero spin densities were found on bridging ligands due to covalency effects. Then, the one-electron wave-functions describing these electrons (magnetic orbitals) are mainly not only of 3d-character, but also include some admixture of the bridging s- and p-orbitals.

Virtual electron transfer that mixes the ground state of the dimer with the excited charge-transfer (CT) states occurs mainly due to the kinetic energy of electrons and gives rise to the kinetic exchange that appears in Andreson's theory [84,85] as a second-order spin-dependent splitting. Figures 1 and 2 illustrate different kinetic exchange mechanisms and their contributions to the overall exchange splitting. It is to be noted that the full spin of the system is conserved in the course of the electron transfer. The ground manifold of the pair includes the spin-singlet ($S = 0$) and spin-triplet ($S = 1$), the corresponding wave-functions are the following:

$$\Psi_{gr}(S=0) = \frac{1}{\sqrt{2}}\left(\left|\varphi_A\bar{\varphi}_B\right| - \left|\bar{\varphi}_A\varphi_B\right|\right), \quad \Psi_{gr}(S=1, M_S=1) = \left|\varphi_A\varphi_B\right|, \tag{2.1}$$

where φ_i and $\bar{\varphi}_i$ are the SOs with spin up and down, respectively, ($\varphi_i \equiv |\varphi(\boldsymbol{r})\uparrow\rangle$ and $\bar{\varphi}_i \equiv |\varphi(\boldsymbol{r})\downarrow\rangle$), and $|\varphi_A\varphi_B|$, etc., are the Slater determinants. For the sake of simplicity, the orbitals are assumed to be orthogonal. Only the spin-triplet wave-function with maximum spin projection is given in Equation (2.1). If the metal ions are isolated from each other, the spin-singlet and spin-triplet states possess the same energies. When the electron transfer is switched on, the ground manifold is split due to the mixing (interaction of configurations) with different CT states. The first kind of CT states (denoted as CT_1 in Figure 1) corresponds to the virtual electron transfer from the single-occupied φ_A orbital of ion A to the single-occupied φ_B orbital of ion B and also from the back transfer $\varphi_B \rightarrow \varphi_A$ (the latter is not shown in Figure 1). In accordance with the Pauli's exclusion principle, these CT states are spin singlets and they are described by the wave-functions

$$\Psi^A_{CT_1} = \left|\varphi_A\bar{\varphi}_A\right|, \quad \Psi^B_{CT_1} = \left|\varphi_B\bar{\varphi}_B\right|. \tag{2.2}$$

The states CT_1 are separated from the ground manifold by a large (in comparison to the interatomic interaction) gap U, where U is the energy of the Coulomb repulsion between two electrons located at the same site. These CT states are connected with the ground spin-singlet by the matrix elements

$$\left\langle \Psi^B_{CT_1} \middle| \hat{V}(\varphi_A \rightarrow \varphi_B) \middle| \Psi_{gr}(S=0) \right\rangle = \left\langle \Psi^A_{CT_1} \middle| \hat{V}(\varphi_B \rightarrow \varphi_A) \middle| \Psi_{gr}(S=0) \right\rangle = \sqrt{2}t_{\varphi\varphi}, \tag{2.3}$$

where $\hat{V}$ is the electron transfer operator and $t_{\varphi\varphi} = \langle\varphi_B|\hat{h}|\varphi_A\rangle$ is the transfer integral ($\hat{h}$ is the one-electron Hamiltonian) for which the dominant contribution is provided by the kinetic energy of the delocalised electron. Using the second-order perturbation

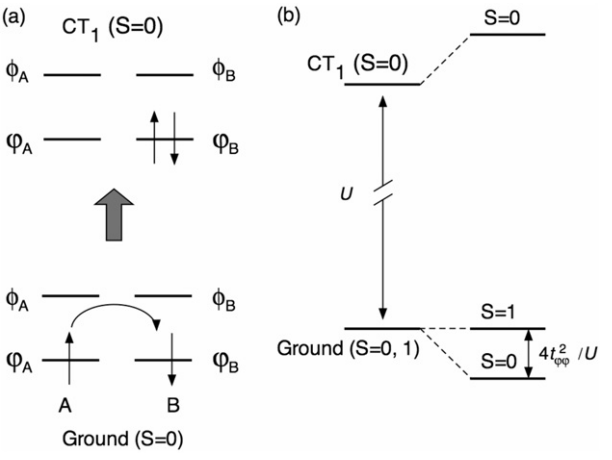

Figure 1. Schematic representation for the mechanism of the antiferromagnetic kinetic exchange: (a) orbital population in the ground and CT configurations and (b) full spin states and exchange splitting (U is the intrasite interelectronic repulsion energy and $t_{\varphi\varphi}$ is the ransfer parameter for the $\varphi_A \rightarrow \varphi_B$ electron hopping).

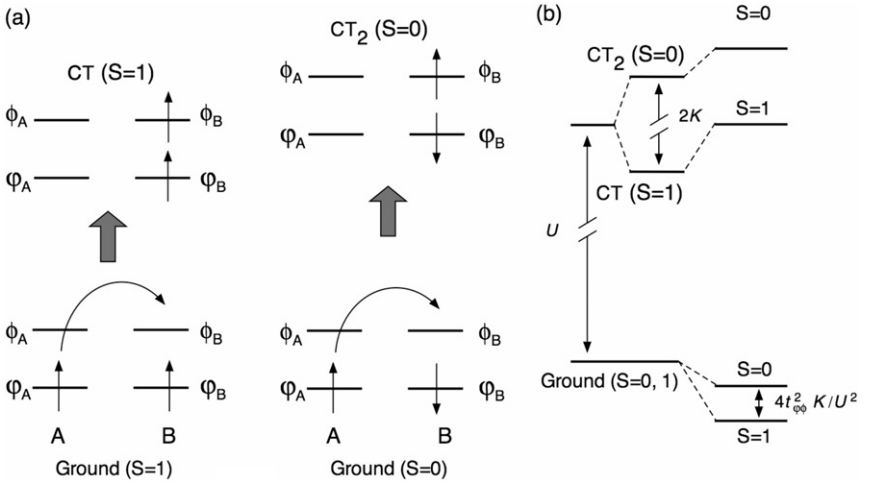

Figure 2. Schematic representation for the mechanism of the antiferromagnetic kinetic exchange: (a) orbital population in the ground and CT configurations and (b) full spin states and exchange splitting (K is the intersite exchange integral and $t_{\varphi\phi}$ is the ransfer parameter for the $\varphi_A \rightarrow \phi_B$ electron hopping).

treatment, one can find that the low-lying spin-singlet $E(S = 0)$ is stabilised with respect to the spin-triplet $E(S = 1)$ due to the $t_{\varphi\varphi}$-transfer processes by the value

$$[E(S = 1) - E(S = 0)]_{\varphi_i \rightarrow \varphi_j} = 4\frac{t_{\varphi\varphi}^2}{U}, \tag{2.4}$$

and hence the virtual electron transfer (second-order process) gives rise to the antiferromagnetic exchange contribution.

Another type of CT state can occur if the centres contain more than one empty orbital in the excited energy pattern. In this case, the CT states can also be obtained by the virtual electron transfer from a half-occupied φ orbital of one centre to an empty orbital ϕ of another centre (Figure 2). This kind of transfer leads to the CT states with $S=0$ (CT_2 state in Figure 2) and $S=1$ (CT($S=1$) state in Figure 2). The gaps between the ground manifold and CT states CT_2 and CT($S=1$) are equal to $U+K$ and $U-K$, respectively, where

$$K = \int\int \varphi_i(1)\phi_i(2)g(1,2)\phi_i(1)\varphi_i(2)\mathrm{d}\tau_1\mathrm{d}\tau_2 \equiv \langle \varphi_i\phi_i|\hat{g}|\phi_i\varphi_i\rangle \tag{2.5}$$

is the intracentre exchange integral and $\hat{g}$ is the interelectronic repulsion, i.e. two-electron part of the Hamiltonian. It is seen that the spin-triplet state CT ($S=1$) is lower in energy than the spin-singlet state CT_2 by the value $2K$ in accordance with the Hund's rule. The wave-functions for the states CT_2 and CT ($S=1$) are given by

$$\begin{aligned} &\Psi^A_{CT_2} = \frac{1}{\sqrt{2}}\left(|\varphi_A\bar{\phi}_A| - |\bar{\varphi}_A\phi_A|\right), \quad \Psi^B_{CT_2} = \frac{1}{\sqrt{2}}\left(|\varphi_B\bar{\phi}_B| - |\bar{\varphi}_B\phi_B|\right), \\ &\Psi^A_{CT}(S=1, M_S=1) = |\varphi_A\phi_A|, \quad \Psi^B_{CT}(S=1, M_S=1) = |\varphi_B\phi_B|, \end{aligned} \tag{2.6}$$

where only the wave-functions with the maximum spin projection are shown for spin-triplet CT states. The matrix elements connecting the spin-triplets prove to be the same as those connecting spin-singlets, namely

$$\begin{aligned} &\left\langle \Psi^B_{CT_2}\middle|\hat{V}(\varphi_A \to \phi_B)\middle|\Psi_{gr}(S=0)\right\rangle \\ &\quad = \left\langle \Psi^A_{CT_2}|\hat{V}(\varphi_B \to \phi_A)|\Psi_{gr}(S=0)\right\rangle = \left\langle \Psi^A_{CT}(S=1)\middle|\hat{V}(\varphi_B \to \phi_A)\middle|\Psi_{gr}(S=1)\right\rangle \\ &\quad = -\left\langle \Psi^B_{CT}(S=1)\middle|\hat{V}(\varphi_A \to \phi_B)\middle|\Psi_{gr}(S=0)\right\rangle = t_{\varphi\phi}, \end{aligned} \tag{2.7}$$

where $t_{\varphi\phi} = \langle\phi_B|\hat{h}|\varphi_A\rangle = \langle\phi_A|\hat{h}|\varphi_B\rangle$ is the corresponding transfer integral. It is seen that the $t_{\varphi\phi}$-transfer stabilises both the spin-singlet and the spin-doublet, but the stabilisation of the spin-triplet is stronger due to the fact that it is closer in energy to the ground manifold. Applying again the perturbation procedure, one can find that the $t_{\varphi\phi}$-transfer stabilises the spin-triplet with respect to the spin-singlet by the value

$$[E(S=0) - E(S=1)]_{\varphi_i \to \phi_j} = 2t^2_{\varphi\phi}\left(\frac{1}{U-K} - \frac{1}{U+K}\right) \approx 4t^2_{\varphi\phi}K/U^2 \tag{2.8}$$

The interelectronic Coloumb repulsion of two electrons at the same centre usually exceeds the intracenter exchange, and therefore in Equation (2.8) it is assumed that $K/U \ll 1$. One can see that the stabilisation of the spin-triplet is smaller than the antiferromagnetic splitting in Equation (2.4). In fact, the ferromagnetic splitting, Equation (2.8), represents the third-order effect with respect to a small factor K/U.

In this context it is worth mentioning the so-called Goodenough–Kanamori rules [4,5], which are closely related to the above consideration of the kinetic exchange pathways and are widely used in molecular magnetism. According to these rules, the exchange coupling

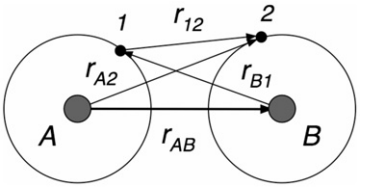

Figure 3. Scheme of the interactions involved in the potential interatomic exchange.

is antiferromagnetic if the virtual electron transfer occurs between overlapping half-filled orbitals, and it is ferromagnetic if the electron virtually jumps from a half-filled to an empty orbital or alternatively, from a filled orbital to a half-filled one.

2.2. *Potential exchange*

Potential exchange is induced by all intercentre Coulomb interactions,

$$\hat{g}' = \frac{e^2}{r_{12}} - \frac{Ze^2}{r_{B1}} - \frac{Ze^2}{r_{A2}} + \frac{Z^2e^2}{r_{AB}}, \tag{2.9}$$

related to this part of the potential energy in the system of two ions, namely, interelectronic repulsion energy (first term), Coulomb attraction of the electrons to the alien centers (second and third terms) and the repulsion of the nuclei. The last three terms do not contribute to the exchange in the model of localised orthogonal orbitals. The meaning of the notations used in Equation (2.9) are explained in Figure 3.

The singlet-triplet gap is expressed through the integral of potential exchange as following:

$$[E(S=0) - E(S=1)]_P = 2\left\langle \varphi_A \phi_B \middle| \hat{g}' \middle| \phi_B \varphi_A \right\rangle. \tag{2.10}$$

The potential exchange is usually small and positive, and therefore leads to a ferromagnetic contribution.

2.3. *Heisenberg–Dirac–van Vleck model, restrictions*

Taking into account both kinetic and potential contribution, one can write down the overall singlet–triplet separation of an exchange-coupled pair with one unpaired electron on each metal centre as follows:

$$E(S=0) - E(S=1) = 2J. \tag{2.11}$$

In this expression, the value J:

$$J = -2t_{\varphi\varphi}^2/U + 2t_{\varphi\phi}^2 K/U^2 + \left\langle \varphi_A \phi_B \middle| \hat{g}' \middle| \phi_B \varphi_A \right\rangle \tag{2.12}$$

is the combined exchange parameter involving potential and kinetic exchange interactions. One can see that the exchange splitting can be reproduced by the eigenvalues of an isotropic spin Hamiltonian:

$$\hat{H}_{ex}(A, B) = -2J\,\hat{\boldsymbol{s}}_A\hat{\boldsymbol{s}}_B, \tag{2.13}$$

in which the parameter J is expressed as the sum of antiferromagnetic and ferromagnetic contributions and the cases $J > 0$ and $J < 0$ are related to the ferromagnetic and antiferromagnetic coupling correspondingly, $\hat{\boldsymbol{s}}_A$ and $\hat{\boldsymbol{s}}_B$ are the spin operators of the ions A and B. In the considered simple cases they are one-electron spin operators. It is important to note that the Hamiltonian, Equation (2.13), has a more general sense and can be extended to the case of many-electron ions. In this case, $\hat{\boldsymbol{s}}_A$ and $\hat{\boldsymbol{s}}_B$ are the full spin operators of the many-electron metal centres. Such many-electron spin-Hamiltonian represents the HDVV exchange model [1,14,15,86,87] that is widely used in molecular magnetism and solid state physics.

In the view of the main topic of this article, it should be stressed that the derivation of the HDVV Hamiltonian is essentially based on the assumptions that the active space of each centre comprises only half-filled magnetic orbitals and double occupied orbitals. This means that the ground terms of the centres are orbitally non-degenerate and possess non-vanishing spins. Therefore, the HDVV model is only applicable to the systems comprising ions whose ground terms are orbitally non-degenerate and well isolated from the excited ones (spin-clusters). This is valid, for example, for the half-filled shells of transition metal ions in a cubic crystal field, for example, high-spin Fe(III) ions with the ground term $^6A_1(t_2^3e^2)$, Cr(III) ions with the half-filled t_2 shell giving rise to $^4A_2(t_2^3)$ term, etc. In general, the gound term proves to be an orbital singlet for all transition metal ions in a strong low-symmetry crystal field that removes the orbital degeneracy and separates the ground state from the excited ones. One should also note that, although the HDVV Hamiltonian is invalid in the case of orbitally degenerate ions, the described basic mechanisms of the exchange (kinetic and potential) are rather general and remain valid in the case of degeneracy as well.

Turning back to the expression for the combined exchange parameter, Equation (2.12), one can see that in most cases the antiferromagnetic contribution dominates. Only when the electron transfer $t_{\varphi\varphi}$ is prevented by the symmetry of the pair, the overall interaction is expected to be ferromagnetic. This conclusion is, however, valid only for non-degenerate states of the interacting metal ions. In degenerate systems, the kinetic exchange is sometimes able to give rise to the ferromagnetic ground state as was first pointed out by McConnell [88] and then discussed by Kollmar and Kahn [89], Weihe and Güdel [90] and also in [91–94]. In the subsequent discussion, we will deal with the situation when the orbitally-dependent exchange stabilises the ferromagnetic state. From this point of view, the use of exchange-coupled metal ions with the unquenched orbital angular momenta can be regarded as a possible strategy for the design of molecular ferromagnets. Another important trend is to obtain orbitally-degenerate clusters exhibiting unusually strong magnetic anisotropy useful for applications.

2.4. *Magnetic anisotropy in spin-clusters*

2.4.1. *Single-ion anisotropy*

Considering magnetic anisotropy, one can distinguish two kinds of anisotropic contributions, namely, single-ion contributions and those appearing due to the anisotropy of the exchange interactions. Both named factors act in spin clusters as well as in degenerate systems, but their manifestations in these two kinds of systems, are different as well as in the corresponding parameters.

In the ground orbital singlet states of the metal ions the first-order orbital angular momentum is quenched. As a result, the spin contribution to the single-ion magnetic moments (and hence to the total magnetic moment of the cluster) dominates. Single-ion anisotropic terms appear in spin-clusters in which the symmetry of the local surroundings of the constituent metal ions is lower than the cubic one as due to the small mixing of the ground spin state of ions with the excited crystal field terms through the SO coupling. This mixing leads to the anisotropic corrections to g-factors and also to the zero-field splitting (ZFS) terms in the spin-Hamiltonian (see [4,15,95,96] and references therein). The ZFS of the state of cluster with the spin S is described by the Hamiltonian

$$\hat{H}_{ZFS} = D_S\left[\hat{S}_Z^2 - \frac{1}{3}S(S+1)\right] + E_S\left(\hat{S}_X^2 - \hat{S}_Y^2\right), \tag{2.14}$$

where the parameters D_S and E_S are the so-called axial and rhombic ZFS parameters. The Hamiltonian, Equation (2.17), is not invariant under arbitrary rotations and therefore brings the magnetic anisotropy into the system. Since the ZFS appears as a second-order correction, the parameters of ZFS can be estimated as $\propto \lambda^2/\Delta E$, where λ is the SO coupling constant and ΔE is a gap in the crystal field energy pattern. Usually, for the transition metal ions $|\lambda/\Delta E| \ll 1$ that determines the smallness of the local contributions to the global anisotropy.

2.4.2. *Exchange anisotropy*

The HDVV Hamiltonian is expressed in terms of the scalar products of spin operators, and therefore it is invariant under any rotations. This means that the Zeeman splitting arising from the interaction of spins with the external magnetic field is independent of the direction of the field. Therefore the exchange coupling in the framework of the HDVV model does not imply magnetic anisotropy. If weak magnetic anisotropy still exists in spin-systems, it appears as a result of small corrections to the HDVV spin Hamiltonian due to the contributions of the excited states admixed by SO coupling to the ground state.

Along with the HDVV terms the exchange Hamiltonian contains anisotropic contributions [4–6,14,15], which can be written in the tensorial form as $\sum_{ij}\hat{\boldsymbol{s}}_i\boldsymbol{T}_{ij}\hat{\boldsymbol{s}}_j$, where the second-order tensor $\boldsymbol{T}_{ij}$ can be divided into the symmetric part $\boldsymbol{G}_{ij}$ and antisymmetric one $\boldsymbol{D}_{ij}$. The corresponding terms are not invariant under the rotations and their explicit form does depend on the point symmetry of the system giving rise to a magnetic anisotropy. Among anisotropic contributions, one should mention the antisymmetric exchange introduced by Dzyaloshinsky [97] using phenomenological symmetry arguments

and deduced explicitly by Moriya [98,99] using the inclusion of SO coupling in the Anderson's theory of superexchange:

$$H_{AS} = \sum_{i,k} \boldsymbol{D}_{ij}[\hat{\boldsymbol{s}}_i \times \hat{\boldsymbol{s}}_k], \tag{2.15}$$

where $\boldsymbol{D}_{ij} = -\boldsymbol{D}_{ji}$ are the antisymmetric vector parameters. Antisymmetric exchange appears as a second-order perturbation through the combined effect of SO interaction and isotropic exchange coupling. Therefore, the $\boldsymbol{D}_{ij}$ parameters can be estimated as $D_{ij} \propto J_{ij}(\lambda/\Delta E)$, where λ is the SO coupling parameter and ΔE is the energy of an appropriate excited state (crystal field splitting). The parameters G_{ij} in the symmetric part of the anisotropic exchange are of the order of $G_{ij} \propto J_{ij}(\lambda/\Delta E)^2$. Usually for the transition metal ions crystal field exeeds SO coupling, $|\lambda/\Delta E| \ll 1$, and hence the magnetically anisotropic interactions are small as compared to the isotropic ones.

Although the local and exchange anisotropic contributions cannot be directly compared, it should be emphasized that in spin-clusters the parameters defining all the above mentioned single-ion and pairwise anisotropic contributions are usually small compared to the isotropic ones, so only relatively weak magnetic anisotropy can be expected for these clusters.

3. Orbital degeneracy and exchange interaction: a preliminary consideration

3.1. *Orbital angular momentum in crystal fields, T–P isomorphism*

An effective quenching of the orbital angular momentum of the metal ion in crystal fields of different symmetries has been understood at the earlier stage of crystal field theory [83] and played a fundamental role in the development of coordination chemistry and solid state physics, in general, and specifically, in the understanding of magnetism. To illustrate the main ideas, let us consider one-electron $3d$-state of a free ion for which l and s are the exact quantum numbers. This state possesses the orbital angular momentum $l = 2$ and spin $s = 1/2$. In the crystal fields of the cubic symmetry, five $3d$ states are split into the orbital triplet ${}^2t_{2g}$ (d_{yz}, d_{xz}, d_{xy}) and the orbital doublet ${}^2e_g(d_{z^2}, d_{x^2-y^2})$, with the ${}^2t_{2g}$-state being the ground one in the octahedral surrounding (Figure 4). The 3×3 matrices of the orbital angular momentum operators defined on the basis of the orbital triplet are given by (see, e.g. the books [100,101])

$$\begin{matrix} & d_{yz} & d_{xz} & d_{xy} \end{matrix}$$

$$\hat{l}_x(t_{2g}) = \begin{pmatrix} 0 & 0 & 0 \\ 0 & 0 & i \\ 0 & -i & 0 \end{pmatrix}, \quad \hat{l}_y(t_{2g}) = \begin{pmatrix} 0 & 0 & -i \\ 0 & 0 & 0 \\ i & 0 & 0 \end{pmatrix}, \quad \hat{l}_z(t_{2g}) = \begin{pmatrix} 0 & i & 0 \\ -i & 0 & 0 \\ 0 & 0 & 0 \end{pmatrix}. \tag{3.1}$$

These matrices obey the same commutation relations as the components of the orbital angular momentum $\hat{l}_x, \hat{l}_y, \hat{l}_z$. Although the operators $\hat{\boldsymbol{l}}^2$ and $\hat{l}_z$ do not commute with the cubic crystal field potential that lowers the spherical symmetry of a free ion, the system in a restricted basis of three t_{2g} orbitals can be described by an effective angular orbital momentum $l = 1$. This means that the cubic crystal field partially reduces the orbital angular momentum of a free ion from $l = 2$ to $l = 1$. By comparing these matrices with

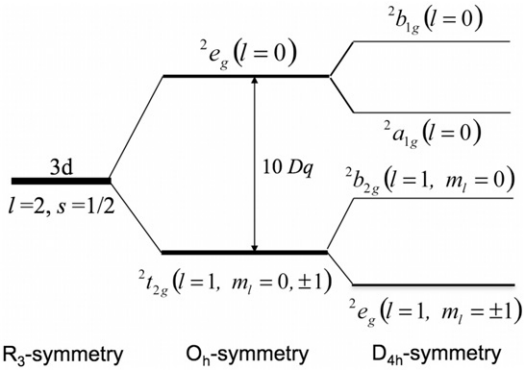

Figure 4. Illustration for the partial quenching of the first-order orbital angular momentum by the cubic and tetragonal crystal fields.

those for the *p*-state (basis p_x, p_y, p_z) of a free atom, one can see that the following simple relation holds:

$$\hat{\boldsymbol{l}}(t_{2g}) = -\hat{\boldsymbol{l}}(p). \tag{3.2}$$

This relation is a particular case of a more general statement that is called *T–P* isomorphism. On the other hand, all matrix elements of the orbital angular momentum operators in the ^2e_g-state are vanishing, so the first-order orbital angular momentum is completely quenched in the cubic ^2e_g-state and only the second-order term arising from the SO mixing of the $^2t_{2g}$ and ^2e_g-states remains.

A crystal field of a lower symmetry produces further quenching of the orbital angular momentum. This is illustrated by the right-hand side of Figure 4. Thus, when the symmetry of the crystal field is reduced from O_h to D_{4h}, the $^2t_{2g}$-level undergoes the splitting into the tetragonal orbital doublet $^2e_g(d_{yz}, d_{xz})$ and the singlet $^2b_{2g}(d_{xy})$. Depending on the sign of the tetragonal crystal field splitting, either orbital singlet or doublet can be the ground state (Figure 4 displays the situation when the orbital doublet is the ground state). When the ^2e_g-state is well separated from the $^2b_{2g}$-state, one can neglect the matrix elements of the orbital angular momentum operators connecting these two states and consider the orbital angular momentum matrices defined on the basis of tetragonal ^2e_g-state. It is seen that all matrix elements of the operators $\hat{l}_x$ and $\hat{l}_y$ are vanishing within the ^2e_g-state, and the matrix of $\hat{l}_z$ is the following:

$$\hat{l}_z(e_g) = \begin{array}{c} \begin{matrix} d_{-1} & d_{+1} \end{matrix} \\ \begin{pmatrix} -1 & 0 \\ 0 & 1 \end{pmatrix} \end{array}, \tag{3.3}$$

where the following complex (circular) basis for d-orbitals is used:

$$d_{-1} = -(d_{xz} - id_{yz})/\sqrt{2},$$
$$d_{+1} = +(d_{xz} + id_{yz})/\sqrt{2}.$$

The matrix in Equation (3.3) in the complex basis d_{-1} and d_{+1} coincides with the matrix of $\hat{l}_z$ in the basis of *p*-functions $p_{-1} = -(p_x - ip_y)/\sqrt{2}$ and $p_{+1} = +(p_x + ip_y)/\sqrt{2}$, so that

the tetragonal ^2e_g-state can be regarded as a state with projections $m_l = \pm 1$ of the orbital angular momentum, whereas the $^2b_{2g}$-state possesses $m_l = 0$. It should be emphasized that in the tetragonal ^2e_g-state the first-order orbital momentum is still not fully quenched. This conclusion is also valid for the axial point groups and, in particular for the, trigonal ^2e-state arising from the cubic $^2t_{2g}$-level. In a field of a lower symmetry, the ^2e_g-state will be evidently split into orbital singlets so that the first-order orbital angular momentum will be fully quenched.

The concept of pseudoangular momentum is rather general and, in particular, is not only restricted to the one-electron case but also valid for the many-electron terms of the transition metal ions. In the present review, we will deal with the cubic orbital triplets $^{2s+1}T_{2g}$ or $^{2s+1}T_{1g}$ (states with $l = 1$ and $m_l = 0, \pm 1$) and also with the tetragonal orbital doublets $^{2s+1}E_g$ (or trigonal orbital doublets arising from the cubic orbital triplets) possessing $m_l = \pm 1$.

3.2. *Single-ion anisotropy in degenerate systems*

As distinguished from spin-systems, the anisotropy in degenerate systems is expected to be strong. Here again the two kinds of the anisotropic contributions can be distinguished, namely the single-ion contributions and the exchange ones.

The origin of a strong single-ion anisotropy in degenerate systems can be illustrated by a scheme of classical motion of the angular momentum in the situation when a cubic orbital triplet is split by an axial crystal field into a singlet and a doublet (Figure 5). While the orbital triplet can be regarded as a state with the orbital angular momentum $l = 1$, the singlet and doublet can be associated with the projections $m_l = 0$ and $m_l = \pm 1$, respectively. Depending on the sign of the axial field, the ground state can be either doublet or singlet. In the former case, the ground state can be regarded as the state in which only two possible values of the angular momentum projection ('up' and 'down') are

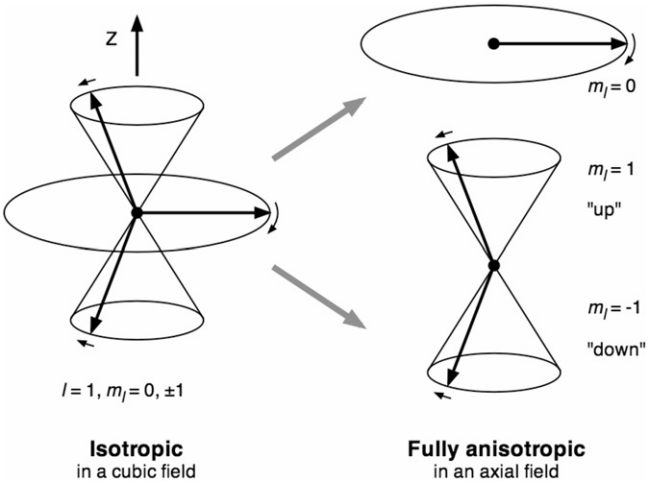

Figure 5. Illustration for the magnetic anisotropy induced by an axial crystal field.

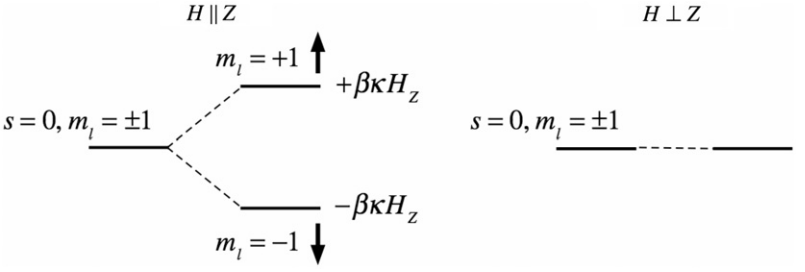

Figure 6. Zeeman splitting of the level with $s = 0$, $m_l = \pm 1$, κ is the orbital reduction factor that is related to a partial delocalisation of the d-orbitals towards the ligands [5].

retained. This immediately leads to a strong uniaxial magnetic anisotropy with Z being the 'easy' axis of magnetisation. In fact, the system shows a linear Zeeman splitting in a parallel (along the axis) field and *does not exhibit splitting in a perpendicular field* (Figure 6). Figure 5 also illustrates the existence of the barrier for the reversal of magnetisation when the doublet ('negate' ZFS) is the ground state. In fact, the system can jump from 'up' ('down') to 'down' ('up') configuration through the exited singlet. On the contrary, provided 'positive' ZFS, the system proves to be barrierless.

As distinguished from the spin, the orbital angular momentum 'feels' the axial crystal field directly, and hence the magnetic anisotropy appears without the inclusion of SO coupling. In this case, the singlet–doublet gap is just the axial crystal field splitting. On the contrary, when the ground state of the ion possesses only spin (spin clusters), this state can be affected by the axial field only through the second-order SO coupling and thus leading to the above-mentioned anisotropy of g-factors and ZFS. Formally, the ZFS for $s = 1$ and the axial field splitting for the orbital triplet ($l = 1$) are similar in the labels of the levels ($m_s = 0$ and $m_s = \pm 1$ for spin states and $m_l = 0$ and $m_l = \pm 1$ for orbital states), but in the former case the ZFS is of the order of 0.1–10 cm^{-1} whereas the axial crystal field splitting for the orbital triplet is about 10^3 cm^{-1}. Just these energies determine the magnitude of the external magnetic field that is able to turn the magnetic moment, and therefore this field can be referred to as a characteristic measure of the magnetic anisotropy or, alternatively, of the barrier for the reversal of magnetisation. In this sense, the direct (first-order) orbital contributions can be referred to as strong, whereas the anisotropy in spin-systems is 'weak'. This is illustrated by Figure 7, which demonstrates the field dependences of magnetic moments of an axial spin ion ($s = 1$, $l = 0$, $D_s = -3\,\mathrm{cm}^{-1}$, $g_s = 2$) and an orbitally degenerate ion ($s = 0$, $l = 1$, $\Delta = -100\,\mathrm{cm}^{-1}$, $g_l = 1$) for the two main directions of the magnetic field. In the case of spin systems, the saturation is reached in the fields that are much lower than those for the degenerate systems. At the same time, the difference between the values of magnetisation in principal directions of the field are much smaller in spin-systems. One can see that, in general, the degenerate systems exhibit a much more pronounced anisotropy than the spin-systems.

3.3. *The concept of the orbitally-dependent exchange: a simple illustration*

Exchange interaction and, in particular, magnetic anisotropy in degenerate systems represents a more complicated phenomenon. In this section we will introduce a key

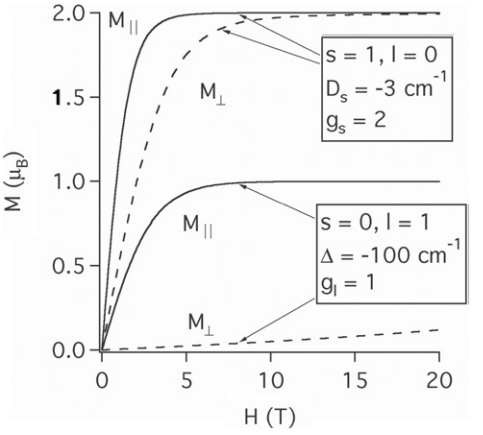

Figure 7. Field dependences (H in Tesla) of magnetisation for an axial spin system, $s=1$, and for orbitally degenerate system, $l=1$ (temperature $T=2\,\mathrm{K}$).

concept related to the exchange interaction in the degenerate systems, namely the concept of the orbitally-dependent exchange. We will show how the orbitally-dependent exchange Hamiltonian naturally appears while considering the interaction between ions with the unquenched orbital angular momenta. This also allows to comprehend the general features of the magnetic anisotropy. The concept of orbitally-dependent exchange can be illustrated by considering potential exchange in a simple case of *s–p* molecule (van Vleck [102] and Levi [103]). In this dimer one atom (A) has an s electron and another one (B) possesses a p electron. There are three possible orbital states of the molecule, which can be referred to as sp_Z, sp_X and sp_Y. Accordingly, one can describe the exchange interaction in the bielectron molecule by means of the following three Hamiltonians:

$$\hat{H}_\alpha = -J_\alpha\left(\frac{1}{2} + 2\hat{\boldsymbol{s}}_A\hat{\boldsymbol{s}}_B\right), \quad \alpha = sp_Z,\ sp_X,\ sp_Y. \tag{3.4}$$

In conformity with the symmetry of the molecule (Figure 8) there are only two independent exchange integrals, which can be associated with the σ- and two equivalent π-bonds:

$$\begin{aligned} J_{sp_Z} &= \int\int s_A^*(1)\,p_{ZB}^*(2)(1/r_{12})s_A(2)\,p_{ZB}(1)\mathrm{d}\tau_1\mathrm{d}\tau_2 \equiv J_\sigma \equiv J_{||}, \\ J_{sp_X} &= J_{sp_Y} \equiv J_\pi \equiv J_\perp. \end{aligned} \tag{3.5}$$

Now instead of three equations (3.4) ($\alpha = sp_Z, sp_X, sp_Y$), one can describe the exchange interaction by the following matrix Hamiltonian operating within the full basis comprising four spin states and three orbital states:

$$\hat{H}_{\mathrm{ex}} = \begin{pmatrix} J_{||}\left(\frac{1}{2} + 2\hat{\boldsymbol{s}}_A\,\hat{\boldsymbol{s}}_B\right) & 0 & 0 \\ 0 & J_\perp\left(\frac{1}{2} + 2\hat{\boldsymbol{s}}_A\,\hat{\boldsymbol{s}}_B\right) & 0 \\ 0 & 0 & J_\perp\left(\frac{1}{2} + 2\hat{\boldsymbol{s}}_A\,\hat{\boldsymbol{s}}_B\right) \end{pmatrix} \equiv -\hat{F}\left(\frac{1}{2} + 2\hat{\boldsymbol{s}}_A\,\hat{\boldsymbol{s}}_B\right). \tag{3.6}$$

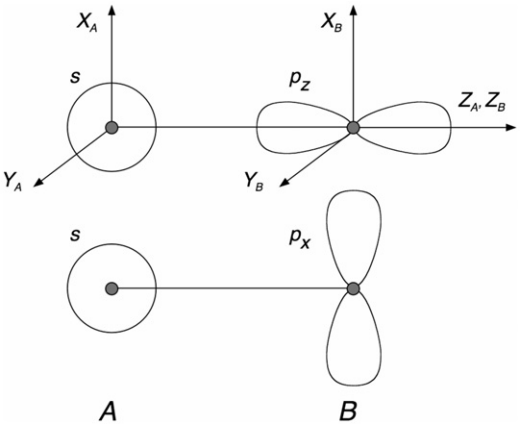

Figure 8. *s–p* molecule: illustration for the two types of the exchange integrals.

Here $\hat{F}$ is the *orbital operator* defined by the diagonal 3×3 matrix on the basis of three biorbital states $|sp_Z\rangle$, $|sp_X\rangle$ and $|sp_Y\rangle$.

$$\hat{F} = \begin{array}{c} \begin{matrix} sp_Z & sp_X & sp_Y \end{matrix} \\ \begin{pmatrix} J_{||} & 0 & 0 \\ 0 & J_{\perp} & 0 \\ 0 & 0 & J_{\perp} \end{pmatrix} \end{array}. \tag{3.7}$$

Each block of the matrix in Equation (3.6) represents a sub-matrix acting in the spin basis of the two centres provided that the orbital state is fixed (sp_x, sp_y, sp_z), and hence the full Hamiltonian is represented by the 12×12 matrix in the basis $|sp_i,\ s_A = 1/2,\ m_{sA},\ s_B = 1/2, m_{sB}\rangle$ ($i = X, Y, Z$, $m_{sB} = \pm1/2, m_{sA} = \pm1/2$).

We thus arrive at the Hamiltonian that contains both spin and orbital operators, and for this reason this Hamiltonian can be referred to as *orbitally-dependent exchange Hamiltonian*. To make this statement more transparent, it is instructive to pass from the real orbitals p_Z, p_X and p_Y to the basis $|l = 1, m_l\rangle$ ordered as $|1, 0\rangle, |1, 1\rangle, |1, -1\rangle$ in which the marix $\hat{F}$ retains its diagonal form, Equation (3.7). This allows one to express the operator $\hat{F}$ in terms of the angular momentum operator as follows:

$$\hat{F} = (1/3)\big(J_{||} + 2J_{\perp}\big) - (1/3)\big(J_{||} - J_{\perp}\big)\Big(3\hat{l}_Z^2 - 2\Big). \tag{3.8}$$

Alternatively, the Hamiltonian, Equation (3.6), can be rewritten as

$$\hat{H} = \frac{1}{6}(J_{||} - J_{\perp})\hat{O}_B - \frac{2}{3}(J_{||} + 2J_{\perp})\hat{\mathbf{s}}_A\hat{\mathbf{s}}_B + \frac{2}{3}\big(J_{||} - J_{\perp}\big)\,\hat{O}_B\,\hat{\mathbf{s}}_A\hat{\mathbf{s}}_B, \tag{3.9}$$

where the constant term is omitted and the orbital operator $\hat{O}_B = (3\hat{l}_z^2 - 2)$ acts in the p-basis of the degenerate centre B. The operator part of the Hamiltonian contains three types of contributions: *orbital part* (first term) that contains only the orbital operator $\hat{O}_B$, *spin part* (second term) that does not contain the orbital operator and is of HDVV form and *mixed spin–orbital part* (third term) that contains the scalar product of spin operators and operator $\hat{O}_B$. Such kind of complicated structure of the Hamiltonian is the main feature of degenerate

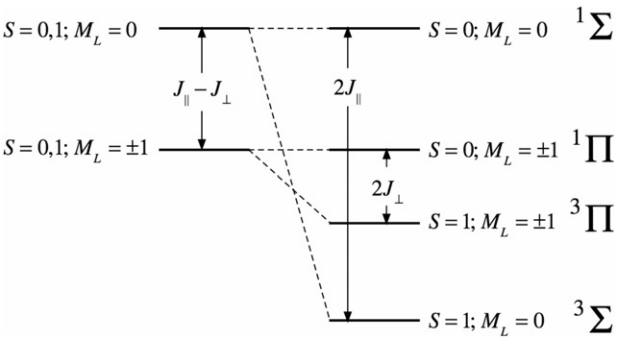

Figure 9. Energy pattern of *s–p*-exchange pair, exchange interactions are assumed to be ferromagnetic (conventional notations for the terms of a diatomic molecule are used).

systems that drastically distinguishes them from spin-clusters. A general form of the orbitally-dependent Hamiltonian will be considered in Section 5. Figure 9 shows the energy pattern of *s–p*-exchange pair in the conventional notations for the terms of a diatomic molecule providing ferromagnetic exchange interactions. One can see that the enegy levels are much more complicated as compared to those in a simple spin model.

3.4. *Exchange anisotropy in degenerate systems*

Let us discuss the magnetic anisotropy of the above-considered diatomic molecule. The HDVV contribution in Equation (3.9) is magnetically isotropic, whereas the two remaining orbitally-dependent terms are obviously anisotropic and have axial symmetry. In particular, the system in $^1\Pi$ term exhibits a fully anisotropic magnetic moment as shown in Figure 9, and for $^3\Pi$ term one can observe an isotropic spin contribution and a fully anisitropic orbital one. One can see that three parameters of the Hamiltonian, Equation (3.9), are expressed in terms of the two fundamental exchange constants $J_{||}$ and $J_\perp$ and therefore they are of the same order of magnitude. In this way, one arrives at the remarkable conclusion that in systems comprising ions with unquenched orbital angular momenta the isotropic and anisotropic contributions to the overall exchange are of the same order of magnitude, and in this sense the magnetic anisotropy can be referred to as strong one. This conclusion marks a fundamental difference between spin-systems in which the anisotropy is small and orbitally degenerate systems possess strong magnetic anisotropy.

Figure 9 shows that, in the example under consideration, the ground state is magnetically isotropic and strong magnetic anisotropy appears when the next two excited levels are populated. The majority of the studies dealing with the problem of the unquenched orbital angular momenta in exchange-coupled molecular systems relates to the clusters containing high-spin Co(II) ions in octahedral or quasioctahedral surroundings. There are two main approaches to treat this kind of systems, namely the microscopic approach proposed by Lines and Ginsberg [104,105] and the phenomenological approach based on the effective pseudo-spin-1/2 Hamiltonian [101,106–112], which describes the interaction between two Co(II) ions in their ground Kramers doublet states. The Lines model takes into account SO coupling acting within the ground cubic $^4T_1$ term of each Co(II) ion and the exchange coupling between the Co(II) ions. According to the Lines'

assumption, this exchange interaction is described by the isotropic HDVV spin Hamiltonian. If the symmetry of the local surroundings of Co(II) ions is lower than the cubic one, a strong (first-order) single-ion anisotropy can be expected. Such anisotropy appears as a result of the splitting of the ground cubic $^4T_1$ term by the low-symmetry (non-cubic) components of the crystal field. In the Lines model this anisotropy was not taken into account, so only high-symmetric systems comprising Co(II) ions in a perfect octahedral ligand field can be treated within this model. As an example, one can mention ref [113]. reporting the susceptibility of the triangular μ_3-oxo-bridged heterometallic complex $[Fe_2CoO(CH_3COO)_6(3\text{-Cl–Py})_3]$ in powder form. The model Hamiltonian is elaborated involving isotropic exchange interactions Fe(III)–Fe(III) and Co(II)–Fe(III) dealing with the real spins of high-spin Co(II) and Fe(III) ions, and also SO coupling and low-symmetry crystal field (C_{2v}) acting within the $^4T_{1g}$ ground manifold of the Co(II) ion. The outlined general model takes into account the strong anisotropic orbital contribution to the magnetic characteristics of the whole system arising from the Co(II) ion with unquenched orbital angular momentum.

On the contrary, the approach based on the pseudo-spin-1/2 Hamiltonian takes into account the anisotropy of the effective exchange parameters and *g*-factors. Since the exchange interaction is assumed to be isotropic, the anisotropy of the effective pseudo-spin-1/2 Hamiltonian is apparently a consequence of the above-mentioned single-ion anisotropy. An important problem that remained unsolved untill recently relates to the elucidation of the microscopic origin of the pseudo-spin-1/2 Hamiltonian, namely, to the establishing of interrelation between the set of the parameters involved in the effective Hamiltonian (which remained unknown in the framework of the phenomenological approach) and the set of microscopic parameters (exchange integral, SO parameter and low-symmetry crystal field parameter). This problem has been discussed in [114], in which the anisotropic pseudo-spin-1/2 Hamiltonian is deduced on the basis of the microscopic Lines model generalised to the case of axially and rombically distorted octahedral surroundings of Co(II) ions (we will refer to this model as *anisotropic Lines model*).

An extension of the anisotropic Lines model to other transition metal ions with unquenched orbital angular momenta has been elaborated in [115,116], in which the magnetic properties of a trigonal bipyramidal cyano-bridged SMM $[Mn^{III}(CN)_6]_2[Mn^{II}(tmphen)_2]_3$ containing orbitally degenerate low-spin Mn(III) ions has been interpreted and possible ways of increasing the barrier for the reversal of magnetisation have been discussed. Some aspects of the above-mentioned problems will be discussed hereafter.

The exchange anisotropy in clusters comprising ions with unquenched orbital angular momenta can be described in the framework of a more general theory that takes into account the *orbitally-dependent* terms of the effective exchange Hamiltonian. Many efforts were applied to construct the exchange Hamiltonian for a pair of orbitally degenerate ions [103,117–130]. First ideas in this area were proposed by van Vleck in his pioneering paper [102]. The theory of the potential exchange between orbitally-degenerate ions was worked out by Levy [117,118], and later on the cubic crystal field has been taken into account [119,120]. In this earlier period it was understood that the exchange interaction in orbitally degenerate systems is orbitally-dependent, and can lead to a strong magnetic anisotropy. Subsequent studies in this area were mainly focused on the consideration of the kinetic exchange mechanism proposed by Anderson [84,85]. Conventionally, this kind of magnetic

exchange dominates in most cases. For the first time, Kugel and Khomskii [121,122] considered the kinetic exchange between the orbitally degenerate ions and developed the theory of orbital ordering in JT crystals on this basis. Orbitally-dependent intercentre coupling also appears due to the JT effect (JTE) and results in a structural ordering in crystals (see the book by Kaplan and Vekhter [123]). Later on, the underlying ideas proposed in the cited works have been applied to the field of the molecular magnetism with their subsequent developing towards a more detailed description of the crystal field states and virtual electron transfer processes in the exchange coupled metal ions. In this context, the articles of Drillon and Georges [124,125], Leuenberger and Güdel [126], Weihe and Güdel [90] and Ceulemens *et al.* [127–129] devoted to the orbitally-dependent kinetic exchange should be mentioned. Although the important features of the exchange in degenerate systems had been understood, several underlying problems proved to be unresolved:

(i) The kinetic exchange Hamiltonian was only built for a pair of ions with simple electronic configurations (mainly the cases of one or two t_2 electrons per site). At the same time, a general form of the orbitally-dependent kinetic exchange Hamiltonian has not been deduced.
(ii) The deduced Hamiltonians were valid only for cubic local surroundings of constituent metal ions and specific overall symmetries of a pair.
(iii) A complex multiplet structure of the energy spectrum of the CT states implied by the Tanabe–Sugano diagrams was ignored.
(iv) Last but not the least, the physical consequences of the orbitally-dependent exchange interactions for the field of molecular magnetism (especially, anomalous magnetic anisotropy) have not been understood to full extent.

A more detailed discussion of these limitations of the conventional approaches will be given in the subsequent sections. Here we will only note that the absence of a general theoretical approach to the problem of orbitally-dependent exchange, precluded from the adequate description of this interaction, in complex systems containing many-electron orbitally degenerate ions and the exchange, coupled pairs of arbitrary overall symmetries. In his book 'Molecular Magnetism' [5], Oliver Kahn indicated that in spite of the existence of a large number of studies devoted to this topic '... the interaction between ions with unquenched angular momenta remains essentially an unsolved problem in the sense that there is no widely accepted model. Each case has been treated in a specific manner with a specific model...'.

In order to overcome the limitations of the conventional approaches, a new method has been recently developed to attack the problem of the kinetic exchange between orbitally degenerate ions [91–94]. As distinguished from the previous works, the orbitally-dependent exchange Hamiltonian has been deduced in a general form, that is, for the arbitrary terms and electronic configurations of the constituent metal ions in crystal fields. The usage of the tensorial properties of the creation and annihilation operators and Wigner–Racah algebra allowed to express the effective exchange Hamiltonian in terms of the irreducible tensors of the point groups of the local surroundings of metal ions, spin operators, the parameters of the constituent moieties (crystal field splitting parameter and Racah parameters) and the set of the intercentre transfer integrals specific for each overall symmetry of the pair. This Hamiltonian proved to be an efficient tool for the description

of the magnetic properties of clusters comprising metal ions with unquenched orbital angular momenta and, especially, their magnetic anisotropy. The developed approach has been applied to the interpretation of the magnetic behaviour of $[Ti_2Cl_9]^{3-}$ dimer [130–132], to the study of the exchange anisotropy in Co(II)-dimers [133,134] and cyanide-based SMMs [135,136].

4. Orbital effects and local magnetic anisotropy in the isotropic exchange model

4.1. *Lines approach to the problem of the magnetic exchange in Co(II) clusters*

The majority of the works, in which the role of the unquenched orbital angular momentum in molecular magnetism was discussed, were devoted to the compounds containing octahedrally coordinated high-spin Co(II) ions. The most widely used model to treat the magnetic behaviour of Co(II) clusters was proposed by Lines [104] and Ginsberg [105] (see the overview in [137].

The two lowest terms of a free Co(II) ion arising from the $3d^7$ configuration are ^4F (ground) and ^4P. The cubic crystal field splits the ^4F term into $^4T_1$, $^4T_2$ and $^4A_2$ terms in such a way that the orbital triplet $^4T_1$ becomes a ground state, while the excited ^4P state results in the $^4T_1$. In addition, two $^4T_1$ terms are mixed by the cubic crystal field so that the ground state is mainly of ^4F character, but also contains an admixture of ^4P. Using the $T-P$ isomorphism [82] (Section 2.2.), one can regard the orbital triplet $^4T_1$ as a state possessing fictitious orbital angular momentum $l = 1$. The matrix of the angular momentum operator $\hat{\boldsymbol{l}}$ within the $^4T_1(^4F)$ manifold proves to be the same as the matrix of $-(3/2)\,\hat{\boldsymbol{l}}$ defined in the atomic p-basis. This orbital angular momentum is coupled with the spin $s = 3/2$ by the SO interaction

$$\hat{H}_{SO} = -(3/2)\kappa\lambda\,\hat{\boldsymbol{l}}\hat{\boldsymbol{s}}, \tag{4.1}$$

where $\lambda \approx -180\ \mathrm{cm}^{-1}$ [5] is the SO coupling parameter for a free Co(II) ion, and κ is the orbital reduction factor. The pseudoangular momentum representation can be used in order to label the fine structure levels in a cubic crystal field. Accordingly, the SO coupling splits the ground $^4T_1$ term into the following states characterised by the total angular momentum j: doublet $j = 1/2$ (Γ_6), quartet $j = 3/2$ (Γ_8) and sextet $j = 5/2$ ($\Gamma_7 + \Gamma_8$) with the energies $(15/4)\,\kappa\lambda$, $(3/2)\,\kappa\lambda$ and $-(9/4)\,\kappa\lambda$, respectively (Figure 10). Alternatively, the Bethe's notations for the double-valued irreducible representation of the point group $\boldsymbol{O}$ are used: Γ_6 is a Kramers doublet with the basis $|j = 1/2, m_j = \pm 1/2\rangle$, Γ_8 is the quadruplet with the basis $|j = 3/2, m_j = \pm 1/2\rangle$, $|j = 3/2, m_j = \pm 3/2\rangle$ and, finally, Γ_7 is the second Kramers doublet in $\boldsymbol{O}$. The basis functions of the low-lying Kramers doublet $j = 1/2$ (Γ_6) can be found making use of the Clebsch–Gordan decomposition

$$\Phi(j, m_j) = \sum_{m_l m_s} C^{j\,m_j}_{1\,m_l 3/2\,m_s} \big| l = 1,\ m_l,\ s = 3/2,\ m_s \big\rangle, \tag{4.2}$$

where $C^{j\,m_j}_{1\,m_l 3/2\,m_s}$ are the Clebsch–Gordan coefficients in the conventional notations [100]. Using Equation (4.2), one finds the following eigen-vectors:

$$\begin{aligned}\Phi(1/2,\ \pm 1/2) = {} & (1/\sqrt{6})\,|1,\ \pm 1, 3/2,\ \mp 1/2\rangle - (1/\sqrt{3})\,|1, 0, 3/2,\ \pm 1/2\rangle \\ & + (1/\sqrt{2})\,|1,\ \mp 1, 3/2,\ \pm 3/2\rangle.\end{aligned} \tag{4.3}$$

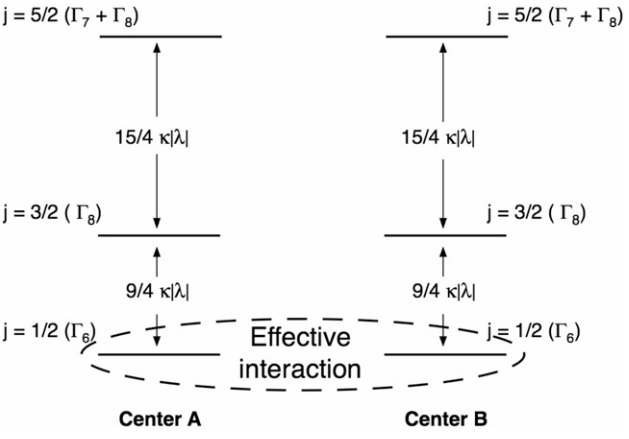

Figure 10. Illustration for the origin of effective pseudo-spin-1/2 Hamiltonian.

The wave-functions for the quartet and sextet are given, for example, in [104,105].

As one could see, a simple HDVV Hamiltonian is, in general, inapplicable for the degenerate systems. Nevertheless, Lines has assumed that the isotropic HDVV Hamiltonian can be approximately applied to treat the magnetic properties of polynuclear Co(II) clusters. The applicability of this approximation will be discussed in Section 6. The Hamiltonian for a dimeric unit AB including isotropic exchange and Zeeman interaction is given as follows:

$$\hat{V} = -2J\hat{\boldsymbol{s}}_A\hat{\boldsymbol{s}}_B - \beta H_Z \sum_i \left[g_e \hat{s}^i_Z - (3/2)\,\kappa\,\hat{l}^i_Z\right]. \tag{4.4}$$

Since the interactions involved in this Hamiltonian are magnetically isotropic, the Hamiltonian holds the same form providing any choice of Z-direction. Each single-ion spin and orbital operator in Equation (4.4) acts within the space comprising 12 wave-functions $\Phi(j, m_j)$, so the Hamiltonian operates in the basis of 12^N states (direct product of the one-site states), where N is the number of the constituent Co(II) ions.

The SO coupling stabilises the Kramers doublet that is separated from the first excited quartet state (the gap is of the order of 300–400 cm^{-1}). This splitting significantly exceeds Zeeman splitting and, in many cases, it also exceeds the splitting caused by the magnetic exchange. For these cases, this makes it possible to consider that the low-lying energy levels of two exchange coupled Co(II) ions are a result of the interaction between two Kramers doublets, as shown in Figure 10, and describe this interaction by a pseudo-spin-1/2-Hamiltonian. The full Hamiltonian $\hat{H}$ can be represented as a sum of the zero-order term $\hat{H}_0 = \hat{H}_{SO}$ and the term $\hat{V}$ (Equation (4.4)) playing a role of perturbation. For the further calculation, the matrices of spin and orbital angular momentum operators $\hat{s}_{Xi}, \hat{s}_{Yi}, \hat{s}_{Zi}$, $\hat{l}_{Xi}, \hat{l}_{Yi}, \hat{l}_{Zi}$ are to be evaluated in the basis $\Phi_i(1/2, 1/2)$, $\Phi_i(1/2, -1/2)$. One can find the following interrelations between the operators $\hat{\boldsymbol{s}}_i$, $\hat{\boldsymbol{l}}_i$ defined in the Kramers-doublet basis and the spin-1/2 operators $\hat{\boldsymbol{\tau}}_i$:

$$\hat{\boldsymbol{s}}_i = (5/3)\hat{\boldsymbol{\tau}}_i, \quad \hat{\boldsymbol{l}}_i = -(2/3)\hat{\boldsymbol{\tau}}_i, \tag{4.5}$$

where $\hat{\tau}_\alpha$ ($\alpha = X, Y, Z$) are related to the Pauli matrices $\hat{\sigma}_\alpha$, as usually $\hat{\tau}_\alpha = (1/2)\,\hat{\sigma}_\alpha$. This allows us to define the first-order effective pseudo-spin-1/2 Hamiltonian operating within the restricted basis of the direct product of Kramers doublets states

$$\hat{H}_{\text{eff}}^{(1)} = -(50/9)J\sum_{i<k}\hat{\boldsymbol{\tau}}_i\hat{\boldsymbol{\tau}}_k + g_0\beta H_Z\sum_i\hat{\tau}_Z^i \tag{4.6}$$

In Equation (3.6), the value

$$g_0 = (1/3)(5g_e + 3\kappa) \tag{4.7}$$

represents the effective g factor for a Kramers doublet.

Lines has mentioned that the Hamiltonian $\hat{H}_{\text{eff}}^{(1)}$ does not provide a satisfactory description of the magnetic properties of Co(II) clusters (even at low temperatures), because it ignores the mixture of the ground states with the excited ones by the exchange and Zeeman interactions. According to his idea, these excited states can be taken into account in an effective field approximation. In the framework of such hybrid theory the exchange interaction was included as a molecular field in the excited single-ion levels, but treated exactly within the ground Kramers doublet states. In this way, Lines has demonstrated how in the effective field approximation the problem of interacting Co(II) ions can be reduced to that of sets of independent fictitious spins, $\tau_i = 1/2$, each with a temperature-dependent g factor $g(T)$. Then the hitherto neglected ground doublet matrix elements of exchange (first term in Equation (4.6)) have been reintroduced into the problem exactly, leading to the resulting cluster Hamiltonian of the form

$$\hat{H}_{\text{eff}} = -(50/9)J\sum_{i<k}\hat{\boldsymbol{\tau}}_i\hat{\boldsymbol{\tau}}_k + g(T)\beta H_Z\sum_i\hat{\tau}_Z^i. \tag{4.8}$$

This Hamiltonian is of the same form as $\hat{H}_{\text{eff}}^{(1)}$, but with g_0 replaced with $g(T)$. As distinguished from the initial Hamiltonian, Equation (4.4), the effective Lines Hamiltonian, Equation (4.8), acts within the restricted space involving ground Kramers doublet states.

4.2. *Pseudo-spin-1/2 Hamiltonian for an exchange-coupled Co(II) pair*

4.2.1. *Brief overview of the existing theories*

The conventional Lines theory deals with the Co(II) ions in a perfect octahedral ligand fields, and hence no magnetic anisotropy is imposed. Let us focus on a more general situation when the symmetry of the positions occupied by Co(II) ions is lower than the cubic one. In this case, the interplay between the SO coupling and the low-symmetry crystal field gives rise to a single-ion anisotropy, this is well studied for Co(II) monomeric compounds (see [5] and references therein). The Lines model generalised to the case of anisotropic orbitally degenerate ions was successfully used for the description of the magnetic behaviour of different clusters containing Co(II) ions [137–140] and other transition metal ions [115,116] with unquenched orbital angular momenta. In these works, instead of the use of the effective field approximation, the direct diagonalisation of the full matrix including SO coupling, low-symmetry crystal field, magnetic exchange and Zeeman interactions was performed. This procedure was significantly simplified by the use of the ITO techniques, the details of this method can be found in many textbooks (see, e.g. [4,14,15,141,142]).

Another kind of theoretical treatment that is widely employed [101,106–112] for the analysis of INS spectra and magnetic properties of Co(II) complexes and extended systems is based on the use of the effective Hamiltonian describing the interaction between the low-lying Kramers doublets. Such pseudo-spin-1/2-formalism is applicable for the description of the magnetic data at low temperatures when only the ground Kramers doublets of the Co(II) ions are populated. There are two different approaches dealing with this formalism, namely, the phenomenological and the microscopic. The main advantage of the phenomenological approach is its simplicity that is a consequence of the fact that the effective pseudo-spin-1/2 Hamiltonian is constructed with the aid of symmetry arguments only. The main disadvantage is a large number of unknown parameters, namely, the components of *J*- and *g*-tensors and the parameters describing temperature-independent paramagnetic (TIP) contribution [143]. On the contrary, the microscopic approach being more complicated allows to find a relationship between the set of phenomenological parameters and the inherent parameters of the system.

4.2.2. *Phenomenological Hamiltonian: inelastic neutron scattering studies of polyoxometalates encapsulating Co(II) clusters*

The usage of the phenomenological pseudo-spin-1/2 Hamiltonian for the description of the low temperature dependence of the magnetic susceptibility often gives a multitude of the sets of the best fit parameters. Without additional independent information about the energy levels, neither the adequacy of a model nor the correctness of these parameters can be tested. From this point of view, the use of spectroscopic techniques providing a direct access to the energy splittings seems to be quite useful.

In a series of recent works [106–112], the INS technique was applied to the study of the magnetic exchange in dimeric, trimeric and tetrameric Co(II) units. The first example of this kind represents the Keggin derivative $K_8[Co_2(D_2O)(W_{11}O_{39})]\cdot nD_2O$ [106]. Encapsulation of two Co(II) ions in the Keggin structure leads to the dimer shown in black in Figure 11. The two Co(II) ions in this complex are inequivalent. The divalent high-spin octahedral cobalt ion has a $^4T_1$ ground state split into six Kramers doublets by the SO coupling and the low-symmetry crystal field, with only the ground Kramers doublet being significantly populated in the temperature range of 1.5–30 K. This gound Kramers doublet can be described by the effective spin $j_1 = 1/2$. The divalent cobalt ion in the tetrahedral environment has a ground orbital singlet $^4A_2$; that is, this state possesses only spin ($s_2 = 3/2$).

The effective Hamiltonian describing the exchange interaction between two Co(II) ions in the Kramers doublet states can be written as

$$\hat{H}_{\mathrm{ex}} = -2J\left[\hat{\tau}_Z^1\hat{s}_Z^2 + \eta\left(\hat{\tau}_X^1\hat{s}_X^2 + \hat{\tau}_Y^1\hat{s}_Y^2\right)\right]. \tag{4.9}$$

Provided $\eta \neq 1$, only M_J (but not J) is a good quantum number and the eigenvectors of the Hamiltonian, Equation (4.9), are given by the following linear combinations:

$$\psi_n(M_J) = \sum_J a_n(J, M_J)\left|j_1, s_2, J, M_J\right\rangle, \tag{4.10}$$

where index n is introduced to distinguish different states with the same M_J value.

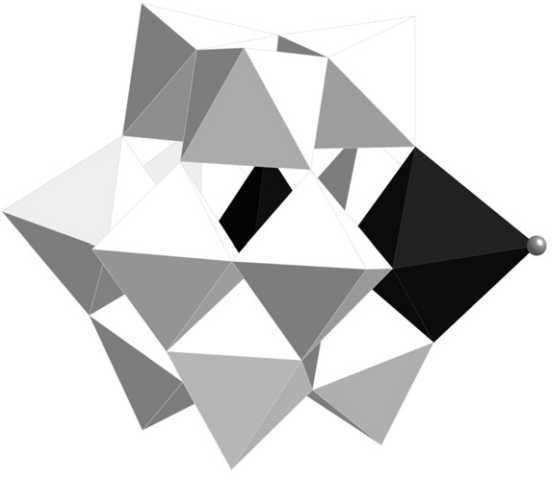

Figure 11. The structure of the $K_8[Co_2(D_2O)(W_{11}O_{39})]$ complex. The black polyhedra contains an oxo-coordinated Co(II) ions, and the white octahedra contains an oxo-coordinated W atoms.

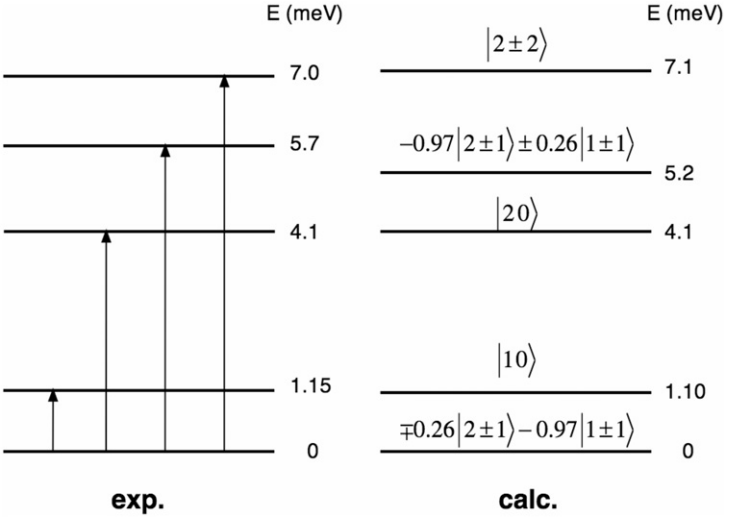

Figure 12. Experimentally determined energy pattern $K_8[Co_2(D_2O)(W_{11}O_{39})]$ complex (left) and that calculated with the best-fit parameters $J = -2.24\,\text{meV}$, $\eta = 0.33$ (right). The observed cold transitions and the calculated wave-functions are shown.

The details of the calculation of neutron cross-section are given in [142], in which the relative INS intensities for all allowed $|\psi_n(M_J)\rangle \rightarrow |\psi_{n'}(M'_J)\rangle$ transitions have been calculated. The analysis of the INS spectra provides the energy-level diagram shown in the left-side part of Figure 12. The best-fit parameters are: $J = -2.24\,\text{meV}$, $\eta = 0.33$. The value of the anisotropy parameter $\eta = 0.33$ indicates that the situation is intermediate

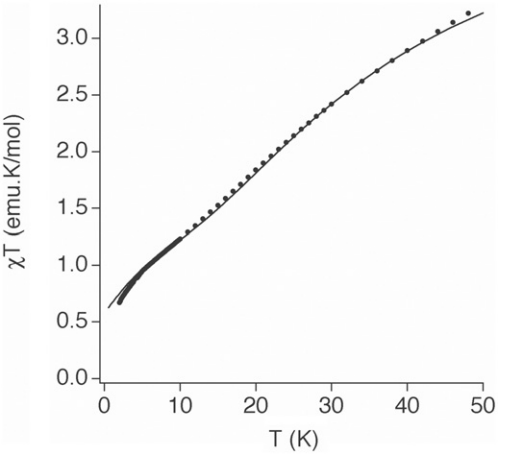

Figure 13. Measured magnetic susceptibility of a polycrystalline sample between 2 and 50 K (full circles) and χT vs. T curve calculated with the set of parameters: $J = -2.24$ meV, $\eta = 0.33$, $g_{\perp} = 2.3$, $g_{||} = 7.0$ (solid line).

between the Heisenberg ($\eta = 1$) and the Ising ($\eta = 0$) limits, and it is more close to the Ising one. The right-hand side of Figure 12 shows the energy levels and corresponding wave-functions calculated with this set of parameters. The obtained wave-functions were used to compute the relative intensities of the observed transitions. The obtained best-fit parameters were further used to calculate the temperature dependence of the magnetic susceptibility. In this calculation, the g value for the tetrahedral Co(II) ion was assumed to be equal to 2, because the octahedral site the ratio $\eta = g_{\perp}/g_{||}$ was fixed and $g_{\perp}$ was the only adjustable parameter. The best-fit to the experimental χT versus T curve was achieved for $g_{\perp} = 2.3$ that corresponds to $g_{||} = 7.0$. The χT versus T curve calculated with this set of parameters is in a perfect agreement with the experimental data (Figure 13). The obtained $g_{||}$ and $g_{\perp}$ are reasonable g-values for a Co(II) site with slightly distorted octahedral coordination [143].

Later on, the exchange interaction in the cobalt tetramer $[Co_4(D_2O)_2(PW_9O_{34})_2]^{10-}$ was studied with the aid of INS technique combined with the analysis of thermodynamic properties including specific heat and magnetic susceptibility [109]. The structure of this compound is shown in Figure 14. It represents a tetrameric rhomb-like centrosymmetrical cluster Co_4O_{16} of D_{2h} symmetry formed by four coplanar edge-sharing CoO_6 octahedra. The following effective pseudo-spin-1/2 exchange Hamiltonian was used to describe the pattern of low-lying energy levels:

$$\hat{H}_{\mathrm{ex}} = -2 \sum_{\alpha = X,\, Y,\, Z} \left[J_{\alpha} \left(\hat{\tau}_{\alpha}^{1} \hat{\tau}_{\alpha}^{3} + \hat{\tau}_{\alpha}^{1} \hat{\tau}_{\alpha}^{4} + \hat{\tau}_{\alpha}^{2} \hat{\tau}_{\alpha}^{3} + \hat{\tau}_{\alpha}^{2} \hat{\tau}_{\alpha}^{4} \right) + J'_{\alpha}\ \hat{\tau}_{\alpha}^{1} \hat{\tau}_{\alpha}^{2} \right]. \tag{4.11}$$

In Equation (4.11) the two dominant exchange pathways J and J' correspond to the interactions along the edges and the short diagonal of the rhomb, respectively, while the interactions along the long diagonal is neglected (Figure 14). The analysis of the INS spectra led us to the following set of parameters: $J_Z = 1.51$ meV, $J_X = 0.70$ meV,

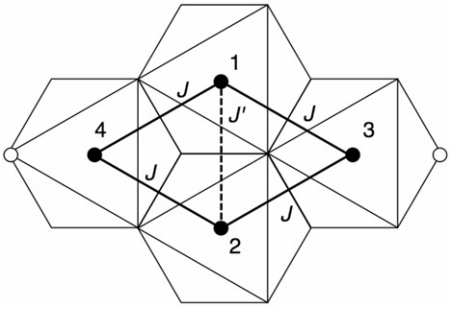

Figure 14. The structure of Co_4O_{16} cluster and the network of the exchange parameters.

$J'_Z = 0.46$ meV, $J'_X = 0.44$ meV, $r = J_X/J_Y = J'_X/J'_Y = 1.6$. Both interactions turned out to be ferromagnetic and anisotropic with $J_Z > J_X, J_Y$ and $J'_Z > J'_X, J'_Y$. This set of parameters allows to reproduce the observed temperature dependence of the magnetic heat capacity and also the experimental χT versus T curve (see [109] for more detail).

The INS technique was also used for the study of the exchange interactions in a more complex pentameric Co(II) cluster $[Co_3W(D_2O)_2(CoW_9O_{34})_2]^{12-}$, which contains three octahedral and two tetrahedral oxo-coordinated Co(II) ions [110]. This study revealed two kinds of highly anisotropic exchange interactions in this compound: a ferromagnetic interaction between the octahedral Co(II) ions and an antiferromagnetic interaction between the octahedral and the tetrahedral Co(II) ions. The set of parameters of the effective pseudo-spin-1/2 Hamiltonian derived from the analysis of INS spectra was shown to reproduce, in a satisfactory manner, the susceptibility, magnetisation and INS properties of the compound.

Finally, we should mention the INS investigations of two trimeric Co(II) clusters: $[Co_3W(D_2O)_2(ZnW_9O_{34})_2]^{12-}$ [111] and $[(NaOH_2)Co_3(D_2O)(P_2W_{15}O_{56})_2]^{17-}$ [112]. In these considerations different orientations of anisotropic exchange tensors were taken into account, which were correlated with the molecular symmetries of the complexes.

Summarising, one can conclude that the INS technique proved to be an efficient tool for the determination of the parameters of the phenomenological pseudo-spin-1/2 Hamiltonian.

4.2.3. *Microscopic approach to the pseudo-spin-1/2 Hamiltonian: discussion of the magnetic anisotropy*

Recently [114], the microscopic Lines model has been generalised to the case of anisotropic Co(II) ions. The system under study represents a pair of the Co(II) ions (A and B) occupying identical octahedral positions, with the local coordinate frames associated with the sites A and B being coplanar.

First, let us consider the case when the octahedral ligand surroundings of Co(II) ions are slightly distorted so that the SO coupling significantly exceeds the low-symmetry crystal field. We also assume that the SO coupling is strong as compared to the exchange interaction. Under these conditions, the full Hamiltonian of the pair can be

split into the non-perturbed SO coupling Hamiltonian $\hat{H}_0$ and the perturbation $\hat{V}$ that includes exchange, Zeeman interactions and low-symmetry crystal field (axial and rhombic):

$$\hat{V} = -2J\hat{\boldsymbol{s}}_A\hat{\boldsymbol{s}}_B + \sum_{i=A,B}\left\{\Delta\left[\left(\hat{l}_Z^i\right)^2 - 2/3\right] + \Delta'\left[\left(\hat{l}_X^i\right)^2 - \left(\hat{l}_Y^i\right)^2\right] + \beta\boldsymbol{H}\left[-(3/2)\kappa\hat{\boldsymbol{l}}_i + g_e\hat{\boldsymbol{s}}_i\right]\right\}, \tag{4.12}$$

where Δ and Δ' are the axial and rhombic crystal field splitting parameters, respectively. The isotropic Heisenberg form of the exchange interaction between the true spins 3/2 is assumed. The Hamiltonian $\hat{H} = \hat{H}_0 + \hat{V}$ operates within the total space

$$\Psi_{j_Aj_B}(m_{jA}m_{jB}) \equiv \Phi_A(j_Am_{jA})\Phi_B(j_Bm_{jB}). \tag{4.13}$$

In order to pass to the effective pseudo-spin-1/2-Hamiltonian, one can apply the second-order perturbation theory. The result for the first-order pseudo-spin-1/2 Hamiltonian is given by Equation (4.6). The presence of the low-symmetry crystal field terms in $\hat{V}$ does not affect this result because the Kramers degeneracy cannot be removed by the crystal field. As a result, the first-order Hamiltonian remains fully isotropic. The second-order term involves the mixing of the ground Kramers doublet space with the excited states and can be defined as

$$\begin{aligned}\left\langle\Psi_{\frac{11}{22}}\left(m'_{jA},m'_{jB}\right)\middle|\hat{H}^{(2)}_{\text{eff}}\middle|\Psi_{\frac{11}{22}}(m_{jA},m_{jB})\right\rangle \\ = -\sum_{j_Aj_B}\frac{1}{\Delta_{j_Aj_B}}\sum_{m''_{jA}m''_{jB}}\left\langle\Psi_{\frac{11}{22}}\left(m'_{jA},m'_{jB}\right)\middle|\hat{V}\middle|\Psi_{j_Aj_B}\left(m''_{jA},m''_{jB}\right)\right\rangle \\ \times\left\langle\Psi_{\frac{11}{22}}(m_{jA},m_{jB})\middle|\hat{V}\middle|\Psi_{j_Aj_B}\left(m''_{jA},m''_{jB}\right)\right\rangle^*,\end{aligned} \tag{4.14}$$

where $\Delta_{j_Aj_B} \equiv E_{j_Aj_B} - E_{1/2\,1/2}$ are the energy gaps between the unperturbed ground and excited levels. By expressing the matrix $\hat{H}^{(2)}_{\text{eff}}$ in terms of $\hat{\tau}^A_\alpha$ and $\hat{\tau}^B_\alpha$, we arrive at the following final expression for the effective pseudo-spin-1/2 Hamiltonian, which includes both $\hat{H}^{(1)}_{\text{eff}}$ and $\hat{H}^{(2)}_{\text{eff}}$:

$$\hat{H}_{\text{eff}} = \sum_{\alpha=X,Y,Z}\left[-2J_\alpha\hat{\tau}^A_\alpha\hat{\tau}^B_\alpha + g_\alpha\beta\left(\hat{\tau}^A_\alpha + \hat{\tau}^B_\alpha\right)H_\alpha - \Lambda_\alpha\beta^2\boldsymbol{H}^2_\alpha\right], \tag{4.15}$$

where H_α is the component of the magnetic field along the α-th direction. The effective exchange parameters involved in this Hamiltonian are given by

$$\begin{aligned}J_Z &= \frac{25}{9}J - \frac{40}{243\kappa\lambda}\left(15J^2 - 4J\Delta\right), \\ J_X &= \frac{25}{9}J - \frac{40}{243\kappa\lambda}\left[15J^2 + 2J\left(\Delta - 3\Delta'\right)\right], \\ J_Y &= \frac{25}{9}J - \frac{40}{243\kappa\lambda}\left[15J^2 + 2J\left(\Delta + 3\Delta'\right)\right],\end{aligned} \tag{4.16}$$

For the principle values of g-tensor, one can find the following expressions:

$$g_Z = g_0 - \frac{16}{243\kappa\lambda}(25J - 3\Delta)\left(\frac{3}{2}\kappa + g_e\right),$$

$$g_X = g_0 - \frac{8}{243\kappa\lambda}\left[50J + 3\left(\Delta - 3\Delta'\right)\right]\left(\frac{3}{2}\kappa + g_e\right), \tag{4.17}$$

$$g_Y = g_0 - \frac{8}{243\kappa\lambda}\left[50J + 3\left(\Delta + 3\Delta'\right)\right]\left(\frac{3}{2}\kappa + g_e\right).$$

Finally, the parameters describing the van Vleck paramagnetism (TIP) are the following:

$$\Lambda_X = \Lambda_Y = \Lambda_Z = -\frac{40}{81\,\kappa\,\lambda}\left(\frac{3}{2}\kappa + g_e\right)^2. \tag{4.18}$$

These equations provide the dependences of the parameters of the pseudo-spin-1/2 Hamiltonian on the basic parameters of the system. The mixing with the excited states results in the appearance of the new terms in the exchange parameters and the principal values of g-tensor. The additional terms in g containing Δ and Δ' arise, as usually, from the one-centre contributions and account for the anisotropy of the system. Provided $\Delta' = 0$, the magnetic anisotropy is axial, and the terms containing Δ' lead to the rhombic anisotropy. The second-order terms also contain magnetically isotropic contributions dependent on the ratio $J/\kappa\lambda$. These terms describe the influence of the bicentre interactions on g-factors. The results show a significant deviation of the molecular g-factors from those for the monomeric moieties. The anisotropy of the exchange parameters (in general, triaxial) appears due to the combined effect of the true isotropic exchange and low-symmetry crystal fields. These parameters also contain isotropic contributions. The second-order term contains the TIP contributions. In the adopted approximation, the TIP proves to be isotropic and independent of the parameters J, Δ and Δ'; it is simply twice the value for the octahedral monomeric unit. Note that the anisotropy of the effective pseudo-spin-1/2 exchange Hamiltonian is in fact the result of single-ion anisotropy rather than a consequence of the exchange anisotropy. The latter could appear only if the orbitally dependent terms are included in the initial exchange Hamiltonian. This will be discussed in Section 6.

Now let us consider another limit when the axial crystal field is strong as compared with the SO coupling and the exchange interaction [144,145]. In this case, the non-perturbed Hamiltonian $\hat{H}_0$ should include the axial components of the crystal field while all other interactions act as a perturbation $\hat{V}$. The axial field splits the cubic $^4T_1$ term of the Co(II) ion into the orbital singlet (state with orbital angular momentum projection $m_l = 0$) and the orbital doublet (state with $m_l = \pm 1$). Let us focus on the case of negative Δ when the ground state is the orbital doublet for which the orbital angular momentum remains unquenched. The SO coupling produces further splitting of these levels into the Kramers doublets. Assuming that the splitting caused by the axial field significantly exceeds the SO splitting and neglecting the SO mixing of the orbital doublet and the orbital singlet, we arrive at the scheme of the energy levels shown in Figure 15. The SO interaction takes an axial form with the only non-vanishing Z-component $\hat{H}_{SO}(s = 3/2, m_l = \pm 1) = -(3/2)\,\kappa\,\lambda\,\hat{l}_Z\,\hat{s}_Z$ within the ground orbital doublet, which leads to the splitting of this term into four equidistant

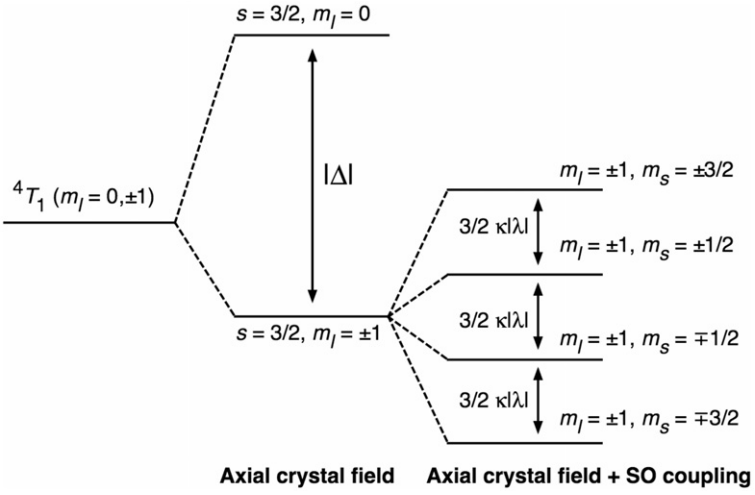

Figure 15. Splitting of the ground cubic $^4T_1(3d^7)$ term of the Co(II) ion by axial crystal field and SO coupling in the limit of a strong negative axial field (spin–orbital mixing of orbital singlet and orbital doublet is neglected).

Kramers doublets with the state based on $m_l = \pm 1, m_s = \mp 3/2$ being of the lowest energy. We will assume that the energy gap between the ground Kramers doublet with $m_l = \pm 1, m_s = \mp 3/2$ and the first excited one ($m_l = \pm 1$, $m_S = \mp 1/2$) exceeds the exchange splitting so that at low temperatures we can restrict ourselves by considering only the ground Kramers doublet for each Co ion. All matrix elements of the operators $\hat{s}_X^i$, $\hat{s}_Y^i$ are vanishing within the basis set of the ground Kramers doublet:

$$\begin{aligned} \langle m_l = \pm 1, m_s = \mp 3/2 | \hat{s}_X^i | m_l = \pm 1, m_s = \mp 3/2 \rangle = 0, \\ \langle m_l = \pm 1, m_s = \mp 3/2 | \hat{s}_Y^i | m_l = \mp 1, m_s = \pm 3/2 \rangle = 0, \end{aligned} \tag{4.19}$$

etc., and hence the Hamiltonian, Equation (3.12), dealing with the 'true' Co(II) spins (s = 3/2) is reduced to the Ising form of the pseudo-spin-1/2 Hamiltonian:

$$H_{\text{eff}} = -2J_{||}\hat{\tau}_Z^A\hat{\tau}_Z^B + g_{||}\beta\left(\hat{\tau}_Z^A + \hat{\tau}_Z^B\right)H_Z - \Lambda_\perp\left(H_X{}^2 + H_Y{}^2\right), \tag{4.20}$$

where the component of the ground Kramers doublet level with $m_l = -1, m_s = 3/2$ ($m_l = 1, m_s = -3/2$) corresponds to the projection $\sigma = 1/2$ ($\sigma = -1/2$) of the pseudo-spin-1/2.

$$J_{||} = 9J - \frac{3J^2}{\kappa|\lambda|}, \quad g_{||} = 3(g_e - \kappa), \quad \Lambda_\perp = \beta^2\left(\frac{g_e^2}{\kappa|\lambda|} + \frac{9\kappa^2}{4|\Delta| + 9\kappa|\lambda|}\right). \tag{4.21}$$

The pseudo-spin-1/2 basis is chosen in such a way that the component of the ground Kramers doublet level with $m_l = -1$, $m_s = 3/2$ ($m_l = 1, m_s = -3/2$) corresponds to the projection $\sigma = 1/2$ ($\sigma = -1/2$) of the pseudo-spin-1/2. The term proportional to J^2 in the expression of $J_{||}$ in Equation (4.21) represents the second-order correction arising from the mixing of the ground and excited manifolds of the cobalt pairs by the exchange

interaction. The TIP contribution $\Lambda_\perp$ in Equation (4.21) appears as a result of the Zeeman mixing of the ground Kramers doublet $|m_l = \pm 1, m_s = \mp 3/2\rangle$ with the three lowest excited states (Figure 15) and the highest orbital singlet. One can see that the system in the ground state is highly anisotropic and, in particular, first-order Zeeman splitting disappears in the perpendicular field. For this reason, the considered case can be referred to as axial or Ising limit.

The theory in its present form is not directly applicable to the case of moderate low-symmetry crystal field when the described perturbation schemes fail. In the last case both the low symmetry crystal field and the SO terms should be included into the zeroth-order Hamiltonian, while the perturbation will only involve the exchange and Zeeman terms. In this approximation the parameters of the effective Hamiltonian calculated up to the first-order prove to be dependent on the parameters Δ and Δ', the procedure for the case of axially distorted systems was outlined in [101]. At the same time, an important effect of the exchange mixing of spin–orbital multiplets was not discussed in [101]. The above-described approach is also restricted by the assumption that the local anisotropy axes for both interacting Co ions are parallel. Recently, a more general case of different orientations of the local anisotropy axes has been analysed and the microscopic derivation of the pseudo-spin-1/2 Hamiltonian for this case has been performed [146].

5. Orbitally dependent exchange: theoretical background

5.1. *Derivation of the orbitally dependent exchange Hamiltonian*

In Section 4, the exchange interaction between the ions possessing unquenched orbital angular momenta has been treated in the framework of the Lines model, that is, the HDVV spin Hamiltonian has been assumed. At the same time, this approximation has a restricted area of applicability and often a more general orbitally dependent exchange Hamiltonian is required. In this section the orbitally dependent kinetic exchange Hamiltonian [91–94] will be described along with its applications to the analysis of the magnetic anisotropy in clusters containing metal ions with unquenched orbital angular momenta.

The ions A and B are assumed to be in the crystal field states ${}^{2s_A+1}\Lambda_A$ and ${}^{2s_B+1}\Lambda_B$, where Λ_A, Λ_B stand for the irreducible representations of the local point groups of the ions and s_A, s_B are the local spins. One or both of these states are assumed to be orbitally degenerate. We will only consider the kinetic exchange interaction that dominates in most cases [84], thus neglecting the potential exchange contribution. According to Anderson's basic concept [84,85] (Section 2.1), the kinetic exchange Hamiltonian operating within the ${}^{2s_A+1}\Lambda_A \otimes {}^{2s_B+1}\Lambda_B$ manifold appears in the second order of perturbation theory when we start with the Hamiltonian

$$\hat{H} = \hat{H}_0 + \hat{V}_{AB}, \tag{5.1}$$

where $\hat{H}_0$ is the unperturbed Hamiltonian that includes local crystal field, intra-center inter-electronic interactions, and inter-centre Coulomb repulsion and $\hat{V}_{AB}$ is the operator of the inter-centre one-electron transfer (Hubbard Hamiltonian) that plays the role of the perturbation. The operator $\hat{V}_{AB}$ can be presented as follows:

$$\hat{V}_{AB} = \sum_{\Gamma_A\gamma_A} \sum_{\Gamma_B\gamma_B} t(\Gamma_A\gamma_A, \Gamma_B\gamma_B) \sum_{\sigma} \left(\hat{c}^{+}_{\Gamma_A\gamma_A\,\sigma} \hat{c}_{\Gamma_B\gamma_B\,\sigma} + \hat{c}^{+}_{\Gamma_B\gamma_B\,\sigma} \hat{c}_{\Gamma_A\gamma_A\,\sigma} \right), \tag{5.2}$$

where the operator $\hat{c}^{+}_{\Gamma_A\gamma_A\sigma}$ ($\hat{c}_{\Gamma_A\gamma_A\sigma}$) creates (destroys) the electron on the orbital $\varphi_{\Gamma_A\gamma_A}$ of the centre A with the spin projection σ, and $t(\Gamma_A\gamma_A, \Gamma_B\gamma_B)$ is the transfer integral. For example, for the important particular case of cubic local symmetry it is convenient to use a strong crystal field scheme, so the irreducible representations Γ_i ($i = A, B$) can be either t_2 or e. Since all transfer pathways $\Gamma_A\gamma_A \leftrightarrow \Gamma_B\gamma_B$ are taken into account in Equation (5.2), the present consideration is quite general and is not restricted to a particular overall symmetry of the system.

The eigenvectors of the Hamiltonian $\hat{H}_0$ belonging to the ${}^{2s_A+1}\Lambda_A\left(d_A^{n_A}\right) \otimes {}^{2s_B+1}\Lambda_B\left(d_B^{n_B}\right)$ manifold can be presented as the product of the one-centre states

$$|\nu_A s_A \Lambda_A m_A \lambda_A, \quad \nu_B s_B \Lambda_B m_B \lambda_B\rangle = |\nu_A s_A \Lambda_A m_A \lambda_A\rangle |\nu_B s_B \Lambda_B m_B \lambda_B\rangle,$$

where m_i ($i = A, B$) is the spin projection, λ_i enumerates the basis of the irreducible representation Λ_i and the symbol ν_i is introduced to specify a given ${}^{2s_i+1}\Lambda_i$ term in the case when several crystal field terms of the same symmetry exist. To find the one-centre wave functions within a strong crystal field scheme, one has to diagonalise the matrices of the intra-centre inter-electronic interaction [100]. As a result, they are represented by the following linear combination of the wave functions forming the many-electron strong crystal field basis:

$$|\nu_i s_i \Lambda_i m_i \lambda_i\rangle = \sum_{k_i} \langle k_i|\nu_i\rangle |d^{n_i}, k_i s_i \Lambda_i m_i \lambda_i\rangle, \tag{5.3}$$

where the symbol k_i indicates the different intermediate states resulting in the $s_i\,\Lambda_i(d^{n_i})$ term. Thus, for the case of cubic local symmetry k_i is defined as follows:

$$k_i \equiv t_2^{m_i}\left(s_i'\Lambda_i'\right)e^{n_i-m_i}\left(s_i''\Lambda_i''\right). \tag{5.4}$$

The operator $\hat{V}_{AB}$ mixes the ground electronic configuration $d_A^{n_A} - d_B^{n_B}$ with the excited CT configurations $d_A^{n_A-1} - d_B^{n_B+1}$ and $d_A^{n_A+1} - d_B^{n_B-1}$. The wave-functions for the CT configurations (the excited eigenvectors of the unperturbed Hamiltonian $\hat{H}_0$) can also be taken as the products of the wave functions of the reduced and oxidised configurations of the constituent ions. We denote the oxidised states of the ion i ($d_i^{n_i-1}$-configuration) by $|\bar{\nu}_i\,\bar{s}_i\,\bar{\Lambda}_i\,\bar{m}_i\,\bar{\lambda}_i\rangle$, and the reduced states ($d_i^{n_i+1}$-configuration) by $|\tilde{\nu}_i\,\tilde{s}_i\,\tilde{\Lambda}_i\,\tilde{m}_i\,\tilde{\lambda}_i\rangle$. The symbol $\bar{\nu}_i(\tilde{\nu}_i)$ is used to distinguish different cubic crystal field terms $\bar{s}_i\bar{\Lambda}_i(\tilde{s}_i\,\tilde{\Lambda}_i)$ of the same symmetry. The wave function of the oxidised crystal field state is given by

$$\left|\bar{\nu}_i\bar{s}_i\bar{\Lambda}_i\bar{m}_i\bar{\lambda}_i\right\rangle = \sum_{\bar{k}_i}\left\langle\bar{k}_i|\bar{\nu}_i\right\rangle\left|d^{n_i-1}, \bar{k}_i\bar{s}_i\bar{\Lambda}_i\bar{m}_i\bar{\lambda}_i\right\rangle, \tag{5.5}$$

and similar expression can be written down for the reduced state. For cubic local symmetry the symbol $\bar{k}_i$ is defined as follows:

$$\bar{k}_i \equiv t_2^{\bar{m}_i}\left(\bar{s}_i'\bar{\Lambda}_i'\right)e^{n_i-\bar{m}_i-1}\left(\bar{s}_i''\bar{\Lambda}_i''\right). \tag{5.6}$$

The coefficients $\langle\bar{k}_i|\bar{\nu}_i\rangle$ in Equation (5.5) form the eigenvectors of the matrices of the intra-centre Coulomb interaction for the $d_i^{n_i-1}$ ion.

The effective second-order Hamiltonian operating within the ${}^{2s_A+1}\Lambda_A(\nu_A) \otimes {}^{2s_B+1}\Lambda_B(\nu_B)$ manifold is the following:

$$\hat{H}^{(2)}(A,B) = -\sum_{\Gamma_A\Gamma_B\Gamma'_A\Gamma'_B}\sum_{\gamma_A\gamma_B\gamma'_A\gamma'_B} t(\Gamma_A\gamma_A,\Gamma_B\gamma_B)t(\Gamma'_B\gamma'_B,\Gamma'_A\gamma'_A) \times \sum_{\sigma\sigma'}\left[\sum_{\bar{\nu}_A\bar{s}_A\bar{\Lambda}_A}\sum_{\tilde{\nu}_B\tilde{s}_B\tilde{\Lambda}_B} \frac{\hat{c}^+_{\Gamma_A\gamma_A\,\sigma}\hat{G}(\bar{\nu}_A\bar{s}_A\bar{\Lambda}_A)\hat{c}_{\Gamma'_A\gamma'_A\sigma'}\hat{c}_{\Gamma_B\gamma_B\sigma}\hat{G}(\tilde{\nu}_B\tilde{s}_B\tilde{\Lambda}_B)\hat{c}^+_{\Gamma'_B\gamma'_B\sigma'}}{\varepsilon_{\bar{\nu}_A}(\bar{s}_A\bar{\Lambda}_A)+\varepsilon_{\tilde{\nu}_B}(\tilde{s}_B\tilde{\Lambda}_B)} + \sum_{\bar{\nu}_B\bar{s}_B\bar{\Lambda}_B}\sum_{\tilde{\nu}_A\tilde{s}_A\tilde{\Lambda}_A} \frac{\hat{c}^+_{\Gamma'_B\gamma'_B\,\sigma'}\hat{G}(\bar{\nu}_B\bar{s}_B\bar{\Lambda}_B)\hat{c}_{\Gamma_B\gamma_B\,\sigma}\hat{c}_{\Gamma'_A\gamma'_A\,\sigma'}\hat{G}\big(\tilde{\nu}_A\tilde{s}_A\tilde{\Lambda}_A\big)\hat{c}^+_{\Gamma_A\gamma_A\,\sigma}}{\varepsilon_{\bar{\nu}_B}(\bar{s}_B\bar{\Lambda}_B)+\varepsilon_{\tilde{\nu}_A}(\tilde{s}_A\tilde{\Lambda}_A)}\right]. \tag{5.7}$$

Here $\varepsilon_{\bar{\nu}_i}(\bar{s}_i\bar{\Lambda}_i)$ is defined as the difference between the energies of $\bar{\nu}_i\bar{s}_i\bar{\Lambda}_i(d_i^{n_i-1})$ and $\nu_i s_i\Lambda_i(d_i^{n_i})$ terms, and $\varepsilon_{\tilde{\nu}_i}(\tilde{s}_i\tilde{\Lambda}_i)$ represents the difference between the energies of $\tilde{\nu}_i\tilde{s}_i\tilde{\Lambda}_i$ $(d_i^{n_i+1})$ and $\nu_i s_i\Lambda_i(d_i^{n_i})$ terms. Finally, $\hat{G}(\bar{\nu}_i\bar{s}_i\bar{\Lambda}_i)$ and $\hat{G}(\tilde{\nu}_i\tilde{s}_i\tilde{\Lambda}_i)$ are the partial projection operators, for instance

$$\hat{G}\big(\bar{\nu}_i\bar{s}_i\bar{\Lambda}_i\big) = \sum_{\bar{m}_i\,\bar{\lambda}_i}\big|\bar{\nu}_i\bar{s}_i\bar{\Lambda}_i\,\bar{m}_i\bar{\lambda}_i\big\rangle\big\langle\bar{\nu}_i\bar{s}_i\bar{\Lambda}_i\bar{m}_i\bar{\lambda}_i\big|. \tag{5.8}$$

In the framework of the many-electron approach, the crystal field states of the ions in their normal, reduced and oxidised forms are determined with due account of all configuration interactions. This leads to the appearance of the complex multiplet structure of the energy patterns of d^{n_i} and $d^{n_i\pm1}$ ions implied by the Tanabe–Sugano diagrams [100]. In this respect, a significant difference between the present many-electron theory of the kinetic exchange and the conventional one-electron approach should be pointed out. This difference can be illustrated by considering the particular case of cubic local symmetry. Since in the one-electron approximation the configuration mixing is not taken into account, each $s_i\,\Lambda_i(d^{n_i})$ term originates from the only $t_2^{m_i}\,e^{n_i-m_i}$ configuration. As a result, the one-site operators $\hat{c}^+_{\Gamma_i\gamma_i\,\sigma}\hat{G}(\bar{\nu}_i\bar{s}_i\bar{\Lambda}_i)\hat{c}_{\Gamma'_i\gamma'_i\,\sigma'}$ and $\hat{c}_{\Gamma_i\gamma_i\,\sigma}\hat{G}(\tilde{\nu}_i\tilde{s}_i\tilde{\Lambda}_i)\hat{c}^+_{\Gamma'_i\gamma'_i\,\sigma'}$ should not change the number of electrons occupying t_2 and e orbitals. This requirement can be satisfied only provided that $\Gamma_i = \Gamma'_i$. Therefore in this approximation, the Hamiltonian, Equation (5.7), can only contain the products of the transfer integrals of the same kind, namely $t(t_2,t_2)t(t_2,t_2)$, $t(e,e)t(e,e)$ and $t(t_2,e)t(t_2,e)$. However, in the framework of the many-electron approach dealing with the configuration interactions, the one-site operator has non-vanishing matrix elements in $s_i\Lambda_i(d^{n_i})$ basis not only for $\Gamma_i = \Gamma'_i$ but also for $\Gamma_i \neq \Gamma'_i$. This means that along with the products of transfer integrals of the same kind, the products of different integrals like $t(t_2,t_2)t(e,e)$ can also contribute to the exchange Hamiltonian.

At the next step, let us pass from the second quantisation representation of the effective Hamiltonian to the exchange Hamiltonian expressed in terms of standard local orbital and spin operators. The creation operator $\hat{c}^+_{\Gamma_i\gamma_i\,\sigma}$ can be regarded as the double tensor operator [147] that acts as a spherical ITO of rank 1/2 in the spin subspace and as ITO of Γ_i type in the coordinate subspace, with two spin projections $\sigma = \pm1/2$ being the components of spherical tensor and γ_i being the components of the cubic tensor of Γ_i type. We will follow the conventionally accepted rule for the choice of phases of spherical ITOs,

$$\hat{c}_{\Gamma_i\gamma_i\,\sigma} = (-1)^{(1/2)-\sigma}\hat{c}^+_{\Gamma_i\gamma_i\,-\sigma}, \tag{5.9}$$

that is implied by the requirement of the Hermitian conjugation of the creation and annihilation operators and the fact that the one-electron basis is real (see the book by Varshalovich *et al*. [141]).

Since the partial projection operators $\hat{G}(\bar{\nu}_i\bar{s}_i\bar{\Lambda}_i)$ and $\hat{G}(\tilde{\nu}_i\tilde{s}_i\tilde{\Lambda}_i)$ are scalars in both coordinate and spin subspaces, the one-site operators $\hat{c}^{+}_{\Gamma_i\gamma_i\,\sigma}\hat{G}(\bar{\nu}_i\bar{s}_i\bar{\Lambda}_i)\hat{c}_{\Gamma'_i\gamma'_i\,\sigma'}$ and $\hat{c}_{\Gamma_i\gamma_i\,\sigma}\hat{G}(\tilde{\nu}_i\tilde{s}_i\tilde{\Lambda}_i)\hat{c}^{+}_{\Gamma'_i\gamma'_i\,\sigma'}$ represent the double tensor operators which are transformed as the direct product $\Gamma_i \otimes \Gamma'_i = \sum\Gamma$ in the coordinate subspace and as the direct product $D^{(1/2)} \otimes D^{(1/2)} = \sum_{k=0,1} D^{(k)}$ in the spin subspace. In general, these double tensor operators are reducible and they can be expressed in terms of ITOs $\hat{X}_{\Gamma\gamma k q}(\Gamma_i\,\Gamma'_i, \bar{\nu}_i\bar{s}_i\bar{\Lambda}_i)$ and $\hat{Y}_{\Gamma\gamma k q}(\Gamma_i\,\Gamma'_i, \tilde{\nu}_i\tilde{s}_i\tilde{\Lambda}_i)$ by means of the following unitary transformations:

$$\hat{c}^{+}_{\Gamma_i\gamma_i\sigma}\hat{G}(\bar{\nu}_i\bar{s}_i\bar{\Lambda}_i)\hat{c}_{\Gamma'_i\gamma'_i\sigma'} = (-1)^{(1/2)-\sigma'}\sum_{k\,q} C^{k\;\;q}_{1/2\sigma 1/2-\sigma'}\sum_{\Gamma\,\gamma}\left\langle\Gamma\gamma \mid \Gamma_i\gamma_i\Gamma'_i\gamma'_i\right\rangle\hat{X}_{\Gamma\gamma kq}(\Gamma_i\Gamma'_i, \bar{\nu}_i\bar{s}_i\bar{\Lambda}_i), \tag{5.10}$$

$$\hat{c}_{\Gamma_i\gamma_i\sigma}\hat{G}(\tilde{\nu}_i\tilde{s}_i\tilde{\Lambda}_i)\hat{c}^{+}_{\Gamma'_i\gamma'_i\sigma'} = (-1)^{(1/2)-\sigma}\sum_{k\,q} C^{k\;\;q}_{1/2-\sigma\;1/2\,\sigma'}\sum_{\Gamma\,\gamma}\left\langle\Gamma\gamma \mid \Gamma_i\gamma_i\Gamma'_i\gamma'_i\right\rangle\hat{Y}_{\Gamma\gamma kq}(\Gamma_i\Gamma'_i, \tilde{\nu}_i\tilde{s}_i\tilde{\Lambda}_i). \tag{5.11}$$

In Equations (5.10) and (5.11), the values $\langle\Gamma\gamma \mid \Gamma_i\gamma_i\Gamma'_i\gamma'_i\rangle$ are the Clebsch–Gordan coefficients for the local point group of the centre *i*. The reverse transformations are the following:

$$\hat{X}_{\Gamma\gamma kq}\left(\Gamma_i\Gamma'_i, \bar{\nu}_i\bar{s}_i\bar{\Lambda}_i\right) = \sqrt{(2k+1)/2}\sum_{\sigma\sigma'} C^{1/2\;\sigma}_{1/2\;\sigma'\;k\;q}\sum_{\gamma_i\,\gamma'_i}\left\langle\Gamma_i\;\gamma_i\;\Gamma'_i\gamma'_i \mid \Gamma\gamma\right\rangle\hat{c}^{+}_{\Gamma_i\gamma_i\sigma}\hat{G}\left(\bar{\nu}_i\bar{s}_i\bar{\Lambda}_i\right)\hat{c}_{\Gamma'_i\gamma'_i\sigma'}, \tag{5.12}$$

$$\begin{aligned}\hat{Y}_{\Gamma\gamma kq}\left(\Gamma_i\Gamma'_i, \tilde{\nu}_i\tilde{s}_i\tilde{\Lambda}_i\right) = (-1)^{k+1}\sqrt{(2k+1)/2}\sum_{\sigma\,\sigma'} C^{1/2\;\sigma'}_{1/2\;\sigma\;k\;q}\\ \times\sum_{\gamma_i\,\gamma'_i}\left\langle\Gamma_i\;\gamma_i\;\Gamma'_i\;\gamma'_i \mid \Gamma\gamma\right\rangle\hat{c}_{\Gamma_i\gamma_i\sigma}\hat{G}\left(\tilde{\nu}_i\tilde{s}_i\tilde{\Lambda}_i\right)\hat{c}^{+}_{\Gamma'_i\gamma'_i\sigma'}.\end{aligned} \tag{5.13}$$

In order to calculate the matrices of the operators $\hat{X}_{\Gamma\gamma k q}(\cdots)$ and $\hat{Y}_{\Gamma\gamma k q}(\cdots)$ within the basis of $\nu_i s_i \Lambda_i(d^n)$, one can apply the Wigner–Eckart theorem [100], for example,

$$\begin{aligned}\left\langle\nu_i s_i\Lambda_i m'_i\lambda'_i\right|\hat{X}_{\Gamma\gamma kq}\left(\Gamma_i\Gamma'_i, \bar{\nu}_i\bar{s}_i\bar{\Lambda}_i\right)\left|\nu_i s_i\Lambda_i m_i\lambda_i\right\rangle = [(2s_i+1)(\Lambda_i)]^{-1/2}\\ \times\left\langle\nu_i s_i\Lambda_i\right\|\hat{X}_{\Gamma k}\left(\Gamma_i\Gamma'_i, \bar{\nu}_i\bar{s}_i\bar{\Lambda}_i\right)\left\|\nu_i s_i\Lambda_i\right\rangle C^{s_i m'_i}_{s_i m_i kq}\left\langle\Lambda_i\lambda'_i \mid \Lambda_i\lambda_i\Gamma\gamma\right\rangle,\end{aligned} \tag{5.14}$$

where (Λ_i) is the dimension of the irreducible representation Λ_i and the notation $\langle\cdots\|\cdots\|\cdots\rangle$ is used for the reduced matrix element. This allows us to express the operators $\hat{X}_{\Gamma\gamma k q}(\cdots)$ and $\hat{Y}_{\Gamma\gamma k q}(\cdots)$ in terms of orbital operators $\hat{O}^{i}_{\Gamma\gamma}$ and spin operators $\hat{s}^{i}_{k\,q}$, for example,

$$\hat{X}_{\Gamma\gamma kq}\left(\Gamma_i\Gamma'_i, \bar{\nu}_i\bar{s}_i\bar{\Lambda}_i\right) = \frac{\left\langle\nu_i s_i\Lambda_i\right\|\hat{X}_{\Gamma k}\left(\Gamma_i\Gamma'_i, \bar{\nu}_i\bar{s}_i\bar{\Lambda}_i\right)\left\|\nu_i s_i\Lambda_i\right\rangle}{\left\langle s_i\right\|\hat{s}^{i}_{k}\left\|s_i\right\rangle\left\langle\Lambda_i\right\|\hat{O}^{i}_{\Gamma}\left\|\Lambda_i\right\rangle}\hat{O}^{i}_{\Gamma\gamma}\hat{s}^{i}_{kq}. \tag{5.15}$$

Here $\hat{O}^{i}_{\Gamma\gamma}$ is the irreducible tensor operator acting in the orbital $\Lambda_i\lambda_i$ manifold. This operator is defined in such a way that

$$\left\langle \Lambda_i \middle\| \hat{O}^{i}_{\Gamma} \middle\| \Lambda_i \right\rangle = (\Lambda_i)^{1/2}, \tag{5.16}$$

so that the matrix elements of this operator coincide with the Clebsch–Gordan coefficients

$$\langle \Lambda_i\lambda_i' | \hat{O}^{i}_{\Gamma\gamma} | \Lambda_i\lambda_i \rangle = \langle \Lambda_i\lambda_i' \mid \Lambda_i\lambda_i\Gamma\gamma \rangle. \tag{5.17}$$

In the case of the cubic symmetry of the ligand surrounding the centre i, $\hat{O}^{i}_{\Gamma\gamma}$ represents the cubic irreducible tensor. The operators $\hat{s}^{i}_{0\,0}$ and $\hat{s}^{i}_{1\,q}$ $(q = 0, \pm 1)$ act in the spin subspace $s_i\, m_i$ and represent the unit operator and the cyclic components of the spin operator, correspondingly. These cyclic components are defined as usually:

$$\hat{s}_{00} = \hat{s}_2,\ \hat{s}_{\pm 1} = \mp\frac{1}{\sqrt{2}}(\hat{s}_x \pm i\hat{s}_y).$$

Now we are in the position to pass from the Hamiltonian, Equation (5.7), expressed in terms of the creation and annihilation operators to the new representation of this Hamiltonian involving the orbital operators $\hat{O}^{i}_{\Gamma\gamma}$ and the one-site spin operators. One thus arrives at the following final formula for the effective exchange Hamiltonian:

$$\begin{aligned}\hat{H}_{\mathrm{ex}}(A,B) = -2 \sum_{\Gamma_A\Gamma_B\Gamma'_A\Gamma'_B} \sum_{\gamma_A\gamma_B\gamma'_A\gamma'_B} \sum_{\Gamma\gamma} \sum_{\Gamma'\gamma'} \langle \Gamma\gamma \mid \Gamma_A\gamma_A\Gamma'_A\gamma'_A \rangle \langle \Gamma'\gamma' \mid \Gamma_B\gamma_B\Gamma'_B\gamma'_B \rangle \hat{O}^{A}_{\Gamma\gamma} \hat{O}^{B}_{\Gamma'\gamma'} \\ \times t(\Gamma_A\gamma_A, \Gamma_B\gamma_B) t\left(\Gamma'_B\gamma'_B, \Gamma'_A\gamma'_A\right) \\ \times \left[F^{(0)}_{\Gamma\Gamma'}\left(\Gamma_A, \Gamma'_A, \Gamma_B, \Gamma'_B\right) + F^{(1)}_{\Gamma\Gamma'}\left(\Gamma_A, \Gamma'_A, \Gamma_B, \Gamma'_B\right) \hat{s}_A \hat{s}_B \right],\end{aligned} \tag{5.18}$$

where the parameters $F^{(0)}_{\Gamma\,\Gamma'}(\cdots)$ and $F^{(1)}_{\Gamma\,\Gamma'}(\cdots)$ are defined as follows:

$$\begin{aligned}F^{(k)}_{\Gamma\Gamma'}\left(\Gamma_A, \Gamma'_A, \Gamma_B, \Gamma'_B\right) = \frac{(-1)^{k+1}}{2\langle s_A \| \hat{s}^{A}_{k} \| s_A \rangle \langle s_B \| \hat{s}^{B}_{k} \| s_B \rangle \sqrt{(\Lambda_A)(\Lambda_B)}} \\ \times \left\{ \sum_{\bar{\nu}_A\bar{s}_A\bar{\Lambda}_A} \sum_{\tilde{\nu}_B\tilde{s}_B\tilde{\Lambda}_B} \left[\varepsilon_{\bar{\nu}_A}\left(\bar{s}_A\bar{\Lambda}_A\right) + \varepsilon_{\tilde{\nu}_B}\left(\tilde{s}_B\tilde{\Lambda}_B\right) \right]^{-1} \right. \\ \times \left\langle \nu_A s_A \Lambda_A \middle\| \hat{X}_{\Gamma k}\left(\Gamma_A\Gamma'_A, \bar{\nu}_A\bar{s}_A\bar{\Lambda}_A\right) \middle\| \nu_A s_A \Lambda_A \right\rangle \langle \nu_B s_B \Lambda_B \middle\| \hat{Y}_{\Gamma' k}\left(\Gamma_B\Gamma'_B, \tilde{\nu}_B\tilde{s}_B\tilde{\Lambda}_B\right) \middle\| \nu_B s_B \Lambda_B \right\rangle \\ + \sum_{\bar{\nu}_B\bar{s}_B\bar{\Lambda}_B} \sum_{\tilde{\nu}_A\tilde{s}_A\tilde{\Lambda}_A} \left[\varepsilon_{\bar{\nu}_B}\left(\bar{s}_B\bar{\Lambda}_B\right) + \varepsilon_{\tilde{\nu}_A}\left(\tilde{s}_A\tilde{\Lambda}_A\right) \right]^{-1} \\ \times \left. \left\langle \nu_B s_B \Lambda_B \middle\| \hat{X}_{\Gamma' k}\left(\Gamma_B\Gamma'_B, \bar{\nu}_B\bar{s}_B\bar{\Lambda}_B\right) \middle\| \nu_B s_B \Lambda_B \right\rangle \left\langle \nu_A s_A \Lambda_A \middle\| \hat{Y}_{\Gamma k}\left(\Gamma_A\Gamma'_A, \tilde{\nu}_A\tilde{s}_A\tilde{\Lambda}_A\right) \middle\| \nu_A s_A \Lambda_A \right\rangle \right\}.\end{aligned} \tag{5.19}$$

As distinguished from the HDVV Hamiltonian containing spin operators only, the effective Hamiltonian, Equation (5.18), operates in both spin and orbital spaces of the interacting orbitally degenerate ions. In fact, this Hamiltonian includes the orbital part (spin-independent) and the mixed part that contains both orbital and spin operators. The last part also contains the orbitally independent term $\propto \hat{\mathbf{s}}_A\,\hat{\mathbf{s}}_B$ as a particular contribution.

5.2. *How to use the developed formalism: an illustrative example*

In spite of the fact that the consideration of the orbitally-dependent exchange in a general form presented in Section 5.1 might look sophisticated, the application of the developed approach is rather simple. Let us illustrate the application of this formalism taking a corner shared bioctahedron (Figure 16) as an example, in which the local ligand octahedral surroundings of the metal ions are strongly stretched along the molecular C_4 axis (Z_A, Z_B axes are chosen to coincide with this C_4 axis) so that the local symmetry of each metal sites is approximately D_{4h} and the overall symmetry of the pair is D_{4h} as well. To demonstrate the procedure, we will focus on the simplest case of one-electron metal ions.

The tetragonal ligand field splits the cubic $^2T_2\left(t_2^1\right)$ term of each metal ion into the orbital doublet ^2E and the orbital singlet $^2B_2$, with the orbital doublet being the ground term in the case of the elongated octahedra. Since the tetragonal splitting is assumed to be large, it is reasonable to consider the $[^2E(e^1)]_A \otimes [^2E(e^1)]_B$-exchange problem neglecting the contributions from the excited $^2B_2$-state (Figure 16b). Substitution of the Clebsch–Gordan coefficients for the D_4 point group into Equation (5.18) gives the following expression for the exchange Hamiltonian:

$$\hat{H}_{\mathrm{ex}}(A,B) = \hat{R}_0 + \hat{R}_1 \hat{\boldsymbol{s}}_A \hat{\boldsymbol{s}}_B. \tag{5.20}$$

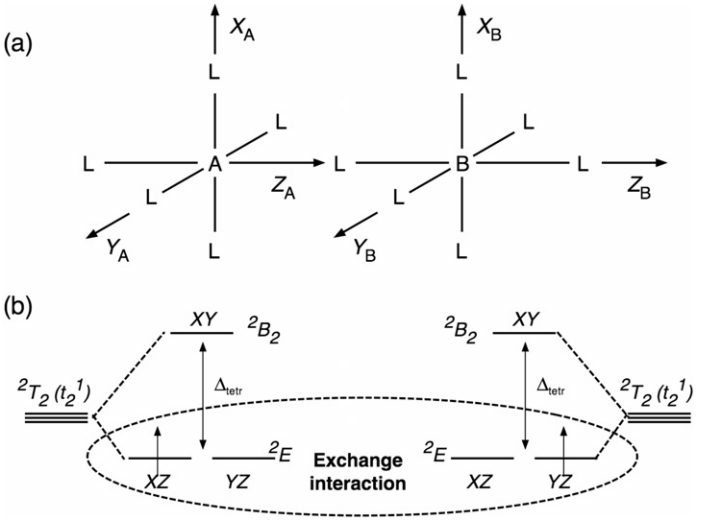

Figure 16. The illustration for the $[^2E(e^1)]_A \otimes [^2E(e^1)]_B$- exchange problem: (a) coordinate axes and (b) tetragonal splittings of local $^2T_2(t_2^1)$ terms and effective exchange coupling.

Here $\hat{R}_k$ ($k = 0, 1$) are the orbital operators defined by

$$\hat{R}_k = -2t_\pi^2\Big[F^{(k)}_{A_1A_1}\hat{O}^A_{A_1}\hat{O}^B_{A_1} + F^{(k)}_{B_1B_1}\hat{O}^A_{B_1}\hat{O}^B_{B_1} + F^{(k)}_{A_2A_2}\hat{O}^A_{A_2}\hat{O}^B_{A_2} + F^{(k)}_{B_2B_2}\hat{O}^A_{B_2}\hat{O}^B_{B_2}\Big], \tag{5.21}$$

and the short notation $F^{(k)}_{\Gamma\Gamma} \equiv F^{(k)}_{\Gamma\Gamma}(e,e,e,e)$ is introduced. The matrices $\hat{\mathbf{O}}_\Gamma$ defined in the tetragonal E-basis θ, ε ($\theta \propto YZ, \varepsilon \propto XZ$), can be expressed in terms of the Pauli matrices:

$$\begin{aligned} \hat{\boldsymbol{O}}_{A_1} &= \begin{pmatrix} 1 & 0 \\ 0 & 1 \end{pmatrix}, \quad \hat{\boldsymbol{O}}_{B_1} = \begin{pmatrix} 1 & 0 \\ 0 & -1 \end{pmatrix} = \hat{\sigma}_Z, \\ \hat{\boldsymbol{O}}_{B_2} &= \begin{pmatrix} 0 & 1 \\ 1 & 0 \end{pmatrix} = \hat{\sigma}_X, \quad \hat{\boldsymbol{O}}_{A_2} = \begin{pmatrix} 0 & 1 \\ -1 & 0 \end{pmatrix} = -i\hat{\sigma}_Y. \end{aligned} \tag{5.22}$$

The following two equivalent π-type transfer pathways are allowed by the tetragonal overall symmetry of the dimer: $\theta_A \leftrightarrow \theta_B$ and $\varepsilon_A \leftrightarrow \varepsilon_B$. The corresponding transfer parameter will be denoted as

$$t_{\theta\theta} = t_{\varepsilon\varepsilon} \equiv t_\pi. \tag{5.23}$$

These transfer processes mix the ground $[^2E(e^1)]_A \otimes [^2E(e^1)]_B$-manifold of the pair with different CT states corresponding to $e^0_A e^2_B$ and $e^2_A e^0_B$ configurations. The oxidised e^0-configuration gives rise to the only $\bar{s}\bar{\Lambda}$ vacuum one-centre state $\psi[^1A_1(e^0)]$. The one-centre $\tilde{s}\tilde{\Lambda}$-states for the reduced e^2-configuration and the energies of these states are given in Table 1. The mixing of the ground manifold with different CT states by the π-type transfer is shown in Figure 17, in which each ground and CT state is represented by the only Slater determinant (microstate).

To illustrate the procedure of the calculation of the reduced matrix elements of the operators $\hat{X}_{\Gamma\gamma kq}\big[ee, {}^1A_1(e^0)\big]$, we will consider in detail one selected reduced matrix element, let us say $\langle e\|\hat{X}_{B_21}\big[ee, {}^1A_1(e^0)\big]\|e\rangle$. Using the values of the Clebsch–Gordan coefficients $\langle E\theta E\varepsilon|B_2\rangle = \langle E\varepsilon E\theta \mid B_2\rangle = 1/\sqrt{2}$ and Wigner coefficient $C^{1/2\,1/2}_{1/2-1/2\,11} = -\sqrt{2/3}$, one finds that

$$\hat{X}_{B_211}\big[ee, {}^1A_1(e^0)\big] = -\frac{1}{\sqrt{2}}\Big\{\hat{c}^+_\theta\hat{G}[0]\hat{c}_{\bar{\varepsilon}} + \hat{c}^+_\varepsilon\hat{G}[0]\hat{c}_{\bar{\theta}}\Big\}. \tag{5.24}$$

In this equation $\hat{G}[0] = |0\rangle\langle 0|$ and a short notation $\big|{}^1A_1\big(e^0\big)\big\rangle \equiv |0\rangle$ for the vacuum state is used. Let us calculate the matrix element

$$\langle\theta|\hat{X}_{B_211}\big[ee, {}^1A_1(e^0)\big]|\bar{\varepsilon}\rangle = -\frac{1}{\sqrt{2}}\big(\langle\theta|\hat{c}^+_\theta|0\rangle\langle 0|c_{\bar{\varepsilon}}|\bar{\varepsilon}\rangle + \langle\theta|\hat{c}^+_\varepsilon|0\rangle\langle 0|\hat{c}_{\bar{\theta}}|\bar{\varepsilon}\rangle\big). \tag{5.25}$$

Since $\hat{c}^+_\varepsilon|0\rangle = |\varepsilon\rangle$, the matrix element vanishes, $\langle\theta|\,\hat{c}^+_\varepsilon|0\rangle = \langle\theta \mid \varepsilon\rangle = 0$, and hence the second term in the parentheses also vanishes. For the first term, one finds that $\langle\theta|\,\hat{c}^+_\theta|0\rangle\langle 0|\,\hat{c}_{\bar{\varepsilon}}\,|\bar{\varepsilon}\rangle = \langle\theta \mid \theta\rangle\ \langle 0 \mid 0\rangle = 1$.

Therefore

$$\langle\theta|\hat{X}_{B_211}\big[ee, {}^1A_1(e^0)\big]|\bar{\varepsilon}\rangle = -\frac{1}{\sqrt{2}}. \tag{5.26}$$

Table 1. The one-centre $\tilde{s}\tilde{\Lambda}$-states for the reduced e^2-configuration and corresponding energies (A, B and C are the Racah parameters).

$\tilde{s}\tilde{\Lambda}(e^2)$-states	Energies of the $\tilde{s}\tilde{\Lambda}(e^2)$-states
$\psi[^1A_1(e^2)] = \frac{1}{\sqrt{2}}\left(\lvert\theta\bar{\theta}\rvert + \lvert\varepsilon\bar{\varepsilon}\rvert\right)$,	$A + 7B + 4C$
$\psi[^1B_1(e^2)] = \frac{1}{\sqrt{2}}\left(\lvert\theta\bar{\theta}\rvert - \lvert\varepsilon\bar{\varepsilon}\rvert\right)$,	$A + B + 2C$
$\psi\left[^1B_2(e^2)\right] = \frac{1}{\sqrt{2}}\left(\lvert\theta\bar{\varepsilon}\rvert - \lvert\bar{\theta}\varepsilon\rvert\right)$,	$A + B + 2C$
$\psi\left[^3A_2(e^2),\ m = 1\right] = \lvert\theta\varepsilon\rvert$	$A - 5B$
$\psi\left[^3A_2(e^2), m = 0\right] = \frac{1}{\sqrt{2}}\left(\lvert\theta\bar{\varepsilon}\rvert + \lvert\bar{\theta}\varepsilon\rvert\right)$	
$\psi\left[^3A_2(e^2),\ m = -1\right] = \lvert\bar{\theta}\bar{\varepsilon}\rvert$	

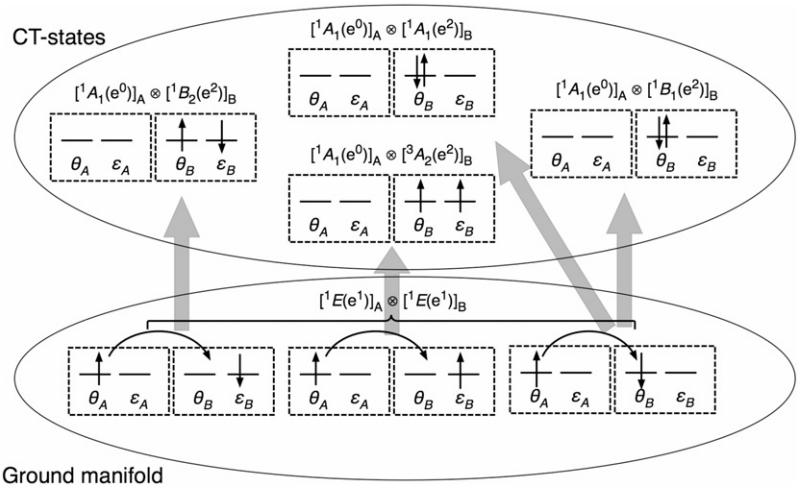

Figure 17. Different one-electron transfer processes and related CT states of $[^1E(e^1)]_A \otimes [^1E(e^1)]_B$-dimer (only the $A \rightarrow B$ transfer is shown).

On the other hand, applying the Wigner–Eckart theorem, Equation (5.14), to the double ITO $\hat{X}_{B_2\,11}[e\,e, {}^1A_1(e^0)]$ and taking into account that $\langle E\theta \mid E\varepsilon\ B_2\rangle = 1$, one can write

$$\langle\theta|\hat{X}_{B_2 11}\left[ee, {}^1A_1(e^0)\right]|\bar{\varepsilon}\rangle = -\frac{1}{\sqrt{6}}\langle e\|\hat{X}_{B_2 1}\left[ee, {}^1A_1(e^0)\right]\|e\rangle. \tag{5.27}$$

Then, by comparing Equations (4.26) and (4.27) one finds that

$$\langle e\|\hat{X}_{B_2 1}\left[ee, {}^1A_1(e^0)\right]\|e\rangle = \sqrt{3}. \tag{5.28}$$

All reduced matrix elements of the operators $\hat{X}_{\Gamma\gamma kq}[ee, {}^1A_1(e^0)]$ calculated in this way are collected in Table 2.

Table 2. Reduced matrix elements of the operators $\hat{X}_{\Gamma\gamma kq}\big[ee, {}^1A_1(e^0)\big]$.

Γ	$\langle e\|\hat{X}_{\Gamma 0}\big[ee, {}^1A_1(e^0)\big]\|e\rangle$	$\langle e\|\hat{X}_{\Gamma 1}\big[ee, {}^1A_1(e^0)\big]\|e\rangle$
A_1	1	$\sqrt{3}$
B_1	-1	$-\sqrt{3}$
A_2	1	$\sqrt{3}$
B_2	1	$\sqrt{3}$

Let us pass to the calculation of the reduced matrix elements of the operator $\hat{Y}_{\Gamma\gamma kq}(ee, \tilde{s}\tilde{\Lambda})$ taking the matrix element $\langle\varepsilon|\,\hat{Y}_{B_2\,1\,1}[\,e\,e, {}^3A_2(e^2)\,]|\bar{\theta}\rangle$ as an example. First, consider

$$\hat{Y}_{B_2 11}\big[ee, {}^3A_2(e^2)\big] = -\frac{1}{\sqrt{2}}\Big\{\hat{c}_{\bar{\theta}}\hat{G}\big[{}^3A_2(e^2)\big]\hat{c}^+_{\varepsilon} + \hat{c}_{\bar{\varepsilon}}\hat{G}\big[{}^3A_2(e^2)\big]\hat{c}^+_{\theta}\Big\}. \tag{5.29}$$

In this equation, the following notation is used:

$$\hat{G}\big[{}^3A_2(e^2)\big] = \sum_{\tilde{m}_s=0,\pm1} \big|{}^3A_2(e^2), m_s\big\rangle\big\langle{}^3A_2(e^2), m_s\big|.$$

Then the matrix element can be presented as a sum of two terms

$$\langle\varepsilon|\,\hat{Y}_{B_2 11}\big[ee, {}^3A_2(e^2)\big]\big|\bar{\theta}\big\rangle = a_1 + a_2, \tag{5.30}$$

where a_1 and a_2 are the following expressions:

$$\begin{aligned} a_1 &= -\frac{1}{\sqrt{2}}\sum_{m_s=0,\pm1}\langle\varepsilon|\hat{c}_{\bar{\theta}}\big|{}^3A_2(e^2), m_s\big\rangle\big\langle{}^3A_2(e^2), m_s\big|\hat{c}^+_{\varepsilon}\big|\bar{\theta}\big\rangle, \\ a_2 &= -\frac{1}{\sqrt{2}}\sum_{m_s}\langle\varepsilon|\hat{c}_{\bar{\varepsilon}}\big|{}^3A_2(e^2), m_s\big\rangle\big\langle{}^3A_2\big(e^2\big), m_s\big|\hat{c}^+_{\theta}\big|\bar{\theta}\big\rangle. \end{aligned} \tag{5.31}$$

One can see that $a_2 = 0$. This follows from the following equations:

$$\begin{aligned} &\big\langle\psi\big[{}^3A_2(e^2), m_s = 1\big]\big|\hat{c}^+_{\theta}\big|\bar{\theta}\big\rangle = \langle|\theta\varepsilon||\theta\bar{\theta}|\rangle = 0, \\ &\big\langle\psi\big[{}^3A_2(e^2), m_s = 0\big]\big|\hat{c}^+_{\theta}\big|\bar{\theta}\big\rangle = \Big\langle\frac{1}{\sqrt{2}}\big(|\theta\bar{\varepsilon}| + |\bar{\theta}\varepsilon|\big)\Big||\theta\bar{\theta}|\Big\rangle = 0, \\ &\big\langle\psi\big[{}^3A_2(e^2), m_s = -1\big]\big|\hat{c}^+_{\theta}\big|\bar{\theta}\big\rangle = \big\langle|\bar{\theta}\bar{\varepsilon}|\,|\,|\theta\bar{\theta}|\big\rangle = 0. \end{aligned} \tag{5.32}$$

To calculate a_1, one should take into account the following interrelations:

$$\begin{aligned} &\big\langle{}^3A_2(e^2), m_s = 1\big|\hat{c}^+_{\bar{\theta}}\,|\varepsilon\rangle = \big\langle|\theta\varepsilon|\;|\;|\bar{\theta}\varepsilon|\big\rangle = 0, \\ &\big\langle{}^3A_2(e^2), m_s = -1\big|\hat{c}^+_{\bar{\theta}}\,|\varepsilon\rangle = \big\langle|\bar{\theta}\bar{\varepsilon}|\;|\;|\bar{\theta}\varepsilon|\big\rangle = 0. \end{aligned} \tag{5.33}$$

For this reason, only the term with $m_s = 0$ contributes to a_1. Then one can apply the following relations:

$$\begin{aligned}
&\langle {}^3A_2(e^2), m_s = 0 | \hat{c}^+_{\bar{\theta}} | \varepsilon \rangle = \left\langle \frac{1}{\sqrt{2}} \left(|\theta\bar{\varepsilon}| + |\bar{\theta}\varepsilon| \right) \,\middle|\, |\bar{\theta}\varepsilon| \right\rangle = \frac{1}{\sqrt{2}}, \\
&\langle {}^3A_2(e^2), m_s = 0 | \hat{c}^+_{\varepsilon} | \bar{\theta} \rangle = \left\langle \frac{1}{\sqrt{2}} \left(|\theta\bar{\varepsilon}| + |\bar{\theta}\varepsilon| \right) \,\middle|\, |\varepsilon\bar{\theta}| \right\rangle = \left\langle \frac{1}{\sqrt{2}} \left(|\theta\bar{\varepsilon}| + |\bar{\theta}\varepsilon| \right) \,\middle|\, -|\bar{\theta}\varepsilon| \right\rangle = -\frac{1}{\sqrt{2}}.
\end{aligned} \tag{5.34}$$

Using these relations, one finds that

$$\begin{aligned}
\langle \varepsilon | \hat{Y}_{B_2 11} \left[ee, {}^3A_2(e^2) \right] | \bar{\theta} \rangle &= -\frac{1}{\sqrt{2}} \langle \varepsilon | \hat{c}_{\bar{\theta}} | {}^3A_2(e^2), m_s = 0 \rangle \langle {}^3A_2(e^2), m_s = 0 | \hat{c}^+_{\varepsilon} | \bar{\theta} \rangle \\
&= -\frac{1}{\sqrt{2}} \langle {}^3A_2(e^2), m_s = 0 | \hat{c}^+_{\bar{\theta}} | \varepsilon \rangle \langle {}^3A_2(e^2), m_s = 0 | \hat{c}^+_{\varepsilon} | \bar{\theta} \rangle = \frac{1}{2\sqrt{2}}.
\end{aligned} \tag{5.35}$$

Then applying the Wigner–Eckart theorem and taking into account that $\langle E\varepsilon | E\theta\ B_2 \rangle = 1$, one finds that

$$\langle \varepsilon | \hat{Y}_{B_2 11} \left[ee, {}^3A_2(e^2) \right] | \bar{\theta} \rangle = -\frac{1}{\sqrt{6}} \langle e \| \hat{Y}_{B_2 1} \left[ee, {}^3A_2(e^2) \right] \| e \rangle. \tag{5.36}$$

It follows from Equations. (5.35) and (5.36) that

$$\langle e \| \hat{Y}_{B_2 1} \left[ee, {}^3A_2(e^2) \right] \| e \rangle = -\sqrt{3}/2. \tag{5.37}$$

All reduced matrix elements of the operators $\hat{Y}_{\Gamma\gamma\, k\, q} \left[ee, \tilde{s}\tilde{\Lambda}(e^2) \right]$, calculated as described above, are given in Table 3.

Using the reduced matrix elements $\langle e \| \hat{X}_{\Gamma k} [ee, {}^1A_1(e^0)] \| e \rangle$ and $\langle e \| \hat{Y}_{\Gamma k} [ee, \tilde{s}\tilde{\Lambda}(e^2)] \| e \rangle$, we obtain the following expressions for the parameters of the Hamiltonian:

$$\begin{aligned}
F^{(0)}_{A_1 A_1} &= \frac{1}{8\varepsilon[{}^1A_1(e^2)]} + \frac{1}{8\varepsilon[{}^1B_1(e^2)]} + \frac{1}{8\varepsilon[{}^1B_2(e^2)]} + \frac{3}{8\varepsilon[{}^3A_2(e^2)]}, \\
F^{(0)}_{B_1 B_1} &= \frac{1}{8\varepsilon[{}^1A_1(e^2)]} + \frac{1}{8\varepsilon[{}^1B_1(e^2)]} - \frac{1}{8\varepsilon[{}^1B_2(e^2)]} - \frac{3}{8\varepsilon[{}^3A_2(e^2)]}, \\
F^{(0)}_{A_2 A_2} &= \frac{1}{8\varepsilon[{}^1A_1(e^2)]} - \frac{1}{8\varepsilon[{}^1B_1(e^2)]} - \frac{1}{8\varepsilon[{}^1B_2(e^2)]} + \frac{3}{8\varepsilon[{}^3A_2(e^2)]}, \\
F^{(0)}_{B_2 B_2} &= \frac{1}{8\varepsilon[{}^1A_1(e^2)]} - \frac{1}{8\varepsilon[{}^1B_1(e^2)]} + \frac{1}{8\varepsilon[{}^1B_2(e^2)]} - \frac{3}{8\varepsilon[{}^3A_2(e^2)]}, \\
F^{(1)}_{A_1 A_1} &= -\frac{1}{2\varepsilon[{}^1A_1(e^2)]} - \frac{1}{2\varepsilon[{}^1B_1(e^2)]} - \frac{1}{2\varepsilon[{}^1B_2(e^2)]} + \frac{1}{2\varepsilon[{}^3A_2(e^2)]},
\end{aligned}$$

Table 3. Reduced matrix elements of the operators $\hat{Y}_{\Gamma\gamma kq}\left[ee, \tilde{s}\tilde{\Lambda}(e^2)\right]$.

$\tilde{s}\tilde{\Lambda}(e^2)$	Γ	$\langle e \Vert \hat{Y}_{\Gamma 0}\left[ee, \tilde{s}\tilde{\Lambda}(e^2)\right] \Vert e\rangle$	$\langle e \Vert \hat{Y}_{\Gamma 1}\left[e\,e,\ \tilde{s}\tilde{\Lambda}(e^2)\right] \Vert e\rangle$
$^1A_1$	A_1	$-1/2$	$-\sqrt{3}/2$
	B_1	$1/2$	$\sqrt{3}/2$
	A_2	$-1/2$	$-\sqrt{3}/2$
	B_2	$-1/2$	$-\sqrt{3}/2$
$^1B_1$	A_1	$-1/2$	$-\sqrt{3}/2$
	B_1	$1/2$	$\sqrt{3}/2$
	A_2	$1/2$	$\sqrt{3}/2$
	B_2	$1/2$	$\sqrt{3}/2$
$^1B_2$	A_1	$-1/2$	$-\sqrt{3}/2$
	B_1	$-1/2$	$-\sqrt{3}/2$
	A_2	$1/2$	$\sqrt{3}/2$
	B_2	$-1/2$	$-\sqrt{3}/2$
$^3A_2$	A_1	$-3/2$	$\sqrt{3}/2$
	B_1	$-3/2$	$\sqrt{3}/2$
	A_2	$-3/2$	$\sqrt{3}/2$
	B_2	$3/2$	$-\sqrt{3}/2$

$$
\begin{aligned}
F^{(1)}_{B_1B_1} &= -\frac{1}{2\varepsilon[^1A_1(e^2)]} - \frac{1}{2\varepsilon[^1B_1(e^2)]} + \frac{1}{2\varepsilon[^1B_2(e^2)]} - \frac{1}{2\varepsilon[^3A_2(e^2)]},\\
F^{(1)}_{A_2A_2} &= -\frac{1}{2\varepsilon[^1A_1(e^2)]} + \frac{1}{2\varepsilon[^1B_1(e^2)]} + \frac{1}{2\varepsilon[^1B_2(e^2)]} + \frac{1}{2\varepsilon[^3A_2(e^2)]},\\
F^{(1)}_{B_2B_2} &= -\frac{1}{2\varepsilon[^1A_1(e^2)]} + \frac{1}{2\varepsilon[^1B_1(e^2)]} - \frac{1}{2\varepsilon[^1B_2(e^2)]} - \frac{1}{2\varepsilon[^3A_2(e^2)]}.
\end{aligned}
\tag{5.38}
$$

These expressions are directly related to the crystal field parameters through the energies listed in Table 1. Now it is convenient to pass from the initial bicentre orbital basis $\theta_A\theta_B$, $\theta_A\varepsilon_B$, $\varepsilon_A\theta_B$ and $\varepsilon_A\varepsilon_B$, to the symmetry adapted orbital basis. Such symmetry-adapted orbital basis and related terms of the $^2E(e^1)$–$^2E(e^1)$ system are given in Table 4. The true symmetry adapted wave-functions with $S = 1$ and $M_S = 1$ are formally obtained from the states given in Table 4 by replacing each product $\varphi_A\,\psi_B$ $(\varphi, \psi = \theta, \varepsilon)$ with the Slater determinant $|\varphi_A\,\psi_B|$, whereas the states with $S = 0$ are obtained using the substitution $\varphi_A\,\psi_B \rightarrow (1/\sqrt{2})(|\varphi_A\,\bar{\psi}_B| - |\bar{\varphi}_A\,\psi_B|)$. In the symmetry-adapted basis constructed as the product of the symmetry-adapted orbital basis and spin basis $|S\,M_S\rangle$, the matrix of the Hamiltonian, Equation (4.20), is diagonal, its eigenvalues are collected in Table 5.

The spin-independent part of the exchange Hamiltonian $\hat{R}_0$ gives rise to four multiplets degenerate with respect to the value of the total spin. The spin-dependent part $\hat{R}_1\,\hat{\boldsymbol{s}}_A\hat{\boldsymbol{s}}_B$ splits each multiplet into spin-singlet $(S = 0)$ and spin-triplet $(S = 1)$, this splitting obeys the Lande's rule. The overall energy pattern represents a result of the overlapping of different Lande's schemes and thus proves to be essentially non-Heisenberg. Figure 18 shows the energy pattern of the orbitally dependent exchange splittings calculated with the values of the Racah parameters obtained for the free Ti(II) ion [148], namely

Table 4. Symmetry adapted orbital basis and related terms of the corner shared $^2E(e^1)$–$^2E(e^1)$ pair of D_{4h} symmetry.

Terms	Symmetry adapted orbital basis
$^3A_{2u}, {}^1A_{1g}$	$(1/\sqrt{2})(\theta_A\theta_B + \varepsilon_A\varepsilon_B)$
$^3B_{2u}, {}^1B_{1g}$	$(1/\sqrt{2})(\theta_A\theta_B - \varepsilon_A\varepsilon_B)$
$^3B_{1u}, {}^1B_{2g}$	$(1/\sqrt{2})(\theta_A\varepsilon_B + \varepsilon_A\theta_B)$
$^3A_{2g}, {}^1A_{1u}$	$(1/\sqrt{2})(\theta_A\varepsilon_B - \varepsilon_A\theta_B)$

Table 5. Eigenvalues of the exchange Hamiltonian, Equation (4.8).

Terms	Energies
$^3A_{2u}, {}^1A_{1g}$	$-\dfrac{2t_\pi^2}{\varepsilon[{}^1A_1(e^2)]}[2 - S(S+1)]$
$^3B_{2u}, {}^1B_{1g}$	$-\dfrac{2t_\pi^2}{\varepsilon[{}^1B_1(e^2)]}[2 - S(S+1)]$
$^3B_{1u}, {}^1B_{2g}$	$-\dfrac{2t_\pi^2}{\varepsilon[{}^1B_2(e^2)]}[2 - S(S+1)]$
$^3A_{2g}, {}^1A_{1u}$	$-\dfrac{2t_\pi^2}{\varepsilon[{}^3A_2(e^2)]}S(S+1)$

$A = 141000\,\mathrm{cm}^{-1}$, $B = 900\,\mathrm{cm}^{-1}$, $C = 3300\,\mathrm{cm}^{-1}$ (these values are close to those found in the cubic crystal field [100]). An independent evaluation of A can be made by comparing the ionisation potentials for the configurations Ti(II)–Ti(III) (2.6525MJ/mol) and Ti(III)-Ti(IV) (4.1746MJ/mol) [149]. This estimation gives $A = 15.03\,\mathrm{eV}$ that is close to the value calculated for the free Ti(II) ion. Similar estimation can be obtained from the formula $A = F_0 - 49F_4$ with the Slater–Condon parameters expressed in terms of B and C (the corresponding expressions are given in the book [100]) Note that the parameter A plays the same role as the CT energy U in Anderson's theory. We also set $t_\pi = 4000\,\mathrm{cm}^{-1}$ that is within the Anderson's estimation [84,85]). The multiplets ($^3A_{2u}, {}^1A_{1g}$), ($^3B_{2u}, {}^1B_{1g}$) and $^3B_{1u}, {}^1B_{2g}$ are split antiferromagnetically whereas the multiplet $^3A_{2g}, {}^1A_{1u}$ is split ferromagnetically. It is seen that the ferromagnetic splitting of the multiplet $^3A_{2g}, {}^1A_{1u}$ is bigger as compared with the antiferromagnetic splittings of the remaining multiplets. This result can be easily understood if one takes into account that only the ground and CT states of the same symmetry are mixed by the electron transfer. Since all CT states are even (symbol g is omitted in the notation of the CT states in Table 1), only the states $^1A_{1g}$, $^1B_{1g}$, $^1B_{2g}$ and $^3A_{2g}$ belonging to the ground manifold of the dimer are stabilised due to the mixing with the CT states possessing the same spin and space symmetry, whereas the odd states $^3A_{2u}$, $^3B_{2u}$, $^3B_{1u}$ and $^1A_{1u}$ keep the same energy. Since the energy of the spin-triplet CT state $^3A_{2g}$ is lower than the energies of the spin-singlet CT states $^1A_{1g}$, $^1B_{1g}$, $^1B_{2g}$, the stabilisation of the $^3A_{2g}$state is the strongest one and hence the overall effect of the orbitally dependent exchange proves to be ferromagnetic (Figure 18).

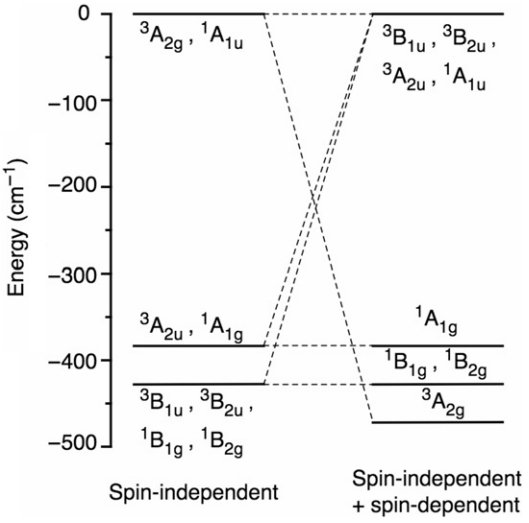

Figure 18. The energy pattern of the exchange splittings for the $[^2E(e^1)]_A \otimes [^2E(e^1)]_B$ - exchange problem (the values of the Racah parameters and transfer integral are explained in the text).

One can also demonstrate that the considered exchange interaction gives rise to a considerable magnetic anisotropy. At this step, we will not discuss this point; the detailed discussion of the magnetic anisotropy caused by the orbitally dependent exchange will be given below.

The described direct way of the calculations of the parameters of the effective exchange Hamiltonian does not involve any conceptual difficulties. Nevertheless, such calculations can be sometimes rather lengthy, especially for the case of constituent metal ions containing large number of unpaired electrons. For this reason, in [93] a more comprehensive but also more complicated in its conceptual background approach to the calculation of the parameters $F^{(k)}_{\Gamma\Gamma'}(\cdots)$ that is based on the use of Racah technique was developed. Here we give only the final expressions that can be used for such evaluation, the procedure of the derivation of these expressions can be found in [93].

The reduced matrix element of the operator $\hat{X}$ can be evaluated as

$$\left\langle \nu_i s_i \Lambda_i \middle\| \hat{X}_{\Gamma k}\left(\Gamma_i \Gamma'_i, \bar{\nu}_i \bar{s}_i \bar{\Lambda}_i\right) \middle\| \nu_i s_i \Lambda_i \right\rangle = (-1)^{\bar{F}} \sqrt{(2k+1)(\Gamma)} \times \left\{ \begin{array}{ccc} s_i & s_i & k \\ 1/2 & 1/2 & \bar{s}_i \end{array} \right\} W\left(\begin{array}{ccc} \Lambda_i & \Lambda_i & \Gamma \\ \Gamma_i & \Gamma'_i & \bar{\Lambda}_i \end{array} \right) \left\langle \nu_i s_i \Lambda_i \middle\| \hat{c}^+_{\Gamma_i 1/2} \middle\| \bar{\nu}_i \bar{s}_i \bar{\Lambda}_i \right\rangle \left\langle \nu_i s_i \Lambda_i \middle\| \hat{c}^+_{\Gamma'_i 1/2} \middle\| \bar{\nu}_i \bar{s}_i \bar{\Lambda}_i \right\rangle, \tag{5.39}$$

and similar formula is valid for the reduced matrix element of $\hat{Y}$ [93]. Here $W\begin{pmatrix} a & b & c \\ d & e & f \end{pmatrix}$ is the W-symbol [150] (the letters a, b, c, d, e, f stand for the irreducible representations), and $\bar{F}$ is the phase factor defined by the following symbolic equations:

$$\bar{F} = F(\Gamma_i, \Gamma'_i, \Gamma) + F(\Lambda_i, \Gamma, \Lambda_i) + F(\bar{\Lambda}_i, \Gamma_i, \Lambda_i) + F(\bar{\Lambda}_i, \Gamma'_i, \Lambda_i) + \Lambda_i + \Gamma'_i + \bar{\Lambda}_i + \Gamma. \tag{5.40}$$

The phase factors of the type $(-1)^{F(a,b,c)}$ are introduced to take into account the difference in phases between the definition of the Clebsch–Gordan coefficients in the book by Sugano *et al.* [100] that we use in this article and the definition of these coefficients given in the book of Grifith [150]. For the point group O, the additional phase factors of the type $(-1)^a$ are calculated using the following conventions: $(-1)^{A_1} = (-1)^E = (-1)^{T_2} = 1$, and $(-1)^{A_2} = (-1)^{T_1} = -1$.

Finally, the reduced matrix elements of the creation operator in Equation (5.39) can be found with the aid of the relationship between these matrix elements and the coefficient of fractional parentage [151]. This gives the following result:

$$\left\langle \nu_i s_i \Lambda_i \left\| \hat{c}^{+}_{\Gamma_i 1/2} \right\| \bar{\nu}_i \bar{s}_i \bar{\Lambda}_i \right\rangle = (-1)^{n_i} \sqrt{n_i (2s_i + 1)(\Lambda_i)} \times \sum_{k_i \bar{k}_i} \langle \nu_i \mid k_i \rangle \left\langle \bar{k}_i \;\middle|\; \bar{\nu}_i \right\rangle \left\langle (d^{n_i - 1}) \bar{k}_i \bar{s}_i \bar{\Lambda}_i, \Gamma_i \middle| \right\} (d^{n_i}) k_i s_i \Lambda_i \rangle. \tag{5.41}$$

In Equation (5.41), the conventional notation $\langle \cdots | \} \cdots \rangle$ is used for the coefficients of fractional parentage [152].

5.3. *Comparison with earlier approaches*

Conceptually, the background of the described approach is close to those of Drillon and Georges [124,125] and Leuenberger and Güdel [126]. However, there are at least two significant differences. The first difference is in the mathematical procedure. In [124–126], the *T–P* isomorphism was employed from the very beginning and the kinetic exchange Hamiltonian was expressed in terms of the fictitious orbital angular momentum operators and spin operators. This implies two restrictions, namely, only the orbital triplets (T_1 or T_2) can be considered, and only the transfer pathways involving the electron jumps from t_2 orbitals can be taken into account. On the contrary, in the present approach we start with the strong crystal field scheme (with subsequent allowance of mixing of all configurations) and express the effective Hamiltonian through the irreducible cubic tensors $\hat{O}^{i}_{\Gamma\gamma}$ and spin operators. Also note that as distinguished from the approaches [124–126], the present consideration exploits the tensorial properties of the fermionic operators and point symmetry arguments. As a consequence, this approach is applicable to all electronic configurations and terms of the constituent metal ions.

The second important difference is that the approach so far discussed takes into account a complex multiplet structure (given by Tanabe–Sugano diagrams) of the energy patterns of metal ions in their normal, oxidised and reduced forms. In fact, in [126] all the energies of the CT states were set to the on-site repulsion energy U involved in the Hubbard Hamiltonian. Although in [124,125] the energies of the CT states were considered to be dependent on the spin, the difference between the energies of the CT states with the same spin was still neglected. At the same time, the discrimination between the energies of different CT states is sometimes important because it affects the mutual disposition of the spin levels arising from the exchange splitting of the ground manifold and, particularly, it can change the spin multiplicity of the ground state. Particularly, the importance of the accurate determination of the multiplet structure of the CT states for the adequate description of the magnetic and orbital ordering in the manganites has been pointed out in [153].

To complete the discussion of the existing approaches, one should mention two studies based on the similar ideas, namely the studies of Weihe and Güdel [90] and Ceulemans *et al.* [127–129]. In [90], the kinetic exchange in μ-oxo–bridged dimeric complexes of D_{4h} symmetry was considered and a direct calculation of the energy pattern was performed by means of the second-order perturbation procedure without using of the effective Hamiltonian. A second-order kinetic exchange Hamiltonian acting within the ground manifold of the pair was deduced in [127–129] and applied to the $[Ti_2Cl_9]^{3-}$ dimer. However, in its final form this Hamiltonian still contains the one-electron fermionic operators acting on the spin–orbitals rather than the many-electron orbital and spin operators, and hence it cannot be regarded as an effective Hamiltonian to the full extent. In fact, according to the conventional definition of the effective Hamiltonian, the last should not only operate within the restricted basis but also should be expressed in terms of the many-electron operators acting within the space specified by the total quantum numbers of the constituents. From this point of view, the Hamiltonian, Equation (5.18), does represent a genuine effective exchange Hamiltonian because it contains only the many-electron orbital and spin operators of the interacting metal ions. To clarify this statement, let us use the analogy with the HDVV spin-Hamiltonian and compare two possible forms of this Hamiltonian. The first form of the HDVV Hamiltonian represents the sum of bi-orbital contributions, namely, $\hat{H}_{\mathrm{ex}} = -2\sum_{\alpha\beta} J_{A\alpha,B\beta}\hat{\boldsymbol{s}}_{A\alpha}\hat{\boldsymbol{s}}_{B\beta}$ (i), where α and β enumerate the magnetic orbitals, and $J_{A\alpha,B\beta}$ are the biorbital exchange parameters. The second form is the conventional HDVV Hamiltonian, i.e. $\hat{H}_{\mathrm{ex}} = -2\,J\,\hat{\boldsymbol{s}}_A\hat{\boldsymbol{s}}_B$ (ii), where $J = (n_A n_B)^{-1}\sum_{\alpha\beta} J_{A\alpha,B\beta}$ is the many-electron exchange parameter (n_A and n_B are the numbers of the magnetic orbitals). The Hamiltonian (i) explicitly contains all exchange pathways and one-electron operators, while the Hamiltonian (ii) is expressed in terms of the full spin operators $\hat{\boldsymbol{s}}_A$, $\hat{\boldsymbol{s}}_B$, and contains the only many-electron exchange parameter J. Although these two forms of the exchange Hamiltonian are equivalent, only the second one can be useful for the parametrisation of the experimental data and has an irrefutable advantage as a computational tool.

5.4. *Orbitally dependent exchange Hamiltonian in terms of spherical irreducible tensor operators*

To simplify the evaluation of the energy pattern and eigen-functions of the orbitally dependent Hamiltonian, the orbital and spin operators can be expressed in terms of the ITOs of R_3 group. The ITO approach based on full symmetry group R_3 is well known as the most efficient computational tool for the evaluation of the energy levels and physical properties of high-nuclearity spin-clusters [4]. Now we will demonstrate that the ITO technique based on R_3 group can be extended to a more general case of degenerate systems. The corresponding approach developed in [94] enables one to benefit from the powerful angular momentum technique and gives a more convenient way to classify the states of the degenerate system by assigning the orbital angular momenta quantum numbers (along with the spin quantum numbers) to the eigenvectors of the effective Hamiltonian. This significantly facilitates also the analysis of the magnetic anisotropy. It is worthwhile to illustrate the main idea by taking a corner-shared bioctahedral system of D_{4h} symmetry (Figure 19) as an example and assuming the ${}^{2S+1}T_2$ or ${}^{2S+1}T_1$ ground

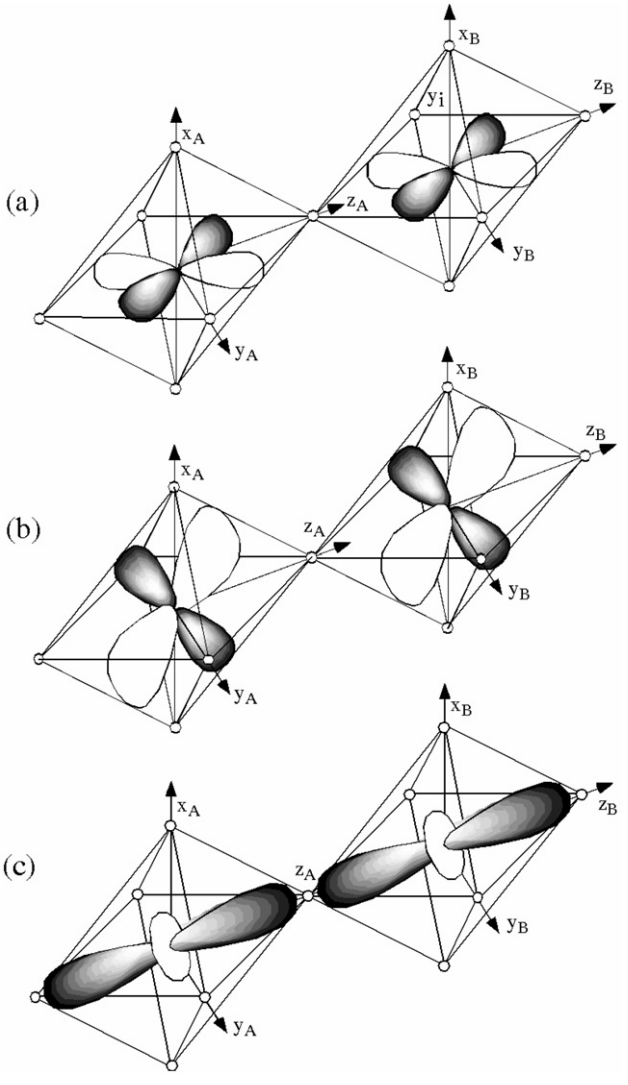

Figure 19. The most efficient transfer pathways in a corner-shared bioctahedron: (a) $\xi - \xi$, (b) $\eta - \eta$ and (c) $u - u$.

terms of the metal ions. Then (in Section 6.1) the magnetic properties of this system will be discussed with the special emphasis on the magnetic anisotropy.

Let us use the conventional notations for the cubic basis [100]: $\xi \propto yz, \eta \propto xz$, $\zeta \propto xy$ (T_2-basis), $u \propto 3z^2 - r^2$, $\mathrm{v} \propto \sqrt{3}(x^2 - y^2)$ (E-basis), and $\alpha \propto \hat{L}_x$, $\beta \propto \hat{L}_y$, $\gamma \propto \hat{L}_z$ (T_1-basis). Figure 19 shows that the main contributions to the kinetic exchange arise from the transfer processes $\xi_A \leftrightarrow \xi_B$, $\eta_A \leftrightarrow \eta_B$ (π-transfer) and $u_A \leftrightarrow u_B$ (σ-transfer). The corresponding transfer integrals will be denoted as follows:

$$t_{\xi\xi} = t_{\eta\eta} \equiv t_\pi, t_{uu} \equiv t_\sigma. \tag{5.42}$$

Table 6. Orbital matrices $\hat{\boldsymbol{O}}_{\Gamma\gamma}$ with $\Gamma = A_1,\ E(\gamma = u, \mathrm{v}),\ T_1(\gamma = \alpha, \beta, \gamma)$ and $T_2(\gamma = \xi, \eta, \zeta)$ defined with the cubic T_2 (upper signs) and T_1 (lower signs) bases.

$\hat{\boldsymbol{O}}_{A_1}$	$\hat{\boldsymbol{O}}_{Eu}$	$\hat{\boldsymbol{O}}_{E\mathrm{v}}$
$\begin{pmatrix} 1 & 0 & 0 \\ 0 & 1 & 0 \\ 0 & 0 & 1 \end{pmatrix}$	$\begin{pmatrix} -1/2 & 0 & 0 \\ 0 & -1/2 & 0 \\ 0 & 0 & 1 \end{pmatrix}$	$\begin{pmatrix} \sqrt{3}/2 & 0 & 0 \\ 0 & -\sqrt{3}/2 & 0 \\ 0 & 0 & 0 \end{pmatrix}$
$\hat{\boldsymbol{O}}_{T_1\alpha}$	$\hat{\boldsymbol{O}}_{T_1\beta}$	$\hat{\boldsymbol{O}}_{T_1\gamma}$
$\begin{pmatrix} 0 & 0 & 0 \\ 0 & 0 & \pm 1/\sqrt{2} \\ 0 & \mp 1/\sqrt{2} & 0 \end{pmatrix}$	$\begin{pmatrix} 0 & 0 & \mp 1/\sqrt{2} \\ 0 & 0 & 0 \\ \pm 1/\sqrt{2} & 0 & 0 \end{pmatrix}$	$\begin{pmatrix} 0 & \pm 1/\sqrt{2} & 0 \\ \mp 1/\sqrt{2} & 0 & 0 \\ 0 & 0 & 0 \end{pmatrix}$
$\hat{\boldsymbol{O}}_{T_2\xi}$	$\hat{\boldsymbol{O}}_{T_2\eta}$	$\hat{\boldsymbol{O}}_{T_2\zeta}$
$\begin{pmatrix} 0 & 0 & 0 \\ 0 & 0 & 1/\sqrt{2} \\ 0 & 1/\sqrt{2} & 0 \end{pmatrix}$	$\begin{pmatrix} 0 & 0 & 1/\sqrt{2} \\ 0 & 0 & 0 \\ 1/\sqrt{2} & 0 & 0 \end{pmatrix}$	$\begin{pmatrix} 0 & 1/\sqrt{2} & 0 \\ 1/\sqrt{2} & 0 & 0 \\ 0 & 0 & 0 \end{pmatrix}$

The consideration will be restricted by the trivalent metal ions possessing ground orbital triplets arising from the t_2^n configurations (e.g. Ti(III) ions ($^2T_2(t_2^1)$), the low-spin Mn(III) ions ($^3T_1(t_2^4)$), etc.). Since the cubic crystal field for these ions is strong, one can expect that these terms arise mainly from t_2^n and neglect the admixture of the states arising from $t_2^{n-m}e^m$ configurations. In this case σ-transfer is excluded because the e-orbitals are unoccupied in the ground state. Retaining only the terms proportional to $t_{\xi\xi}^2$, $t_{\eta\eta}^2$ and $t_{\xi\xi}t_{\eta\eta}$ in Equation (5.18), one can present the kinetic exchange Hamiltonian acting within the ground $[^{2s+1}\Lambda(t_2^n)]_A \otimes [^{2s+1}\Lambda(t_2^n)]_B$ manifold ($\Lambda = T_1, T_2$) in the same form as that in Equation (5.20), with the orbital operators $\hat{R}_k$ being the following:

$$\begin{aligned}\hat{R}_k = -(2/3)t_\pi^2\Big[&2F^{(k)}_{A_1A_1}\hat{O}^A_{A_1}\hat{O}^B_{A_1} + F^{(k)}_{EE}\Big(\hat{O}^A_{Eu}\hat{O}^B_{Eu} + 3\hat{O}^A_{E\mathrm{v}}\hat{O}^B_{E\mathrm{v}}\Big) \\ &-\sqrt{2}F^{(k)}_{A_1E}\Big(\hat{O}^A_{A_1}\hat{O}^B_{Eu} + \hat{O}^A_{Eu}\hat{O}^B_{A_1}\Big) + 3F^{(k)}_{T_1T_1}\hat{O}^A_{T_1\gamma}\hat{O}^B_{T_1\gamma} + 3F^{(k)}_{T_2T_2}\hat{O}^A_{T_2\zeta}\hat{O}^B_{T_2\zeta}\Big].\end{aligned} \tag{5.43}$$

In Equation (5.43), the short notations $F^{(k)}_{\Gamma\Gamma'} \equiv F^{(k)}_{\Gamma\,\Gamma'}(t_2, t_2, t_2, t_2)$ are introduced. The matrices $\hat{\boldsymbol{O}}_{\Gamma\gamma}$ defined in the cubic $T_2(T_1)$ basis are given in Table 6. If the symmetry of the ligand surroundings of the constituent metal ions is lower than the cubic one, the Hamiltonian of the system also contains the terms of the low-symmetry (non-cubic) components of the crystal field, which splits the ground cubic orbital triplet. The one-centre operator of the low-symmetry crystal field can be written as

$$\hat{H}^i_{cr} = \Delta\left[\hat{l}^2_{zi} - \frac{1}{3}l(l+1)\right] + \Delta'\left(\hat{l}^2_{xi} - \hat{l}^2_{yi}\right) = -\frac{2}{3}\Delta\hat{O}^i_{Eu} + \frac{2}{\sqrt{3}}\Delta'\hat{O}^i_{E\mathrm{v}}, \tag{5.44}$$

where the parameters describing the axial and rhombic distortions are assumed to be equal for both ions. Then for the pair of metal ions, one can write

$$\hat{H}_{cr} = -\frac{2}{3}\Delta\left(\hat{O}^A_{A_1}\hat{O}^B_{Eu} + \hat{O}^A_{Eu}\hat{O}^B_{A_1}\right) + \frac{2}{\sqrt{3}}\Delta'\left(\hat{O}^A_{A_1}\hat{O}^B_{Ev} + \hat{O}^A_{Ev}\hat{O}^B_{A_1}\right). \tag{5.45}$$

Now we can find the relationship between the matrices $\hat{O}_{\Gamma\gamma}$ and the matrices $\hat{l}_x, \hat{l}_y, \hat{l}_z$ defined in the p-basis. The possibility to use $\hat{l}_x, \hat{l}_y, \hat{l}_z$ defined in p-basis (instead of T_2 or T_1) is due to the T–P isomorphism that in the case of pure t_2^n configuration is described by the symbolic equation

$$\hat{\boldsymbol{l}}(P) = -\hat{\boldsymbol{l}}(T_1 \text{ or } T_2). \tag{5.46}$$

For the sake of definiteness we will consider the ground term $^{2s+1}T_2$. In the point group O the operators $\hat{l}_x, \hat{l}_y, \hat{l}_z$ form the basis of T_1, and the matrices $\hat{O}_{T_1\gamma}$ are related to $\hat{l}_x, \hat{l}_y, \hat{l}_z$ as follows:

$$\hat{O}_{T_1\alpha} = (\mathrm{i}/\sqrt{2})\hat{l}_x, \quad \hat{O}_{T_1\beta} = (\mathrm{i}/\sqrt{2})\hat{l}_y, \quad \hat{O}_{T_1\gamma} = (\mathrm{i}/\sqrt{2})\hat{l}_z. \tag{5.47}$$

The matrices $\hat{O}_{E\gamma}$ and $\hat{O}_{T_2\gamma}$ can also be expressed in terms of the components $\hat{l}_x, \hat{l}_y, \hat{l}_z$ using the relation (T_2 and E are contained in the direct product $T_1 \times T_1$)

$$\hat{O}_{\Gamma\gamma} = K_\Gamma \sum_{\gamma_1\gamma_2} \langle T_1\gamma_1 T_1\gamma_2 \mid \Gamma\gamma\rangle \hat{O}_{T_1\gamma_1}\hat{O}_{T_1\gamma_2}, \tag{5.48}$$

where the factors K_Γ are calculated by means of comparing the corresponding bilinear forms with the matrices $\hat{O}_{\Gamma\gamma}$. Applying this procedure, one finds that

$$E\begin{cases} \hat{O}_{Eu} = -(3/2)\left[\hat{l}_z^2 - (1/3)l(l+1)\right], \\ \hat{O}_{Ev} = -(\sqrt{3}/2)\left(\hat{l}_x^2 - \hat{l}_y^2\right). \end{cases}$$

$$T_2\begin{cases} \hat{O}_{T_2\xi} = -(1/\sqrt{2})\left(\hat{l}_y\hat{l}_z + \hat{l}_z\hat{l}_y\right), \\ \hat{O}_{T_2\eta} = -(1/\sqrt{2})\left(\hat{l}_x\hat{l}_z + \hat{l}_z\hat{l}_x\right), \\ \hat{O}_{T_2\zeta} = -(1/\sqrt{2})\left(\hat{l}_x\hat{l}_y + \hat{l}_y\hat{l}_x\right). \end{cases} \tag{5.49}$$

At the next step, one can express $\hat{l}_x, \hat{l}_y, \hat{l}_z$ in terms of the cyclic components $\hat{l}_{1q}(q = 0, \pm 1)$. Then, the bilinear forms $\hat{l}_x, \hat{l}_y$, etc., are expressed through the irreducible tensor products by means of the inverse Clebsch–Gordan transformation [141]:

$$\hat{l}_{1q_1}\hat{l}_{1q_2} = \sum_{nq} C^{nq}_{1q_1 1q_2}\hat{T}_{nq}, \quad \left\{\hat{l}_1 \otimes \hat{l}_1\right\}_{nq} \equiv \hat{T}_{nq}. \tag{5.50}$$

In order to unify the notations we also denote $\hat{l}_{1q_1} \equiv \hat{T}_{1q}$. By combining these results, we arrive at the following expressions for the cubic ITOs $\hat{O}_{\Gamma\gamma}$ in terms of spherical ITOs $\hat{T}_{nq}$:

$$\begin{aligned}
&\hat{O}_{A_1} = \hat{T}_{00},\\
&\hat{O}_{Eu} = -\sqrt{3/2}\hat{T}_{20},\\
&\hat{O}_{Ev} = -(\sqrt{3}/2)\left(\hat{T}_{22} + \hat{T}_{2-2}\right),\\
&\hat{O}_{T_1\alpha} = -(\mathrm{i}/2)\left(\hat{T}_{11} - \hat{T}_{1-1}\right), \quad \hat{O}_{T_1\beta} = -(1/2)\left(\hat{T}_{11} + \hat{T}_{1-1}\right), \quad \hat{O}_{T_1\gamma} = (\mathrm{i}/\sqrt{2})\,\hat{T}_{10},\\
&\hat{O}_{T_2\xi} = -(\mathrm{i}/\sqrt{2})\left(\hat{T}_{21} + \hat{T}_{2-1}\right), \quad \hat{O}_{T_2\eta} = (1/\sqrt{2})\left(\hat{T}_{21} - \hat{T}_{2-1}\right), \quad \hat{O}_{T_2\zeta} = (\mathrm{i}/\sqrt{2})\left(\hat{T}_{22} - \hat{T}_{2-2}\right).
\end{aligned} \tag{5.51}$$

The orbital operators $\hat{O}^A_{\Gamma\gamma}$ and $\hat{O}^B_{\Gamma\gamma}$ are defined in the local frames $x_A y_A z_A$ and $x_B y_B z_B$. In the D_{4h} case they are collinear, and hence the orbital operators defined in these frames retain their forms also in the molecular coordinate frame XYZ that is collinear to the local ones ($Z||C_4$). In this case, one can pass to the site-coupled representation using again the relation between the direct product of the spherical ITOs and the irreducible tensor products [141]

$$\hat{T}^A_{nq}\hat{T}^B_{n'q'} = \sum_{br} C^{br}_{nqn'q'}\left\{\hat{T}^A_n \otimes \hat{T}^B_{n'}\right\}_{br}. \tag{5.52}$$

These equations allow us to express all products $\hat{O}^A_{\Gamma\gamma}\hat{O}^B_{\Gamma'\gamma'}$ in terms of the irreducible tensor products $\{\hat{T}^A_k \otimes \hat{T}^B_n\}_{br}$ [93]. The results are collected in Table 7. Finally, according to a general rule [141], the scalar product $\hat{\boldsymbol{s}}_A\hat{\boldsymbol{s}}_B$ should be replaced with $-\sqrt{3}\left\{\hat{s}^A_1 \otimes \hat{s}^B_1\right\}_{00}$.

Along with the exchange interaction and low-symmetry crystal field contribution, the full Hamiltonian of the cluster should also include SO and Zeeman interactions. The corresponding expressions for the ${}^{2s+1}T_2\left(t_2^n\right) - {}^{2s+1}T_2\left(t_2^n\right)$ pair in terms of spherical ITOs are the following:

$$\hat{H}_{SO} = -\kappa\lambda\sum_q (-1)^q\left(\hat{T}^A_{1q}\hat{s}^A_{1-q} + \hat{T}^B_{1q}\hat{s}^B_{1-q}\right), \tag{5.53}$$

$$\hat{H}_Z = \beta\sum_q (-1)^q\left[-\kappa\left(\hat{T}^A_{1q} + \hat{T}^B_{1q}\right) + g_e\left(\hat{s}^A_{1q} + \hat{s}^B_{1q}\right)\right]H_{1-q} \tag{5.54}$$

SO coupling $\lambda > 0$ for t_2^n configurations with $n \le 3$, and $\lambda < 0$ when $n > 3$, the Zeeman term contains both spin and orbital parts. Using the results listed in Table 7 and Equations (5.53) and (5.54), one can present the full effective Hamiltonian, including both orbitally dependent exchange and one-centre interactions (low-symmetry crystal field, SO coupling and Zeeman interaction) in the following general form:

$$\hat{H}_{\mathrm{ef}}(A,B) = \sum_{n,n'}\sum_{b,r}\sum_{k,k'}\sum_{d,\lambda} G_{b,r,d,\lambda}(n,n',k,k')\left\{\hat{T}^A_n \otimes \hat{T}^B_{n'}\right\}_{br}\left\{\hat{s}^A_k \otimes \hat{s}^B_{k'}\right\}_{d,-\lambda}, \tag{5.55}$$

where the coefficients $G_{b,r,d,\lambda}(n,n',k,k')$ are the functions of the parameters $F^{(k)}_{\Gamma\Gamma'}$, λ, κ, Δ and Δ'. The expressions of the non-zero coefficients $G_{b,r,\mathrm{d},\lambda}(n,n',k,k')$ are collected in Table 8.

As a basis, one can use the wave-functions $|l_A l_B s_A s_B L S M_L M_S\rangle$ in which the single-ion fictitious orbital angular momenta $l_A = l_B = 1$ are coupled to give the total orbital angular momentum L of the dimer ($L = 0, 1, 2$), and the local spins s_A and s_B are coupled to give

Table 7. Relations between the direct products $\hat{O}^A_{\Gamma\gamma}\hat{O}^B_{\Gamma'\gamma'}$ defined in cubic basis and irreducible tensor products $\left\{\hat{T}^A_k \otimes \hat{T}^B_n\right\}_{br}$.

$\hat{O}^A_{\Gamma\gamma}\hat{O}^B_{\Gamma'\gamma'}$	Expression in terms of $\left\{\hat{T}^A_k \otimes \hat{T}^B_n\right\}_{br}$
$\hat{O}^A_{A_1}\hat{O}^B_{A_1}$	$\left\{\hat{T}^A_0 \otimes \hat{T}^B_0\right\}_{00}$
$\hat{O}^A_{Eu}\hat{O}^B_{Eu}$	$(3/\sqrt{20})\left\{\hat{T}^A_2 \otimes \hat{T}^B_2\right\}_{00} - (3/\sqrt{14})\left\{\hat{T}^A_2 \otimes \hat{T}^B_2\right\}_{20} + (9/\sqrt{70})\left\{\hat{T}^A_2 \otimes \hat{T}^B_2\right\}_{40}$
$\hat{O}^A_{Ev}\hat{O}^B_{Ev}$	$(3/\sqrt{20})\left\{\hat{T}^A_2 \otimes \hat{T}^B_2\right\}_{00} + (3/\sqrt{14})\left\{\hat{T}^A_2 \otimes \hat{T}^B_2\right\}_{20} + (3/\sqrt{280})\left\{\hat{T}^A_2 \otimes \hat{T}^B_2\right\}_{40}$ $+ (3/4)\left\{\hat{T}^A_2 \otimes \hat{T}^B_2\right\}_{44} + (3/4)\left\{\hat{T}^A_2 \otimes \hat{T}^B_2\right\}_{4-4}$
$\hat{O}^A_{A_1}\hat{O}^B_{Eu} + \hat{O}^A_{Eu}\hat{O}^B_{A_1}$	$-\sqrt{3/2}\left[\left\{\hat{T}^A_0 \otimes \hat{T}^B_2\right\}_{20} + \left\{\hat{T}^A_2 \otimes \hat{T}^B_0\right\}_{20}\right]$
$\hat{O}^A_{T_1\gamma}\hat{O}^B_{T_1\gamma}$	$(1/\sqrt{12})\left\{\hat{T}^A_1 \otimes \hat{T}^B_1\right\}_{00} - (1/\sqrt{6})\left\{\hat{T}^A_1 \otimes \hat{T}^B_1\right\}_{20}$
$\hat{O}^A_{T_2\zeta}\hat{O}^B_{T_2\zeta}$	$(1/\sqrt{5})\left\{\hat{T}^A_2 \otimes \hat{T}^B_2\right\}_{00} + \sqrt{2/7}\left\{\hat{T}^A_2 \otimes \hat{T}^B_2\right\}_{20} + (1/\sqrt{70})\left\{\hat{T}^A_2 \otimes \hat{T}^B_2\right\}_{40}$ $-(1/2)\left\{\hat{T}^A_2 \otimes \hat{T}^B_2\right\}_{44} - (1/2)\left\{\hat{T}^A_2 \otimes \hat{T}^B_2\right\}_{4-4}$
$\hat{O}^A_{A_1}\hat{O}^B_{Ev} + \hat{O}^A_{Ev}\hat{O}^B_{A_1}$	$-\frac{\sqrt{3}}{2}\left[\left\{\hat{T}^A_0 \otimes \hat{T}^B_2\right\}_{22} + \left\{\hat{T}^A_0 \otimes \hat{T}^B_2\right\}_{2-2} + \left\{\hat{T}^A_2 \otimes \hat{T}^B_0\right\}_{22} + \left\{\hat{T}^A_2 \otimes \hat{T}^B_0\right\}_{2-2}\right]$

Table 8. Non-zero coefficients $G_{b,r,d,\lambda}(n,\ n',\ k,\ k')$.

$G_{b,r,\mathrm{d},\lambda}(n,n',k,k')$	Expression
$G_{0,0,0,0}(0,0,k,k)$	$-(4/3)t_\pi^2 F^{(k)}_{A_1A_1}$
$G_{0,0,0,0}(2,2,k,k)$	$-(2/\sqrt{5})t_\pi^2\left[2F^{(k)}_{EE} + F^{(k)}_{T_2T_2}\right]$
$G_{2,0,0,0}(2,2,k,k)$	$-(4/\sqrt{14})t_\pi^2\left[F^{(k)}_{EE} + F^{(k)}_{T_2T_2}\right]$
$G_{4,0,0,0}(2,2,k,k)$	$-(1/\sqrt{70})t_\pi^2\left[9F^{(k)}_{EE} + 2F^{(k)}_{T_2T_2}\right]$
$G_{4,\pm4,0,0}(2,2,k,k)$	$-(1/2)t_\pi^2\left[3F^{(k)}_{EE} - 2F^{(k)}_{T_2T_2}\right]$
$G_{0,0,0,0}(1,1,k,k)$	$-(1/\sqrt{3})t_\pi^2 F^{(k)}_{T_1T_1}$
$G_{2,0,0,0}(1,1,k,k)$	$(2/\sqrt{6})t_\pi^2 F^{(k)}_{T_1T_1}$
$G_{2,0,0,0}(0,2,k,k) = G_{2,0,0,0}(2,0,k,k)$	$-(2/\sqrt{3})t_\pi^2 F^{(k)}_{A_1E} + (1-k)\sqrt{2/3}\Delta$
$G_{2,\pm2,0,0}(0,2,0,0)$	$-\Delta'$
$G_{1,0,1,0}(1,0,1,0)$	$-\kappa\lambda$
$G_{1,\pm1,1,\pm1}(1,0,1,0)$	$\kappa\lambda$
$G_{1,0,0,0}(1,0,0,0)$	$-\kappa\beta H_{10}$
$G_{1,\pm1,0,0}(1,0,0,0)$	$\kappa\beta H_{1\mp1}$
$G_{0,0,1,0}(0,0,1,0)$	$g_e\beta H_{10}$
$G_{0,0,1,\pm1}(0,0,1,0)$	$-g_e\beta H_{1\mp1}$

the total spin S. This basis corresponds to the Russel–Saunders scheme for dimer. Then using the ITO technique, one can obtain the following formula for the matrix elements of the Hamiltonian:

$$\begin{aligned}
&\langle l_A l_B s_A s_B L' S' M'_L M'_S | \hat{H}_{\mathrm{ef}}(A,B) | l_A l_B s_A s_B L S M_L M_S \rangle \\
&\quad = \sqrt{(2L+1)(2S+1)} \sum_{n,n'} \sum_{b,r} \sum_{k,k'} \sum_{d,\lambda} G_{b,r,d,\lambda}(n,n',k,k') \sqrt{(2b+1)(2d+1)} \\
&\qquad \times \begin{Bmatrix} n & n' & b \\ 1 & 1 & L' \\ 1 & 1 & L \end{Bmatrix} \begin{Bmatrix} k & k' & d \\ s_A & s_B & S' \\ s_A & s_B & S \end{Bmatrix} \langle 1 \| \hat{T}^A_n \| 1 \rangle \langle 1 \| \hat{T}^B_{n'} \| 1 \rangle \langle s_A \| \hat{s}^A_k \| s_A \rangle \\
&\qquad \times \langle s_B \| \hat{s}^B_{k'} \| s_B \rangle C^{L' M'_L}_{L M_L b r} C^{S' M'_S}_{S M_S d-\lambda},
\end{aligned} \tag{5.56}$$

where the orbital and spin one-centre reduced matrix elements are calculated as

$$\begin{aligned}
&\langle 1 \| \hat{T}^f_0 \| 1 \rangle = \sqrt{3}, \quad \langle 1 \| \hat{T}^f_1 \| 1 \rangle = \sqrt{6}, \quad \langle 1 \| \hat{T}^f_2 \| 1 \rangle = \sqrt{5}, \\
&\langle s_f \| \hat{s}^f_0 \| s_f \rangle = \sqrt{2s_f + 1}, \quad \langle s_f \| \hat{s}^f_1 \| s_f \rangle = \sqrt{s_f(s_f+1)(2s_f+1)}.
\end{aligned} \tag{5.57}$$

6. Orbitally dependent exchange: applications, magnetic anisotropy

6.1. *Corner-shared bioctahedral* $^2T_2(t_2^1) - {}^2T_2(t_2^1)$ *cluster*

Let us apply the so far described approach to a simplest corner-shared bioctahedral cluster of D_{4h} symmetry formed by two one-electron centers, this system can be referred to as $^2T_2(t_2^1) - {}^2T_2(t_2^1)$ pair. In this case, the CT states represent the products of the oxidised vacuum state (term $^1A_1$ arising from the t_2^0-configuration) and the following reduced $\tilde{s}\,\tilde{\Lambda}$ states belonging to d^2 configuration: $^3T_1(t_2^2, t_2e)$, $^1A_1(t_2^2, e^2)$, $^1E(t_2^2, e^2)$ and $^1T_2(t_2^2, t_2e)$. One can see that only these CT states are mixed with the ground one by means of the electron hopping of $t_2 \rightarrow t_2$ type. In fact, considering, for example, the reduced state $^3T_2(t_2e)$, one can see that this state can be obtained from the ground $t_2^1 - t_2^1$ configuration only *via* the transfer of $t_2 \rightarrow e$ type, which is forbidden in the case of the overall D_{4h} symmetry.

Since each $\tilde{s}\,\tilde{\Lambda}$ state is the result of the mixing of only two electronic configurations, the corresponding wave-functions can be found analytically by considering the 2×2 matrices of intra-centre Coulomb interaction (see the book by Sugano *et al.* [100]). Then the parameters $F^{(k)}_{\Gamma\Gamma'}$ involved in the exchange Hamiltonian can be presented as follows:

$$F^{(k)}_{\Gamma\Gamma'} = 2 \sum_{\tilde{s}\tilde{\Lambda}} N^{(k)}_{\Gamma\Gamma'}(\tilde{s}\tilde{\Lambda}) \left\{ \frac{\cos^2[\theta(\tilde{s}\tilde{\Lambda})]}{\varepsilon_1(\tilde{s}\tilde{\Lambda})} + \frac{\sin^2[\theta(\tilde{s}\tilde{\Lambda})]}{\varepsilon_2(\tilde{s}\tilde{\Lambda})} \right\}, \tag{6.1}$$

where $N^{(k)}_{\Gamma\Gamma'}(\tilde{s}\tilde{\Lambda})$ are the numerical factors, which are calculated following the procedure described in Section 5. The angles $\theta(\tilde{s}\tilde{\Lambda})$ defining the mixing of the repeating $\tilde{s}\tilde{\Lambda}$ terms are

calculated as follows:

$$\tan\left[2\theta\left({}^3T_1\right)\right] = \frac{12B}{10Dq + 9B}, \quad \tan\left[2\theta\left({}^1A_1\right)\right] = \frac{2\sqrt{6}(2B + C)}{20Dq - 2B - C},$$
$$\tan\left[2\theta({}^1E)\right] = -\frac{4\sqrt{3}B}{20Dq - B}, \quad \tan\left[2\theta\left({}^1T_2\right)\right] = \frac{4\sqrt{3}B}{10Dq - B}. \tag{6.2}$$

The energies $\varepsilon_{\tilde{\nu}}(\tilde{s}\tilde{\Lambda})$ of the CT states are counted from the energy of the pair of the non-interacting ${}^2T_2(t_2^1)$ ions, and their expressions in terms of the Racah parameters A, B, C and parameter Dq are given in [100].

First, let us analyse the eigenvalues of the exchange Hamiltonian defined by Equation (5.20), leaving outside all other interactions. One can find these eigenvalues by using the symmetry-adapted basis constructed from the initial orbital basis $\xi_A\xi_B$, $\xi_A\eta_B$, $\xi_A\zeta_B$, $\eta_A\xi_B$, $\eta_A\eta_B$, $\eta_A\zeta_B$, $\zeta_A\xi_B$, $\zeta_A\eta_B$ and $\zeta_A\zeta_B$. The symmetry-adapted orbital basis and related terms of the ${}^2T_2(t_2^1) - {}^2T_2(t_2^1)$ system are collected in Table 9. In the effective symmetry-adapted basis (the product of the symmetry adapted orbital basis and spin basis $|SM_S\rangle$), the matrix of the exchange Hamiltonian is diagonal, its eigenvalues are collected in Table 10. Note that the symmetry-adapted orbital basis and the eigenvalues are valid not only for ${}^2T_2(t_2^1) - {}^2T_2(t_2^1)$ pair but also for an arbitrary ${}^{2s+1}T_2(t_2^n) - {}^{2s+1}T_2(t_2^n)$ pair of D_{4h} symmetry.

For the numerical evaluation of the energy pattern, we use the same values for the Racah parameters and a transfer integral as in the above consideration. The cybic field parameter Dq is set to $1000\,\mathrm{cm}^{-1}$, that is, a typical value for divalent metal ions [100]. The energy pattern of ${}^2T_2(t_2^1) - {}^2T_2(t_2^1)$ pair calculated with this set of parameters is shown in Figure 20, where the irreducible representations of D_{4h} and the labels $|LSM_LM_S\rangle \equiv |S, LM_L\rangle$ obtained with the aid of spherical ITO approach are indicated. The spin-independent part of the kinetic exchange Hamiltonian splits the ground ${}^2T_2(t_2^1) \otimes {}^2T_2(t_2^1)$ manifold of the pair into six levels (Figure 20a). These levels undergo further splitting under the action of spin-dependent part of the Hamiltonian (Figure 20b). These splittings are defined by the parameters $J_1, J_2, \ldots, J_6$ collected in Table 11. The scheme of the energy levels consists of six superimposed groups of levels, and the energy levels within each group obey the Lande's rule. At the same time, the whole energy pattern does not obey this rule, that is, this pattern is essentially non-Heisenberg. The levels ${}^3A_{2g}$, ${}^1A_{1u}$ and ${}^{1,3}E_g$, ${}^{1,3}E_u$ are split in a ferromagnetic fashion, meanwhile all other levels are split antiferromagnetically.

Table 9. Symmetry-adapted orbital basis and related terms of the corner-shared ${}^2T_2(t_2^1)$–${}^2T_2(t_2^1)$ pair of D_{4h} symmetry.

Terms	Symmetry-adapted orbital basis
${}^3A_{2u}, {}^1A_{1g}$	$\zeta_A\zeta_B$
${}^3A_{2u}, {}^1A_{1g}$	$(1/\sqrt{2})(\xi_A\xi_B + \eta_A\eta_B)$
${}^3B_{2u}, {}^1B_{1g}$	$(1/\sqrt{2})(\xi_A\xi_B - \eta_A\eta_B)$
${}^3A_{2g}, {}^1A_{1u}$	$(1/\sqrt{2})(\xi_A\eta_B - \eta_A\xi_B)$
${}^3B_{1u}, {}^1B_{2g}$	$(1/\sqrt{2})(\xi_A\eta_B + \eta_A\xi_B)$
${}^3E_g, {}^1E_u$	$(1/\sqrt{2})(\eta_A\zeta_B - \zeta_A\eta_B)$, $(1/\sqrt{2})(\zeta_A\xi_B - \xi_A\zeta_B)$
${}^3E_u, {}^1E_g$	$(1/\sqrt{2})(\eta_A\zeta_B + \zeta_A\eta_B)$, $(1/\sqrt{2})(\zeta_A\xi_B + \xi_A\zeta_B)$

Table 10. Eigenvalues of the exchange Hamiltonian for the $^{2s+1}T_2(t_2^n)-^{2s+1}T_2(t_2^n)$ pair of D_{4h} symmetry.

Terms	Energies
$^3A_{2u}, {}^1A_{1g}$	$-(2/3)t_\pi^2 \sum_{k=0,1}\left[2F^{(k)}_{A_1A_1}+F^{(k)}_{EE}-2\sqrt{2}F^{(k)}_{A_1E}\right]P_k(s^g,S)$
$^3A_{2u}, {}^1A_{1g}$	$-(2/3)t_\pi^2 \sum_{k=0,1}\left[2F^{(k)}_{A_1A_1}+(5/2)F^{(k)}_{EE}+\sqrt{2}F^{(k)}_{A_1E}+(3/2)F^{(k)}_{T_1T_1}+(3/2)F^{(k)}_{T_2T_2}\right]P_k(s^g,S)$
$^3B_{2u}, {}^1B_{1g}$	$-(2/3)t_\pi^2 \sum_{k=0,1}\left[2F^{(k)}_{A_1A_1}+(5/2)F^{(k)}_{EE}+\sqrt{2}F^{(k)}_{A_1E}-(3/2)F^{(k)}_{T_1T_1}-(3/2)F^{(k)}_{T_2T_2}\right]P_k(s^g,S)$
$^3A_{2g}, {}^1A_{1u}$	$-(2/3)t_\pi^2 \sum_{k=0,1}\left[2F^{(k)}_{A_1A_1}-2F^{(k)}_{EE}+\sqrt{2}F^{(k)}_{A_1E}+(3/2)F^{(k)}_{T_1T_1}-(3/2)F^{(k)}_{T_2T_2}\right]P_k(s^g,S)$
$^3B_{1u}, {}^1B_{2g}$	$-(2/3)t_\pi^2 \sum_{k=0,1}\left[2F^{(k)}_{A_1A_1}-2F^{(k)}_{EE}+\sqrt{2}F^{(k)}_{A_1E}-(3/2)F^{(k)}_{T_1T_1}+(3/2)F^{(k)}_{T_2T_2}\right]P_k(s^g,S)$
$^3E_g, {}^1E_u, {}^3E_u, {}^1E_g$	$-(2/3)t_\pi^2 \sum_{k=0,1}\left[2F^{(k)}_{A_1A_1}-(1/2)F^{(k)}_{EE}-(1/\sqrt{2})F^{(k)}_{A_1E}\right]P_k(s^g,S)$

Note: The functions $P_k(s^g,S)$ are the following: $P_0(s^g,S)=1$, and $P_1(s^g,S)=(1/2)[S(S+1)-2s^g(s^g+1)]$.

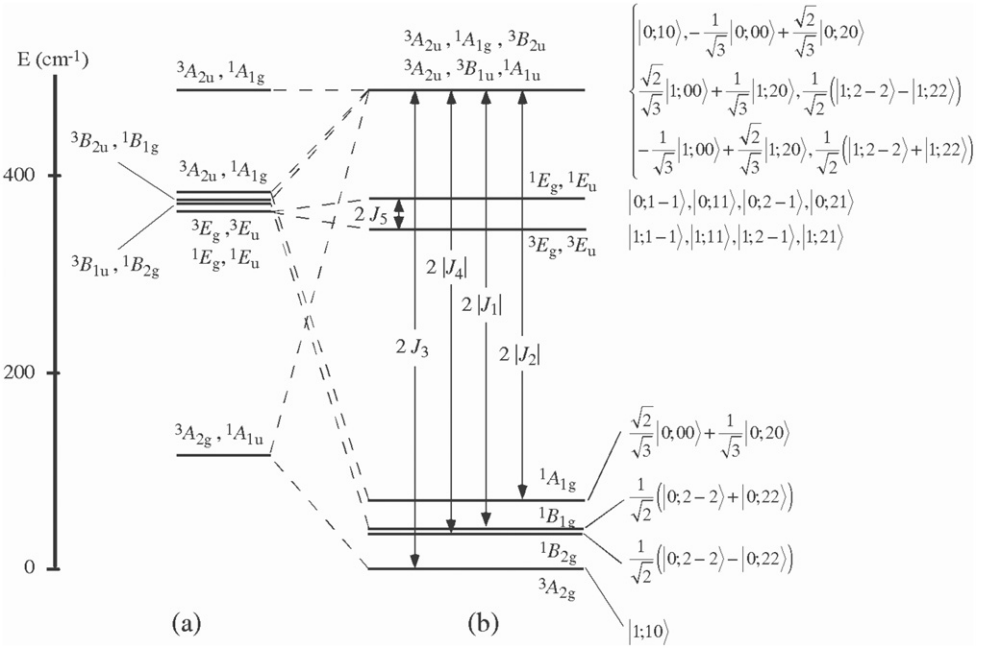

Figure 20. The pattern of the exchange splittings for the D_{4h} cluster: (a) spin-independent splittings and (b) full splittings.

The ferromagnetic splitting of the ground level $^3A_{2g}, {}^1A_{1u}$ is strong (the corresponding parameter $J_3 \approx 235\text{cm}^{-1}$) because J_3 contains only strong ferromagnetic contribution associated with the spin-triplet $^3T_1$ state in the CT spectrum. For this reason, the overall effect of the kinetic exchange is the stabilisation of the ferromagnetic ground state $^3A_{2g}$.

Table 11. Parameters defining the spin-dependent splittings of the energy levels (eigenvalues of the spin-independent part of the exchange Hamiltonian) of the bioctahedral $^2T_2(t_2^1)$–$^2T_2(t_2^1)$ cluster of D_{4h} symmetry.

Level	Parameter	Expression
$^3B_{2u}, {}^1B_{1g}$	J_1	$-2t_\pi^2\left\{\frac{\cos^2[\theta(^1E)]}{\varepsilon_1(^1E)}+\frac{\sin^2[\theta(^1E)]}{\varepsilon_2(^1E)}\right\}$
$^3A_{2u}, {}^1A_{1g}$	J_2	$-(2t_\pi^2/3)\left\{\frac{2\cos^2[\theta(^1A_1)]}{\varepsilon_1(^1A_1)}+\frac{2\sin^2[\theta(^1A_1)]}{\varepsilon_2(^1A_1)}+\frac{\cos^2[\theta(^1E)]}{\varepsilon_1(^1E)}+\frac{\cos^2[\theta(^1E)]}{\varepsilon_2(^1E)}\right\}$
$^3A_{2g}, {}^1A_{1u}$	J_3	$2t_\pi^2\left\{\frac{\cos^2[\theta(^3T_1)]}{\varepsilon_1(^3T_1)}+\frac{\sin^2[\theta(^3T_1)]}{\varepsilon_2(^3T_1)}\right\}$
$^3B_{1u}, {}^1B_{2g}$	J_4	$-2t_\pi^2\left\{\frac{\cos^2[\theta(^1T_2)]}{\varepsilon_1(^1T_2)}+\frac{\sin^2[\theta(^1T_2)]}{\varepsilon_2(^1T_2)}\right\}$
$^{1,3}E_g, {}^{1,3}E_u$	J_5	$(t_\pi^2/2)\left\{\frac{\cos^2[\theta(^3T_1)]}{\varepsilon_1(^3T_1)}+\frac{\sin^2[\theta(^3T_1)]}{\varepsilon_2(^3T_1)}-\frac{\cos^2[\theta(^1T_2)]}{\varepsilon_1(^1T_2)}-\frac{\cos^2[\theta(^1T_2)]}{\varepsilon_1(^1T_2)}\right\}$
$^3A_{2u}, {}^1A_{1g}$	J_6	0

At the same time, the splitting of the first excited level $^{1,3}E_g, {}^{1,3}E_u$ is weak ($J_3 \approx 5\ \mathrm{cm}^{-1}$) due to the competition of ferromagnetic (coming from $^3T_1$ states in the CT spectrum) and antiferromagnetic (coming from $^1T_2$ states in the CT spectrum) contributions. The highest level $^3A_{2u}, {}^1A_{1g}$ remains unsplit ($J_6 = 0$). All other levels undergo strong antiferromagnetic splittings ($J_1 \approx J_2 \approx J_4 \approx -216\,\mathrm{cm}^{-1}$) arising from the uncompensated contributions of different CT spin singlets. It is remarkable that all spin triplets arising from the antiferromagnetically split levels coincide with the highest unsplit level $^3A_{2u}, {}^1A_{1g}$.

The above consideration shows that, in the case of orbitally degenerate ions, one cannot predict (with exception of some special particular situations) the spin of the ground state using only the Goodenough and Kanamori rules [86]. In fact, in the case of orbital degeneracy, both ferromagnetic and antiferromagnetic one-electron transfer processes are operative so that the microscopic calculation of the energy levels becomes inevitable for the elucidation of the overall effect of the exchange interaction.

The ground $^3A_{2g}$ state with $L = 1$ and $M_L = 0$ does not contribute to the orbital part of the magnetic susceptibility in a parallel field ($H||C_4$), so that $\chi_{||}^{\mathrm{orb}} = 0$ in the low-temperature limit (since all $|S, L\, M_L\rangle$ states are the eigenvectors of $\hat{L}_Z$, the TIP does not appear in a parallel field). The first-order orbital contribution in a perpendicular field is also vanishing. At the same time, the second-order contribution to $\chi_{\perp}^{\mathrm{orb}}$ (TIP) is non-zero. As a result, weak magnetic anisotropy with $\chi_{||} < \chi_{\perp}$ can be expected at low temperatures.

The matrix elements $\langle {}^1B_{2g}({}^1B_{1g})|\hat{L}_Z|{}^1B_{2g}({}^1B_{1g})\rangle$ vanish as well as the matrix elements connecting $^1B_{2g}$ and $^1B_{1g}$ with the rest of states. Nevertheless, the states $^1B_{2g}$ and $^1B_{1g}$ contribute to $\chi_{||}^{\mathrm{orb}}$, and this contribution appears in the first order of perturbation theory because $\langle {}^1B_{2g}|\hat{L}_Z|{}^1B_{1g}\rangle \neq 0$ and the gap between $^1B_{2g}$ and $^1B_{1g}$ is rather small ($\approx 0.02\,\mathrm{cm}^{-1}$). The proximity of these two levels takes place due to the fact that the CT states, ^1E and $^1T_2$, are almost degenerate (see Tanabe–Sugano diagram for d^2 ion [100]). On the contrary, $\chi_{\perp}^{\mathrm{orb}}$ appears only as a second-order effect. Therefore, the orbital contribution of the states $^1B_{2g}$ and $^1B_{1g}$ to the overall magnetic susceptibility is strongly anisotropic with $\chi_{||}^{\mathrm{orb}}({}^1B_{2g}, {}^1B_{1g}) >> \chi_{\perp}^{\mathrm{orb}}({}^1B_{2g}, {}^1B_{1g})$.

To illustrate the peculiarities of the magnetic susceptibility arising from the orbital contributions to the magnetic exchange, we have plotted the $\chi_{||}^{\mathrm{orb}}$ versus T and $\chi_{\perp}^{\mathrm{orb}}$ versus T

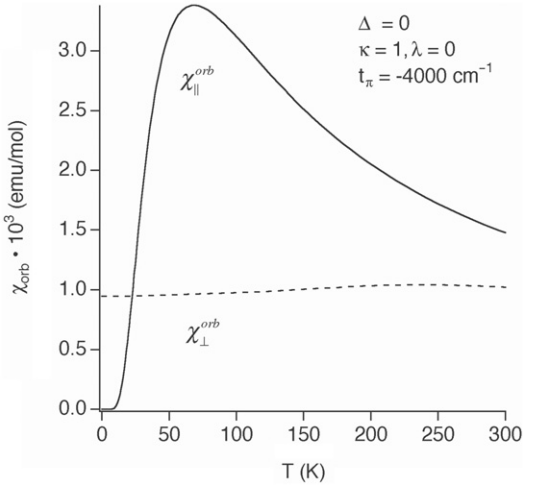

Figure 21. Orbital contribution to the magnetic susceptibility.

dependences in which only the orbital part of Zeeman interaction is taken into account (Figure 21). One can see that $\chi_{\perp}^{\mathrm{orb}}$ is almost temperature independent. On the contrary, $\chi_{||}^{\mathrm{orb}} = 0$ in the low-temperature limit is in conformity with the above qualitative consideration. Then, $\chi_{||}^{\mathrm{orb}}$ rapidly increases with the increase of the temperature and reaches a pronounced maximum at $T \approx 50$ K. This kind of behaviour is evidently explained by the population of the levels ${}^1B_{2g}$ and ${}^1B_{1g}$. Summarising, one can conclude that the exchange Hamiltonian for a corner-shared ${}^2T_2(t_2) - {}^2T_2(t_2)$ pair is fully anisotropic in the sense that $\chi_{||}^{\mathrm{orb}}$ appears as the effect of the first order, meanwhile $\chi_{\perp}^{\mathrm{orb}}$ is a second-order effect.

In the above discussion, it is assumed that the ligand surroundings of the metal ions represent a perfect octahedzon ($\Delta = 0$). Now, let us briefly discuss the case of tetragonally distorted surroundings of the metal ions. Figure 22 shows the energy levels of the pair as the functions of the parameter Δ, provided that $\Delta > 0$. The increase of Δ transforms the ground spin-triplet state $|1, 10\rangle$ formed by the exchange interaction into the paramagnetic mixture of two states, with one being the spin-singlet and another one being the spin triplet. These two states originate from the orbital state $\zeta_A\,\zeta_B$ corresponding to the terms ${}^3A_{2u}$, ${}^1A_{1g}$ of the undistorted system (Table 9). Since the weak $\zeta_A \leftrightarrow \zeta_B$ transfer is neglected, the exchange interaction does not operate within the ground manifold. Both states forming the ground manifold possess $M_L = 0$, so the first-order contributions to $\chi_{||}^{\mathrm{orb}}$ and $\chi_{\perp}^{\mathrm{orb}}$ vanish as well as the second-order contribution to $\chi_{||}^{\mathrm{orb}}$. The second-order contribution to $\chi_{\perp}^{\mathrm{orb}}$ is non-zero, this contribution decreases with the increase of Δ. Therefore, one arrives at the conclusion that at low temperatures $\chi_{\perp} > \chi_{||}$. This means that the low-symmetry crystal field is able to reverse the sign of the magnetic anisotropy produced by the exchange interaction. This conclusion is illustrated by Figure 23 showing the orbital part of the magnetic susceptibility for $\Delta = 150\,\mathrm{cm}^{-1}$. At low temperature, one obtains the TIP contribution $\chi_{\perp}^{\mathrm{orb}}$, meanwhile $\chi_{||}^{\mathrm{orb}}$ tends to 0 when $T \to 0$. The increase of $\chi_{||}^{\mathrm{orb}}$ with the temperature is due to the population of the levels with $M_L = \pm 1$ and $M_L = \pm 2$ that are close to the ground level at $\Delta = 150\ \mathrm{cm}^{-1}$ (Figure 22). On the other hand, the depopulation of the ground level results in the decrease of $\chi_{\perp}^{\mathrm{orb}}$ when $T > 50$–60 K.

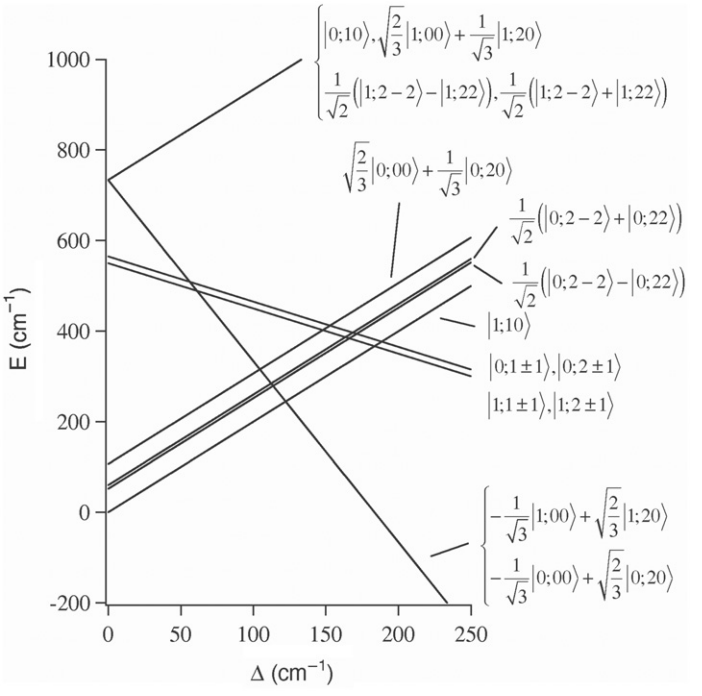

Figure 22. Combined effect of the exchange interaction and positive tetragonal crystal field.

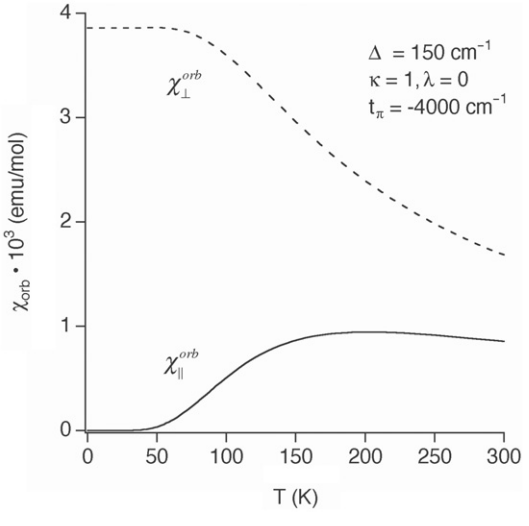

Figure 23. Orbital part of the magnetic susceptibility and influence of the tetragonal crystal field.

In the opposite case of the negative values of Δ, the state $|1,10\rangle$ always remains the ground one; but the ferromagnetic effect is weak because the excited spin singlets are close in energy to the ground state. This result is in line with what one can obtain considering the $[^2E(e^1)]_A \otimes [^2E(e^1)]_B$-exchange problem.

The above discussion demonstrates that the approach based on the use of spherical ITOs provides not only an efficient computational tool, but it is also of great help in the understanding of the magnetic properties of systems containing ions with unquenched orbital angular momenta. Untill now the effect of SO coupling on the magnetic anisotropy has not been analysed. The role of this interaction will be discussed later on in connection with the analysis of the magnetic behaviour of the $[Ti_2Cl_9]^{3-}$ cluster.

6.2. *Orbitally dependent exchange in $[Ti_2Cl_9]^{3-}$*

6.2.1. *Exchange Hamiltonian of a face-shared bioctahedral $^{2s+1}T_2(t_2^n)$–$^{2s+1}T_2(t_2^n)$ cluster*

Now following ref [130] we will apply the technique of the orbitally-dependent Hamiltonian to the analysis of the magnetic properties of the face-shared bioctahedral $d^1(^2T_2) - d^1(^2T_2)$ dimer (D_{3h}). The Ti(III) ions form well-isolated dimers of this kind in the crystal structure of $Cs_3Ti_2Cl_9$ [154,155] and $Cs_3Ti_2Br_9$ [156], whose magnetic and spectroscopic properties were a subject of the discussion for almost two decades [125–130,155]. A spectacular feature of the magnetic behaviour of the $[Ti_2Cl_9]^{3-}$ entity is a significant magnetic anisotropy [155] that indicates the importance of the orbital interactions. This relatively simple system represents a good test for the theory of the orbitally dependent exchange.

The molecular structure of $[Ti_2Cl_9]^{3-}$ and the local coordinate frames associated with the metal sites are shown in Figure 24. It is convenient to introduce the trigonal local coordinates X_A, Y_A, Z_A and X_B, Y_B, Z_B with Z_A (Z_B) axes directed along the C_3 axis. In Figure 24, these frames are shown together with the cubic ones (x_A, y_A, z_A and x_B, y_B, z_B). The molecular frame is chosen to coincide with the local trigonal frame X_A, Y_A, Z_A. The real trigonal forms of t_2 and e orbitals on each metal centre are defined by

$$t_2\text{-basis}\begin{cases} a_2 = d_{Z^2}, \\ \theta_2 = (1/\sqrt{3})\left(-d_{XZ} + \sqrt{2}d_{X^2-Y^2}\right), \\ \varepsilon_2 = (1/\sqrt{3})(-d_{YZ} - \sqrt{2}d_{XY}). \end{cases} \qquad (6.3)$$

$$e\text{-basis}\begin{cases} \theta = (1/\sqrt{3})\left(d_{X^2-Y^2} + \sqrt{2}d_{XZ}\right), \\ \varepsilon = (1/\sqrt{3})\left(-d_{XY} + \sqrt{2}d_{YZ}\right). \end{cases}$$

These orbitals refer to the local trigonal X_i, Y_i, Z_i ($i = A, B$) frames, where the index i is omitted. The θ, ε and θ_2, ε_2 functions are the components of a trigonal e representations. The same notations will be used for the many-electron wave-functions, namely, we use θ_2, ε_2, a_2 for T_2 basis and θ, ε for E basis. In addition, the T_1 basis will be denoted by θ_1, ε_1, a_1.

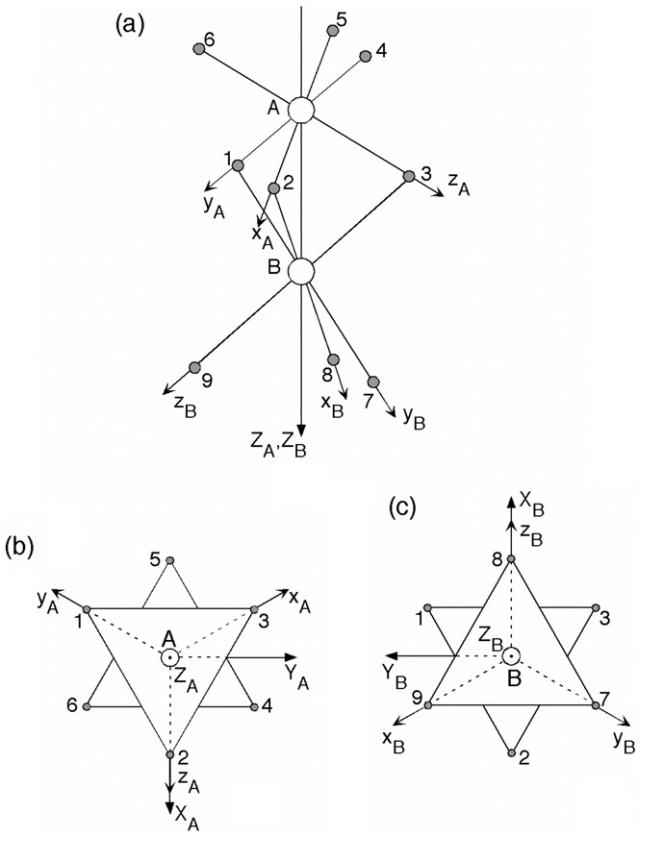

Figure 24. Cartesian cubic and trigonal frames for a face-shared binuclear system: local cubic frames (a), local trigonal frames for the sites A (b) and B (c).

The real trigonal basis $(\theta_2, \varepsilon_2, a_2, \theta_1, \varepsilon_1, a_1, \theta, \varepsilon)$ is related to the cubic one $(\xi, \eta, \zeta, \alpha, \beta, \gamma, u, \mathrm{v})$ as follows:

$$
\begin{aligned}
T_1\text{-basis} &\begin{cases} \theta_1 = (1/\sqrt{6})\,(2\gamma - \alpha - \beta), \\ \varepsilon_1 = (1/\sqrt{2})\,(\alpha - \beta), \\ a_1 = \left(1/\sqrt{3}\right)(\alpha + \beta + \gamma). \end{cases} \\
T_2\text{-basis} &\begin{cases} \theta_2 = (1/\sqrt{6})(2\zeta - \xi - \eta), \\ \varepsilon_2 = (1/\sqrt{2})(\xi - \eta), \\ a_2 = (1/\sqrt{3})(\xi + \eta + \zeta). \end{cases} \\
\text{E-basis} &\begin{cases} \theta = u \\ \varepsilon = \upsilon. \end{cases}
\end{aligned}
\tag{6.4}
$$

Let us assume that the ground ${}^{2s+1}T_2$ term of each metal ion originates only from the t_2^n electronic configuration, so that solely the transfer processes involving the electrons of the t_2 shells should be taken into account. Then t here are the following two non-vanishing (under the trigonal symmetry conditions) transfer integrals describing the $t_2^A \leftrightarrow t_2^B$ electron

hopping: $t(a_2^A, a_2^B) \equiv t_a$ and $t(\theta_2^A, \theta_2^B) = t(\varepsilon_2^A, \varepsilon_2^B) \equiv t_e$. The kinetic exchange Hamiltonian for the $[^{2s+1}T_2(t_2^n)]_A - [^{2s+1}T_2(t_2^n)]_B$ pair of D_{3h} symmetry can be presented in the form given by Equations (5.20), in which the operators $\hat{R}_k$ represent the sum of three contributions

$$\hat{R}_k = \hat{R}_k^{(a)} + \hat{R}_k^{(ae)} + \hat{R}_k^{(e)}. \tag{6.5}$$

Here $\hat{R}_k^{(a)}$ is the term proportional to t_a^2. This term can be expressed as

$$\hat{R}_k^{(a)} = -(2/3)t_a^2\Big[F^{(k)}_{A_1A_1}\hat{O}^A_{A_1}\hat{O}^B_{A_1} + 2F^{(k)}_{T_2T_2}\hat{O}^A_{T_2a_2}\hat{O}^B_{T_2a_2} + \sqrt{2}F^{(k)}_{A_1T_2}\Big(\hat{O}^A_{A_1}\hat{O}^B_{T_2a_2} + \hat{O}^A_{T_2a_2}\hat{O}^B_{A_1}\Big)\Big], \tag{6.6}$$

where the short notation $F^{(K)}_{\Gamma\Gamma'}(t_2\,t_2\,t_2\,t_2) \equiv F^{(K)}_{\Gamma\Gamma'}$ is used. The term proportional to $t_a\,t_e$ is given by

$$\begin{aligned}\hat{R}_k^{(ae)} = -(2/3)t_at_e\Big[&2F^{(k)}_{EE}\Big(\hat{O}^A_{E\theta}\hat{O}^B_{E\theta} + \hat{O}^A_{E\varepsilon}\hat{O}^B_{E\varepsilon}\Big) + 3F^{(k)}_{T_1T_1}\Big(\hat{O}^A_{T_1\theta_1}\hat{O}^B_{T_1\theta_1} + \hat{O}^A_{T_1\varepsilon_1}\hat{O}^B_{T_1\varepsilon_1}\Big)\\ &+ F^{(k)}_{T_2T_2}\Big(\hat{O}^A_{T_2\theta_2}\hat{O}^B_{T_2\theta_2} + \hat{O}^A_{T_2\varepsilon_2}\hat{O}^B_{T_2\varepsilon_2}\Big)\\ &-\sqrt{2}F^{(k)}_{ET_2}\Big(\hat{O}^A_{E\theta}\hat{O}^B_{T_2\theta_2} + \hat{O}^A_{T_2\theta_2}\hat{O}^B_{E\theta} + \hat{O}^A_{E\varepsilon}\hat{O}^B_{T_2\varepsilon_2} + \hat{O}^A_{T_2\varepsilon_2}\hat{O}^B_{E\varepsilon}\Big)\Big].\end{aligned} \tag{6.7}$$

Finally, the term proportional to t_e^2 is the following:

$$\begin{aligned}\hat{R}_k^{(e)} = -(2/3)t_e^2\Big[&2F^{(k)}_{A_1A_1}\hat{O}^A_{A_1}\hat{O}^B_{A_1} + F^{(k)}_{EE}\Big(\hat{O}^A_{E\theta}\hat{O}^B_{E\theta} + \hat{O}^A_{E\varepsilon}\hat{O}^B_{E\varepsilon}\Big) + 3F^{(k)}_{T_1T_1}\hat{O}^A_{T_1a_1}\hat{O}^B_{T_1a_1}\\ &+ F^{(k)}_{T_2T_2}\Big(2\hat{O}^A_{T_2\theta_2}\hat{O}^B_{T_2\theta_2} + 2\hat{O}^A_{T_2\varepsilon_2}\hat{O}^B_{T_2\varepsilon_2} + \hat{O}^A_{T_2a_2}\hat{O}^B_{T_2a_2}\Big) - \sqrt{2}F^{(k)}_{A_1T_2}\Big(\hat{O}^A_{A_1}\hat{O}^B_{T_2a_2} + \hat{O}^A_{T_2a_2}\hat{O}^B_{A_1}\Big)\\ &+\sqrt{2}F^{(k)}_{ET_2}\Big(\hat{O}^A_{E\theta}\hat{O}^B_{T_2\theta_2} + \hat{O}^A_{T_2\theta_2}\hat{O}^B_{E\theta} + \hat{O}^A_{E\varepsilon}\hat{O}^B_{T_2\varepsilon_2} + \hat{O}^A_{T_2\varepsilon_2}\hat{O}^B_{E\varepsilon}\Big)\Big].\end{aligned} \tag{6.8}$$

The orbital matrices $\hat{\boldsymbol{O}}_{\Gamma\gamma}$ defined with the real trigonal T_2 basis are given in Table 12. The parameters $F^{(k)}_{\Gamma\Gamma'}$ for $\big[^2T_2(t_2^1)\big]_A - \big[^2T_2(t_2^1)\big]_B$dimer (the case of $[Ti_2Cl_9]^{3-}$) are given by Equation (6.1).

6.2.2. *Energy pattern and magnetic anisotropy*

Before proceeding to the analysis of the magnetic properties of $[Ti_2Cl_9]^{3-}$, we will discuss the magnetic anisotropy caused by the orbitally dependent exchange. At this step, only the exchange interaction will be taken into account. In the evaluation of the energy pattern and subsequent calculations of the magnetic properties of $[Ti_2Cl_9]^{3-}$, we assume the same A, B, C and Dq values for Ti(II) ion as those used in Section 5. The pattern of the exchange splittings can be evaluated either by the diagonalisation of the exchange Hamiltonian expressed in terms of irreducible cubic tensors and spin operators, with the aid of the symmetry-adapted orbital basis given in Table 13, or by the diagonalisation of the exchange Hamiltonian expressed in terms of spherical ITOs. These two possibilities provide two alternative ways of classification of the eigenvectors, which can be referred to as $S\,\Gamma$-classification and $S, L\,M_L$-classification. Note that under the trigonal crystal field splitting of the ground $^2T_2$ term of the Ti(III) ion, the ground manifold $\big[^2T_2(t_2^1)\big]_A \otimes \big[^2T_2(t_2^1)\big]_B$ splits into the groups of states $(^2A_1)_A \otimes (^2A_1)_B$ ($a \otimes a$-group),

Table 12. The orbital matrices $\hat{\boldsymbol{O}}_{\Gamma\gamma}$ with $\Gamma = A_1,\ E(\gamma = \theta, \varepsilon),\ T_1(\gamma = \theta_1, \varepsilon_1, a_1),\ T_2(\gamma = \theta_2, \varepsilon_2, a_2)$ defined with the real trigonal T_2 basis $(\theta_2, \varepsilon_2, a_2)$.

$$\hat{\boldsymbol{O}}_{A_1} = \begin{pmatrix} 1 & 0 & 0 \\ 0 & 1 & 0 \\ 0 & 0 & 1 \end{pmatrix}$$

$$\hat{\boldsymbol{O}}_{E\theta} = \begin{pmatrix} 1/2 & 0 & 1/\sqrt{2} \\ 0 & -1/2 & 0 \\ 1/\sqrt{2} & 0 & 0 \end{pmatrix}$$

$$\hat{\boldsymbol{O}}_{E\varepsilon} = \begin{pmatrix} 0 & -1/2 & 0 \\ -1/2 & 0 & 1/\sqrt{2} \\ 0 & 1/\sqrt{2} & 0 \end{pmatrix}$$

$$\hat{\boldsymbol{O}}_{T_1\theta_1} = \begin{pmatrix} 0 & 0 & 0 \\ 0 & 0 & 1/\sqrt{2} \\ 0 & -1/\sqrt{2} & 0 \end{pmatrix}$$

$$\hat{\boldsymbol{O}}_{T_1\varepsilon_1} = \begin{pmatrix} 0 & 0 & -1/\sqrt{2} \\ 0 & 0 & 0 \\ 1/\sqrt{2} & 0 & 0 \end{pmatrix}$$

$$\hat{\boldsymbol{O}}_{T_1 a_1} = \begin{pmatrix} 0 & 1/\sqrt{2} & 0 \\ -1/\sqrt{2} & 0 & 0 \\ 0 & 0 & 0 \end{pmatrix}$$

$$\hat{\boldsymbol{O}}_{T_2\theta_2} = \begin{pmatrix} 1/\sqrt{3} & 0 & -1/\sqrt{6} \\ 0 & -1/\sqrt{3} & 0 \\ -1/\sqrt{6} & 0 & 0 \end{pmatrix}$$

$$\hat{\boldsymbol{O}}_{T_2\varepsilon_2} = \begin{pmatrix} 0 & -1/\sqrt{3} & 0 \\ -1/\sqrt{3} & 0 & -1/\sqrt{6} \\ 0 & -1/\sqrt{6} & 0 \end{pmatrix}$$

$$\hat{\boldsymbol{O}}_{T_2 a_2} = \begin{pmatrix} -1/\sqrt{6} & 0 & 0 \\ 0 & -1/\sqrt{6} & 0 \\ 0 & 0 & 2/\sqrt{6} \end{pmatrix}$$

Table 13. Symmetry adapted orbital basis for the face-shared ${}^2T_2(t_2^1) - {}^2T_2(t_2^1)$ bioctahedron, related terms and corresponding groups of states in a trigonal crystal field.

Terms	Symmetry-adapted orbital basis	Group of states
$1,{}^3A_2''[{}^1A_1']$	$a_2^A a_2^B$	$a \otimes a$
$2,{}^3E''[{}^1E']$	$(1/\sqrt{2})(\varepsilon_2^A a_2^B + a_2^A \varepsilon_2^B),\ (1/\sqrt{2})(\theta_2^A a_2^B + a_2^A \theta_2^B)$	$a \otimes e$
${}^3E'[{}^1E'']$	$(1/\sqrt{2})(\theta_2^A a_2^B - a_2^A \theta_2^B),\ (1/\sqrt{2})(\varepsilon_2^A a_2^B - a_2^A \varepsilon_2^B)$	
$2,{}^3A_2''[{}^1A_1']$	$(1/\sqrt{2})(\theta_2^A \theta_2^B + \varepsilon_2^A \varepsilon_2^B)$	$e \otimes e$
${}^3A_2'[{}^1A_1'']$	$(1/\sqrt{2})(\varepsilon_2^A \theta_2^B - \theta_2^A \varepsilon_2^B)$	
$1,{}^3E''[{}^1E']$	$(1/\sqrt{2})(\theta_2^A \varepsilon_2^B + \varepsilon_2^A \theta_2^B),\ (1/\sqrt{2})(\varepsilon_2^A \varepsilon_2^B - \theta_2^A \theta_2^B)$	

$({}^2A_1)_A \otimes ({}^2E)_B, ({}^2E)_A \otimes ({}^2A_1)_B$, ($a \otimes e$-group) and $({}^2E)_A \otimes ({}^2E)_B$ ($e \otimes e$-group), and each term in Table 13 arises from one of this group (last line in Table 13).

Figure 25 shows the energy levels as a function of the ratio t_e/t_a in the range $-1 \le t_e/t_a \le 1$. One can see that the energy pattern is symmetric with respect to the change of the sign of t_e/t_a. In a wide range of t_e/t_a, the ground state is the spin-singlet ${}^1A_1'$. Only at $|t_e/t_a| > 0.9$ the spin-triplet ${}^3E'$ (or ${}^3E''$) becomes the ground state. The highest excited state is accidentally degenerate and comprises several multiplets, mainly spin triplets. It is to be noted that the energy gap between highest and lowest levels is almost independent of the ratio t_e/t_a (except the terminal parts of the diagram) and mainly depends on t_a.

The following three special high-symmetric cases are seen in Figure 25: a pseudo-spherical case ($t_e/t_a = 1$), a spherical case ($t_e/t_a = -1$) and an axial case ($t_e/t_a = 0$). In each of these cases the energy pattern exhibits a high degree of accidental degeneracy. This is a clear indication that the effective exchange Hamiltonian belongs to a more general

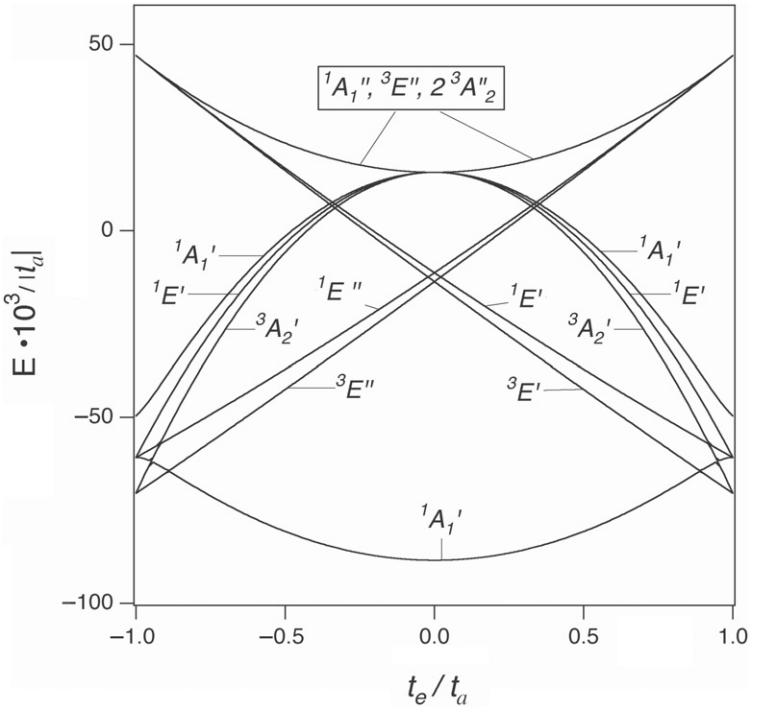

Figure 25. Dependence of the energy pattern formed by the magnetic exchange in the face-shared ${}^2T_2(t_2^1) - {}^2T_2(t_2^1)$ dimer on the ratio t_e/t_a.

symmetry group than the point symmetry group D_{3h}. The terms pseudo-spherical, spherical and axial are closely related to the magnetic anisotropy and will be clarified below.

Let us consider first the pseudo-spherical and spherical limits, which are shown in the left and right sides of Figure 26, correspondingly. Since the diagram is symmetric, the energies of the levels in these two cases are the same. In both limits the energy pattern includes five accidentally degenerate levels, with the corresponding energies being determined by the following four parameters:

$$J_1 = t_a^2 F({}^3T_1), \quad J_2 = -t_a^2 F({}^1T_2), \quad J_3 = -t_a^2 F({}^1E), \quad J_4 = -t_a^2 F({}^1A_1). \tag{6.9}$$

It is to be noted that $F({}^1T_2) \approx F({}^1E)$ because the reduced states ${}^1T_2$ and ${}^1E$ are almost degenerate. For this reason the second and the third excited levels are almost degenerate. Figure 26 shows that in spite of the fact that the energies at $t_e/t_a = 1$ and $t_e/t_a = -1$ are the same, the wave-functions are different. This leads to a drastic difference in the magnetic behaviour of the system in these two limits. In the pseudo-spherical limit ($t_e/t_a = 1$) the ground level with $S = 1$ comprises the orbital singlet ${}^3A_2'$, and the orbital doublet ${}^3E'$, which can be associated with the wave-functions $|1, 10\rangle$, and $|1, 2 \pm 1\rangle$, respectively. One can see that $|1, 2 \pm 1\rangle$ states contribute strongly to $\chi_{||}$, while the matrix elements of $\hat{L}_X$ and $\hat{L}_Y$ disappear within the ground ${}^3A_2'$, ${}^3E'$ manifold. Inspecting in the same way the remaining $|S, L\, M_L\rangle$ states, one can see that the operator $\hat{L}_Z$ has non-vanishing matrix elements within all levels with $M_L \neq 0$ ($L = 1, 2$).

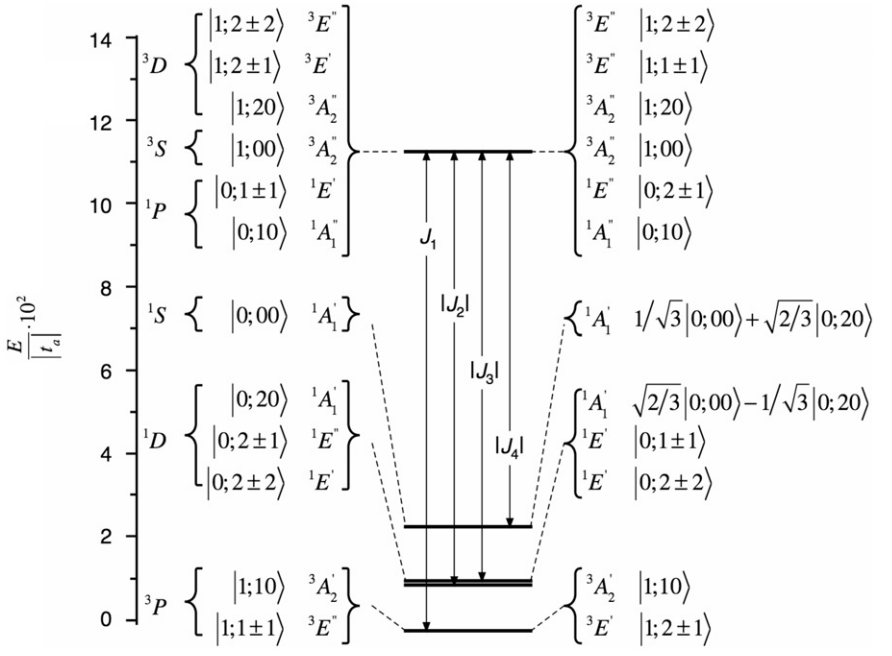

Figure 26. The pattern of the exchange splittings in the spherical (left-side labels) and pseudo-spherical (right-side labels) limits.

On the contrary, the matrix elements of $\hat{L}_X$ and $\hat{L}_Y$ vanish within each level. Moreover, these operators do not mix the different levels belonging to the low-lying group, which includes the ground and the two excited levels. Only the matrix elements connecting these levels with the highest highly degenerate level are non-vanishing, giving rise to the relatively small second-order orbital contributions to $\chi_\perp$. It means that, in this case, the magnetic anisotropy is strong with $\chi_{||} > \chi_\perp$. Finally, it is notable that each level in the case $t_e/t_a = 1$ is $(2L+1)$-fold degenerate like in the system of spherical symmetry, but it does not correspond to a definite value of $L = M_L^{\max}$ (e.g. the values $L = 1$ and $L = 2$ are present in the ground state with $M_L = -1, 0, 1$). For this reason, we refer to this case as pseudo-spherical limit. Indeed, in this case the system is strongly magnetically anisotropic. It is remarkable, however, that the pseudo-spherical limit occurs under the 'spherical' condition ($t_a = t_e$) for the transfer integrals.

The main feature of the energy pattern in the spherical limit ($t_e/t_a = -1$) is that each level can be associated with one or several atomic SL terms. In fact, the ground level comprises accidentally degenerate states $^3A_2'(|1,10\rangle)$ and $^3E''(|1,1\pm1\rangle)$ and thus can be regarded as an atomic term with $L = 1$ and $S = 1$ (^3P-term), the first excited state represents a ^1D term, etc. This means that, as distinguished from the previous case, the system at $t_e/t_a = -1$ is magnetically isotropic. Therefore, this case can be referred to as true spherical limit.

The last special case is the axial limit ($t_e = 0$). The corresponding energy pattern is shown in Figure 27. The ground state is the orbital and spin singlet $^1A_1'$ that corresponds

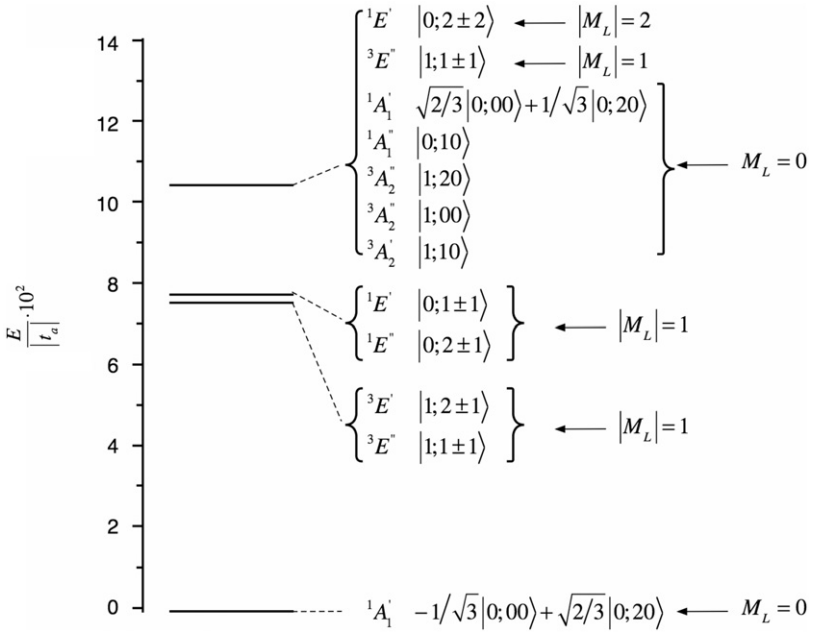

Figure 27. The pattern of the exchange splittings in the axial limit.

to the wave-functions $-\sqrt{1/3}|0,00\rangle + \sqrt{2/3}|0,20\rangle$. The first excited group of levels consists of two closely spaced sublevels. One of them (first excited level) comprises spin triplets $^3E'(|1,2\pm1\rangle)$, $^3E''(|1,1\pm1\rangle)$ and the second excited level includes spin singlets $^1E'(|0,1\pm1\rangle)$, $^1E''(|0,2\pm1\rangle)$. Finally, the highest level comprises both spin-triplets and spin-singlets. It should be noted that this energy scheme is similar to that obtained in [126], but in [126] the spin-triplets $^3E', ^3E''$ and the spin-singlets $^1E', ^1E''$ were found to be accidentally degenerate because the differences between the energies of different CT states were neglected. In the low-temperature limit $\chi_{||} = 0$ because in the ground state $M_L = 0$ and $S = 0$. At the same time, the perpendicular magnetic susceptibility appears as a TIP due to the mixing of the ground state with the excited states $|0,2\pm1\rangle$ ($^1E''$) by the orbital part of Zeeman interaction. We thus find that $\chi_{||} < \chi_{\perp}$, that is the anisotropy has the opposite sign compared to the pseudo-spherical case. Note that $\chi_{||} < \chi_{\perp}$ not only in the axial limit but also for all t_e/t_a in the range $|t_e/t_a| < 0.9$ (Figure 25), where the ground term is $^1A_1'$ (superposition of $|0,00\rangle$ and $|0,20\rangle$). At the same time, $\chi_{||} > \chi_{\perp}$ for the ground terms $^3E''(t_e/t_a < -0.9)$ or $^3E'(t_e/t_a > 0.9)$ possessing $M_L = \pm1$.

In all cases, with the exception of the true spherical limit, the magnetic anisotropy is axial (the energies depend on $|M_L|$) and dependent on the ratio t_e/t_a. In this view, it should be noted that we use the term 'axial' for the limiting case $t_e = 0$ only to emphasize the axial interrelation between t_e and t_a. One can also note that in all cases the states of the system are the eigenvectors of $\hat{L}_Z$, and hence no second-order Zeeman effect is possible in the parallel field.

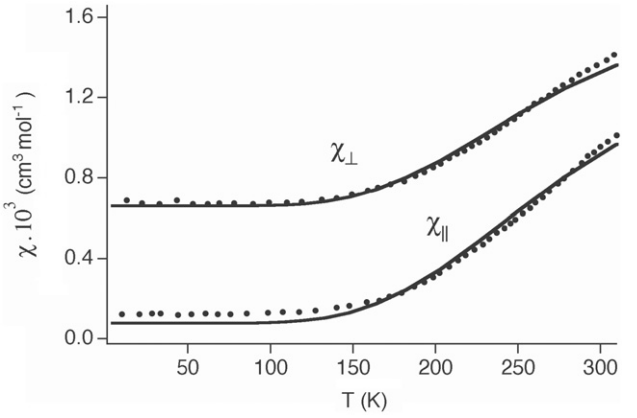

Figure 28. Magnetic behaviour of the $[Ti_2Cl_9]^{3-}$ unit, comparison with the theoretical curve (solid line) calculated with $t_a = -5208\ cm^{-1}$, $\Delta = -320\ cm^{-1}$ and $\kappa = 0.71$.

6.2.3. *Magnetic behaviour of the $[Ti_2Cl_9]^{3-}$ binuclear unit*

The first study of magnetic and spectroscopic properties of the salts $[M_2X_9]^{3-}$ (X = Br, I) containing first-row transition metal ions were reported in [154]. Later on [155], a detailed magnetic and spectroscopic study on crystalline samples of $Cs_3Ti_2Cl_9$ was performed. It was observed that the infrared absorption spectra exhibits a broad featureless band located in the region 800–3000 cm^{-1} that cannot be assigned to a single Ti(III) ion transition. The temperature dependencies of $\chi_{||}$ and $\chi_{\perp}$ measured in [155] (dotted lines in Figure 28) indicated that the low-temperature magnetic susceptibility is small and strongly anisotropic with $\chi_{\perp} > \chi_{||}$. A remarkable feature of the experimental data is that the magnetic anisotropy decreases with the increase of temperature. Both $\chi_{||}$ and $\chi_{\perp}$ decrease when the samples cool down and they become temperature independent at $T < 100$ K. These data clearly show that the ground state of the pair is non-magnetic.

The measurements of the infrared reflectivity from a single crystal of $Cs_3Ti_2Cl_9$ showed the broad signals between 350 and 950 cm^{-1} [157]. Since no vibrational transitions could be expected in this energy range, these signals are of the magnetic origin indicating that the first excited level has the energy of at least 450 cm^{-1}. A similar conclusion was made for a polycrystalline sample of $Rb_3Ti_2Br_9$ on the basis of the INS experiments exhibiting a broad band of magnetic origin between 400 and 600 cm^{-1} [157].

Some preliminary remarks concerning the relevant values of the key parameters are to be made. First, the results of the extended Hückel calculations performed in [126] have demonstrated that $t_a^2 \gg t_e^2$ (axial limit) and t_e and t_a are of opposite signs. This result is consistent with the fact that the t_a transfer corresponds to a strong (due to the short intermetallic distance) through-space interaction (Figure 29), whereas the t_e transfer is responsible for the weaker through-ligand interaction. The conclusion about strong difference in the magnitudes of t_e and t_a has been confirmed by the *ab initio* calculations of Ceulemans *et al.* [127–129]. In [127], the ratio t_a/t_e was roughly estimated as $t_a/t_e \approx -6.5$ (-7 in [128,129]). This corresponds to $t_e/t_a \approx -0.154$. In [130], this ratio was used in the best-fit procedure.

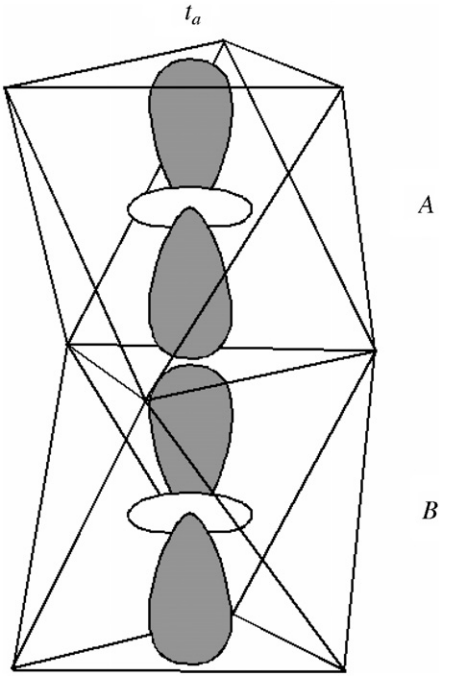

Figure 29. Overlap scheme associated with the t_a transfer.

Since the ratio t_e/t_a is close to the axial limit, it is worthwhile to inspect the effect of the trigonal field in this limit. Figure 30 shows that the negative trigonal field does not change the ground state $^1A_1'$ leading only to its additional stabilisation. The spin triplet $^3A_2''$ arising from the highest group of levels is stabilised in the same way, so in a strong crystal field limit the pair of the levels $^1A_1'$, $^3A_2''$ arising from the $a \times a$-group (Table 13) proves to be well isolated. Provided strong positive trigonal field, the ground level is accidentally degenerate comprising the states $^1A_1'$, $^1E'$, $^3A_2'$, $^3E''$, $^3A_2''$, $^1A_1''$, which arise from the $e \times e$ group. This degeneracy is obviously due to the fact that only the electron transfer of the e–e type is able to split the $e \times e$ group, but such transfer is excluded in the axial limit. At low temperature, $[Ti_2Cl_9]^{3-}$ exhibits almost diamagnetic behaviour, so one can expect the crystal field is negative and the diamagnetic state $^1A_1'$ is the ground one. Note that this conclusion is common for all cited theoretical studies of $[Ti_2Cl_9]^{3-}$. For this reason, one can consider only the values $\Delta < 0$ in the best-fit procedure.

Figure 30 gives some qualitative hints about the influence of the trigonal crystal field on the magnetic behaviour. First, one can see that all wave-functions depicted in Figure 30 are the eigenvectors of $\hat{L}_Z$, so that first-order Zeeman splitting as well as the TIP contribution vanish within the ground level and therefore $(\chi_{||})_{T\to 0} = 0$. At the same time, $(\chi_{\perp})_{T\to 0}$ appears as a second-order effect due to the mixing of the ground $^1A_1'$ term with the orbital doublets $^1E'$ and $^1E''$. Since $^1A_1'$ and $^1E'$, $^1E''$ terms belong to $a \times a$ and $a \times e$ groups, respectively, the $^1A_1' - ^1E'$, $^1E''$ gap linearly increases with the increase of $|\Delta|$. As a consequence, the value $(\chi_{\perp})_{T\to 0}$ is expected to decrease with the increase of the trigonal

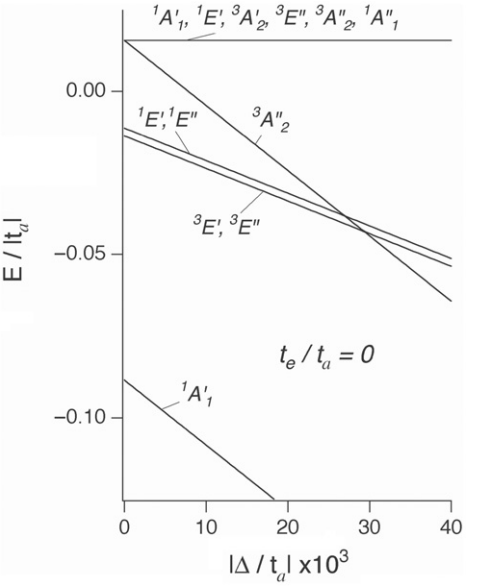

Figure 30. Influence of the negative trigonal field on the energy pattern in the axial limit.

field. Inclusion of SO coupling leads to a small admixture of the magnetic states to the ground diamagnetic level and as a result $(\chi_{||})_{T\to 0}$ becomes non-vanishing.

In the best-fit procedure in [130] the values for the cubic crystal field and Racah parameters for the Ti(II) ion (reduced state) are given in Section 4, the value $\lambda = 155\,\mathrm{cm}^{-1}$ for a free Ti(III) ion [5] is also adopted. Finally, three parameters t_a, Δ and κ are varied in the fitting of the magnetic data, with Δ being negative in accordance with the above arguments. The best-fit was achieved for $t_a = -5208\,\mathrm{cm}^{-1}$, $\Delta = -320\,\mathrm{cm}^{-1}$ and $\kappa = 0.71$. The $\chi_{||}$ versus T and $\chi_{\perp}$ versus T curves calculated with the set of the best-fit parameters are shown in Figure 28 (solid lines) along with the above-described experimental ones. The theoretical curve for $\chi_{\perp}$ is in a good agreement with the experimental data in the low-temperature region (below 170 K). The calculated $\chi_{||}$ at low temperatures is also in a satisfactory agreement with the experimental values. It is also remarkable that the theory reproduces the slopes of $\chi_{||}$ and $\chi_{\perp}$. Finally, it is seen that, in a good agreement with the experimental data, the calculated magnetic anisotropy remains constant below 100 K and decreases with the increase of T in the high-temperature region ($T > 150$ K).

Figure 31 shows the energy scheme calculated (without taking into account the SO coupling) with the set of the best fit parameters. The ground state is $^1A'_1$, and the first excited state $^3A''_2$ is separated by the gap 706 cm^{-1} from the ground one ($a \times a$-group). The next four orbital doublets $^3E''$, $^1E''$, $^3E'$ and $^1E'$ ($a \times e$-manifold) fill the gap that is approximately $135\,\mathrm{cm}^{-1}$. This group of levels is close to the level $^3A''_2$. Finally, the $e \times e$-group of levels forms a narrow band at about $1340\,\mathrm{cm}^{-1}$.

6.2.4. *Discussion of the rival models for the exchange in* $[Ti_2Cl_9]^{3-}$

To understand the magnetic behaviour of $[Ti_2Cl_9]^{3-}$, Briat *et al.* [155] employed the theoretical model proposed by Kahn [158]. This model takes into account the local

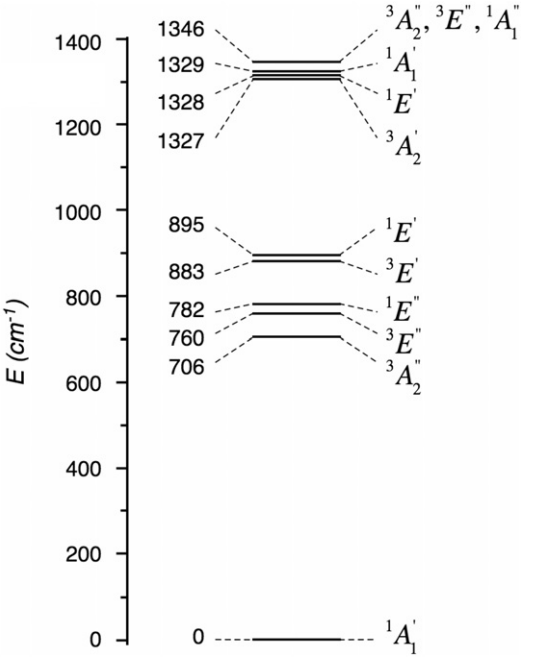

Figure 31. Energy pattern of the $[Ti_2Cl_9]^{3-}$ unit calculated with the set of the best fit parameters.

trigonal crystal field stabilising the orbital singlet of each Ti(III) ion, the SO coupling, the isotropic magnetic exchange and the orbit–orbit interaction of the form $-K\hat{\boldsymbol{l}}_A\hat{\boldsymbol{l}}_B$. Although this model does not take into account all relevant terms involved in the orbitally dependent exchange Hamiltonian, it provided an important indication on the range of parameters. Particularly, the gap between $^1A_1'$ and $^3A_2''$ was estimated to be around 630 cm^{-1}, this value provides a satisfactory explanation of the slope of $\chi_{||}$ versus T and $\chi_{\perp}$ versus T curves observed at $T > 100$ K.

A more comprehensive model was developed by Drillon and Georges [125]. This model was based on the approach proposed by these authors to solve the problem of the kinetic exchange in the orbitally degenerate systems [124]. The orbitally dependent kinetic exchange, the SO coupling and trigonal crystal field were included in the model. In [125] the cubic one-electron basis was used, in which there are two non-vanishing (under D_{3h} symmetry) transfer integrals $t \equiv t(\xi^A, \xi^B) = t(\eta^A, \eta^B) = t(\zeta^A, \zeta^B)$ (diagonal transfer) and $t' \equiv t(\xi^A, \eta^B) = t(\eta^A, \zeta^B) = t(\xi^A, \zeta^B)$ (off-diagonal transfer). These transfer integrals are illustrated by Figure 32. Using Equation (6.4), one finds the following relationship between the transfer integrals defined in trigonal and cubic bases:

$$t_a = t + 2t', \quad t_e = t - t'. \tag{6.10}$$

In [125] the crossing transfer integral was neglected ($t' = 0$), and this assumption is equivalent to the pseudo-spherical limit ($t_e/t_a = 1$) in our terminology. Within this approximation, the kinetic exchange Hamiltonian was found to contain only the scalar

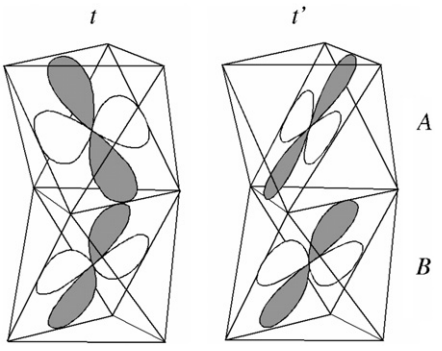

Figure 32. Overlap schemes associated with the diagonal t (a) and off-diagonal t' (b) transfer integrals.

products, namely, $\hat{\boldsymbol{l}}_A\hat{\boldsymbol{l}}_B$, $(\hat{\boldsymbol{l}}_A\hat{\boldsymbol{l}}_B)^2$, $\hat{\boldsymbol{l}}_A\hat{\boldsymbol{l}}_B\hat{\boldsymbol{s}}_A\hat{\boldsymbol{s}}_B$, $(\hat{\boldsymbol{l}}_A\hat{\boldsymbol{l}}_B)^2\ \hat{\boldsymbol{s}}_A\hat{\boldsymbol{s}}_B$ and $\hat{\boldsymbol{s}}_A\hat{\boldsymbol{s}}_B$. For this reason in [125] the kinetic exchange Hamiltonian was regarded as fully isotropic, and LS labels ($L = 0, 1, 2$, $S = 0, 1$) for its eigenvalues were used. At the same time, according to [125], the inclusion of the crossing transfer terms ($t' \neq 0$) should lead to the magnetic anisotropy due to the appearance of the contributions like $\hat{l}_Z^A\,\hat{l}_Z^B$, etc. Since the crossing transfer terms were regarded as small corrections, these authors arrived at the conclusion that the exchange anisotropy was a minor effect and the main reason for the observed anisotropy of $[Ti_2Cl_9]^{3-}$ was the combined action of trigonal crystal field and SO coupling, i.e. the single-ion anisotropy. This conclusion is in a clear contradiction with the results of [130] so far discussed. In fact, we have shown that the exchange Hamiltonian is fully anisotropic with $\chi_\perp < \chi_{||}$ even providing $t' = 0$. We have also shown that the inclusion of the crossing terms tends to change the sign of the anisotropy. This means that the crossing terms cannot be regarded as the only source of the exchange anisotropy.

In order to clarify the origin of this discrepancy, let us analyse a selected orbital contribution to the kinetic exchange Hamiltonian, defined in the complex trigonal basis

$$-2t_a^2F^{(0)}_{T_1T_1}\left(\hat{O}^A_{T_1a_1}\hat{O}^B_{T_1a_1} + \hat{O}^A_{T_1\theta_1}\hat{O}^B_{T_1\theta_1} + \hat{O}^A_{T_1\varepsilon_1}\hat{O}^B_{T_1\varepsilon_1}\right). \tag{6.11}$$

This contribution originates from the terms $\hat{R}_0^{(ae)}$ and $\hat{R}_0^{(e)}$ provided that $t_e = t_a$. One can present this term as

$$J\left(\hat{l}_Z^A\hat{l}_Z^B + \hat{l}_X^A\hat{l}_X^B + \hat{l}_Y^A\hat{l}_Y^B\right), \tag{6.12}$$

where $J = -2\ t_a^2\ F^{(0)}_{T_1\,T_1}$. This expression has a form of a scalar product $\hat{\boldsymbol{l}}_A\hat{\boldsymbol{l}}_B$ but, in fact, it is not a scalar product, because $\hat{\boldsymbol{l}}_A$ and $\hat{\boldsymbol{l}}_B$ are defined in different local trigonal coordinate frames rotated with respect to each other by the angle π around the common trigonal Z_A, Z_B axis. Transforming the operator $\hat{\boldsymbol{l}}_B$ to the molecular frame one arrives at the anisotropic operator

$$J\left(-\hat{\boldsymbol{l}}_A\hat{\boldsymbol{l}}_B + 2\hat{l}_Z^A\hat{l}_Z^B\right). \tag{6.13}$$

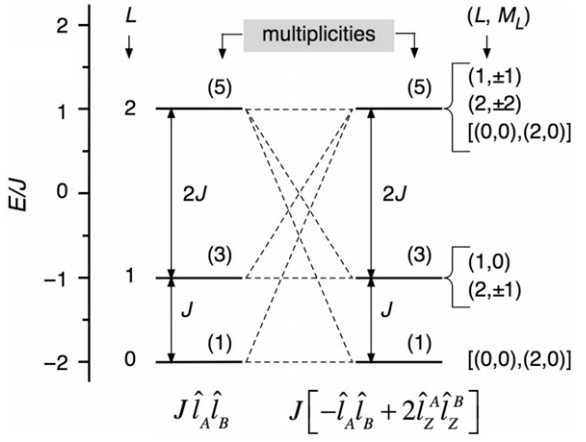

Figure 33. Correlation diagram for the isotropic (a) and anisotropic (b) operators of orbital interactions provided that $J > 0$: [(0, 0), (2, 0)] is the notation of the mixed states with $L = 0$ and $L = 2$.

Figure 33 represents the diagram correlating the eigenvalues of the anisotropic operator, Equation (6.13), with those of isotropic operator $J\hat{\boldsymbol{l}}_A\hat{\boldsymbol{l}}_B$. One can see that in this special case the anisotropic operator gives rise to the same scheme of the energy levels, obeying the Lande rule, as the isotropic operator does, but the eigenvectors of these two operators are different. The eigenvalues of the anisotropic operator, Equation (6.13), depend on $|M_L|$ (Figure 33b), while in the isotropic case L ($L = 0, 1, 2$) is a good quantum number (Figure 33a). This consideration shows that the conclusion made in [125] about the isotropic character of the exchange Hamiltonian and misleading labelling of the eigenvectors could be the result of overlooking the assignment of the operators $\hat{\boldsymbol{l}}_A$ and $\hat{\boldsymbol{l}}_B$ to different coordinate frames. In this view, conclusion [130] about the role of crossing transfer terms also differs from the conclusion made in [125]. One should also mention the critical comments of Ceulemans *et al.* [127,129] addressed to the study of Drillon and Georges. According to the statement of Ceulemans *et al.*, the isotropy of the magnetic exchange obtained in [125] was the consequence of ignoring the difference (in sign and magnitude) between hopping integrals t_a and t_e. However, as we have demonstrated, the condition $t_e = t_a$ corresponds to the pseudo-spherical (but not true spherical) limit, and the magnetic exchange in this limit is fully anisotropic.

Leuenberger and Güdel [126] proposed a model that is similar to that developed in [125] in its background, but it is quite different in the mathematical procedure and in the assumption about the relative importance of the relevant transfer pathways. As distinguished from the model in [125], it was implied a strong difference between the transfer integrals t_a and t_e (see discussion in the previous section). In this point, the model in [126] seems to be more realistic than that developed in [125].

Finally, let us give a brief overview of the results obtained in the framework of *ab initio* calculations. In the study of Ceulemans *et al.* [127], a complete active space (CAS) SCF

wave-function constituted the zeroth-order wave-function in a perturbation treatment of the electron correlation. The CASSCF wave-function was constructed by distributing two electrons in the titanium 3d-derived active orbitals. The remaining dynamical electron correlation energy was obtained from the second-order perturbation theory (CASPT2). Then the two sets of such CASPT2 calculations were performed. In the first set, denoted as CASPT2(v), only the valence electrons originating from Ti 3d and Cl 3s,3p were correlated. In a second set, denoted as CASPT2(c), authors also included the Ti 3s, 3p electrons. The following three contraction schemes (denoted as A, B, C) were used: 6s4p3d1f on Ti, and 4s3p on Cl (basis A); 9s7p5d1f on Ti, and 4s3p on Cl (basis B); 6s4p3d1f on Ti, and 4s3p1d on Cl (basis C). Accordingly, the following five versions of the *ab initio* calculations were presented in [127]: CASPT2(v)A, CASPT2(v)C, CASPT2(c)A, CASPT2(c)B and CASPT2(c)C. These versions give quite different results both for the $^1A_1'$, $^3A_2''$ gap and for the relative positions of the $a \times a$, $a \times e$ and $e \times e$ groups. By comparing our energy pattern (Figure 31) calculated with the set of the best-fit parameters with these results we see that our scheme is most close (at least qualitatively) to the result obtained by CASPT2(v)A, mainly in the positions of the levels arising from $a \times a$ and $a \times e$ groups that are responsible for the magnetic behaviour below 300 K.

Concluding this discussion one should mention the *ab initio* study of Chen *et al.* [159]. The $^1A_1'$, $^3A_2''$ gap reported in their paper (320 cm^{-1}) proves to be too small to account for the experimentally observed slope of $\chi(T)$ at $T > 150$ K, and the position of the excited levels ($a \times e$-group is in the range of 1680–1850 cm^{-1}) is too high to be able to explain the observed low-temperature magnetic anisotropy and its temperature dependence.

6.3. *Orbitally dependent exchange between many-electron metal ions*

6.3.1. *Exchange Hamiltonian for a corner-shared bioctahedral Co(II) cluster*

The conditions of the applicability of HDVV exchange Hamiltonian remained out of the framework of the Lines theory considered in Section 3. At the same time, the *ab initio* calculations [160] performed for the binuclear chlorine-bridged Co(II) complexes $L_3CoCl_3CoL_3$ have shown that the energy pattern formed by the superexchange is more complex than that obtained within the isotropic Lines model. A more comprehensive study of the problem of exchange interaction in Co(II) clusters was performed in [161,162]. As distinguished from the phenomenological Lines theory, this approach is microscopic in its nature. Within this approach, it was possible to reveal the underlying mechanisms governing the magnetic anisotropy or, in other words, to understand how the magnetic anisotropy of the system depends on the basic parameters. As an illustration, let us consider a corner-shared bioctahedral Co(II) cluster of D_{4h} symmetry (Figure 19). In this case, the main contributions to the superexchange arise from the following most efficient transfer pathways: $\xi \leftrightarrow \xi$, $\eta \leftrightarrow \eta$ (π-transfer) and $u \leftrightarrow u$ (σ-transfer). In [161,162] a simplified version of the theory that neglects the differences between the energies of the CT states was applied. This can be done provided that $A \gg B, C, Dq$. Within this approximation, the energies of all CT states corresponding to the $(d^8)_A - (d^6)_B$ and $(d^6)_A - (d^8)_B$ configurations are assumed to be equal to an effective excitation energy ε_e,

and the kinetic exchange Hamiltonian is presented in the form of Equation (5.20), in which the operators $\hat{R}_k$ are given by

$$\begin{aligned}\hat{R}_k = \frac{1}{\varepsilon_e}\Big\{&\Big[(2/3)t_\pi^2 P^{(k)}_{A_1A_1}(t_2t_2t_2t_2) + (1/2)t_\sigma^2 P^{(k)}_{A_1A_1}(eeee)\Big]\hat{O}^A_{A_1}\hat{O}^B_{A_1}\\ &+\Big[(1/3)t_\pi^2 P^{(k)}_{EE}(t_2t_2t_2t_2) + (1/2)t_\sigma^2 P^{(k)}_{EE}(eeee)\Big]\hat{O}^A_{Eu}\hat{O}^B_{Eu} + t_\pi^2 P^{(k)}_{EE}(t_2t_2t_2t_2)\hat{O}^A_{Ev}\hat{O}^B_{Ev}\\ &+ t_\pi^2 P^{(k)}_{T_1T_1}(t_2t_2t_2t_2)\hat{O}^A_{T_1\gamma}\hat{O}^B_{T_1\gamma} + (3/2)t_\pi t_\sigma P^{(k)}_{T_1T_1}(t_2et_2e)\Big(\hat{O}^A_{T_1\alpha}\hat{O}^B_{T_1\alpha} + \hat{O}^A_{T_1\beta}\hat{O}^B_{T_1\beta}\Big)\\ &+ t_\pi^2 P^{(k)}_{T_2T_2}(t_2t_2t_2t_2)\hat{O}^A_{T_2\zeta}\hat{O}^B_{T_2\zeta} + (1/2)t_\pi t_\sigma P^{(k)}_{T_2T_2}(t_2et_2e)\Big(\hat{O}^A_{T_2\xi}\hat{O}^B_{T_2\xi} + \hat{O}^A_{T_2\eta}\hat{O}^B_{T_2\eta}\Big)\\ &-\Big[\Big(\sqrt{2}/3\Big)t_\pi^2 P^{(k)}_{A_1E}(t_2t_2t_2t_2) + (1/2)t_\sigma^2 P^{(k)}_{A_1E}(eeee)\Big]\Big(\hat{O}^A_{A_1}\hat{O}^B_{Eu} + \hat{O}^A_{Eu}\hat{O}^B_{A_1}\Big)\Big\}.\end{aligned} \tag{6.14}$$

In Equation (6.15), the parameters $P^{(k)}_{\Gamma\Gamma'}(\Gamma_A,\Gamma'_A,\Gamma_B,\Gamma'_B)$ play the same role as the parameters $F^{(k)}_{\Gamma\Gamma'}(\Gamma_A,\Gamma'_A,\Gamma_B,\Gamma'_B)$ in a more general theory described above.

The wave-function of the ground state of Co(II) ion represents a mixture of two $^4T_1$ terms arising from two strong crystal field electronic configurations $t_2^5e^2$ and $t_2^4e^3$:

$$\Phi_{gr}(^4T_1) = C_1\big|t_2^5(^2T_2)e^2(^3A_2),{}^4T_1\big\rangle + C_2\big|t_2^4(^3T_1)e^3(^2E),{}^4T_1\big\rangle, \tag{6.15}$$

where the coefficients are found by diagonalising the matrix of the Coulomb mixing of two $^4T_1$-terms [100]. One can find the following expressions for these coefficients:

$$C_{1(2)} = \sqrt{(1^+_{(-)}w)/2}, \quad w = \frac{9B+10Dq}{\sqrt{(9B+10Dq)^2+144B^2}}. \tag{6.16}$$

Provided $Dq/B \ll 1$ (weak crystal field limit), one finds $C_1 = 2/\sqrt{5}, C_2 = 1/\sqrt{5}$. In this case, Equation (6.15) becomes the wave-function of ^4F-state of a free Co(II)-ion. In a strong field limit ($Dq/B \gg 1$) one obtains $C_1 = 1$, $C_2 = 0$. Using the explicit forms of the wave functions $\big|t_2^5e^2,{}^4T_1\big\rangle$ and $\big|t_2^4e^3,{}^4T_1\big\rangle$, in terms of Slater determinants, one can calculate the set of the exchange parameters $P^{(k)}_{\Gamma\Gamma'}(\Gamma_A,\Gamma'_A,\Gamma_B,\Gamma'_B)$ (see [161] for details). The results of these calculations are given in Table 14. These results combined with Equation (6.16) provide the dependencies of the parameters $P^{(k)}_{\Gamma\Gamma'}$ on the ratio B/Dq.

It is convenient to present the SO coupling operating within the ground $^4T_1$-state in the following form:

$$\hat{H}_{SO} = -(3/2)\kappa_c a\lambda\Big(\hat{\boldsymbol{s}}_A\hat{\boldsymbol{l}}_A + \hat{\boldsymbol{s}}_B\hat{\boldsymbol{l}}_B\Big), \tag{6.17}$$

where κ_c is the contribution of the covalence to the orbital reduction factor, and $a = -C_2^2 + (2/3)(C_1+C_2)^2)$. The factor $-(3/2)a$ appears to distinguish between the matrices of the orbital angular momentum defined in the $\Phi_{gr}(^4T_1)$ and p-bases. In the weak crystal field limit $a = 1$, and in strong crystal field limit $a = 2/3$. In order to focus on the magnetic anisotropy produced by the orbitally dependent exchange interaction, we assume

Table 14. Non-vanishing parameters $P^{(k)}_{\Gamma\Gamma'}(\Gamma_A, \Gamma'_A, \Gamma_B, \Gamma'_B)$.

$P^{(0)}_{\Gamma\Gamma'}(\Gamma_A, \Gamma'_A, \Gamma_B, \Gamma'_B)$	$P^{(1)}_{\Gamma\Gamma'}(\Gamma_A, \Gamma'_A, \Gamma_B, \Gamma'_B)$
$P^{(0)}_{A_1A_1}(t_2t_2t_2t_2) = \frac{1}{6\varepsilon_e}(5C_1^2 + 4C_2^2)(C_1^2 + 2C_2^2)$	$P^{(1)}_{A_1A_1}(t_2t_2t_2t_2) = -\frac{2}{27\varepsilon_e}(C_1^2 + 2C_2^2)^2$
$P^{(0)}_{A_1A_1}(eeee) = \frac{1}{4\varepsilon_e}(2C_1^2 + 3C_2^2)(2C_1^2 + C_2^2)$	$P^{(1)}_{A_1A_1}(eeee) = -\frac{1}{9\varepsilon_e}(2C_1^2 + C_2^2)^2$
$P^{(0)}_{EE}(t_2t_2t_2t_2) = -\frac{1}{3\varepsilon_e}(C_1^2 - C_2^2)^2$	$P^{(1)}_{EE}(t_2t_2t_2t_2) = -\frac{4}{27\,\varepsilon_e}(C_1^2 - C_2^2)^2$
$P^{(0)}_{EE}(eeee) = -\frac{1}{4\,\varepsilon_e}C_2^4$	$P^{(1)}_{EE}(eeee) = -\frac{1}{9\,\varepsilon_e}C_2^4$
$P^{(0)}_{T_1T_1}(t_2t_2t_2t_2) = \frac{1}{8\,\varepsilon_e}(2C_1^2 - C_2^2)^2$	$P^{(1)}_{T_1T_1}(t_2t_2t_2t_2) = \frac{1}{18\varepsilon_e}(2C_1^2 - C_2^2)^2$
$P^{(0)}_{T_2T_2}(t_2t_2t_2t_2) = -\frac{1}{8\,\varepsilon_e}(2C_1^2 + C_2^2)^2$	$P^{(1)}_{T_2T_2}(t_2t_2t_2t_2) = -\frac{1}{18\varepsilon_e}(2C_1^2 + C_2^2)^2$
$P^{(0)}_{T_1T_1}(et_2et_2) = P^{(0)}_{T_1T_1}(t_2et_2e) = \frac{1}{4\,\varepsilon_e}C_1^2C_2^2$	$P^{(1)}_{T_1T_1}(et_2et_2) = P^{(1)}_{T_1T_1}(t_2et_2e) = \frac{1}{9\varepsilon_e}C_1^2C_2^2$
$P^{(0)}_{T_2T_2}(et_2et_2) = P^{(0)}_{T_2T_2}(t_2et_2e) = -\frac{3}{4\,\varepsilon_e}C_1^2C_2^2$	$P^{(1)}_{T_2T_2}(et_2et_2) = P^{(1)}_{T_2T_2}(t_2et_2e) = -\frac{1}{3\varepsilon_e}C_1^2C_2^2$
$P^{(0)}_{A_1E}(t_2t_2t_2t_2) = P^{(0)}_{EA_1}(t_2t_2t_2t_2)$	$P^{(1)}_{A_1E}(t_2t_2t_2t_2) = P^{(1)}_{EA_1}(t_2t_2t_2t_2)$
$= \frac{\sqrt{2}}{6\,\varepsilon_e}(C_1^2 - C_2^2)(2C_1^2 + C_2^2)$	$= -\frac{2\sqrt{2}}{27\varepsilon_e}(C_1^2 - C_2^2)(C_1^2 + 2C_2^2)$
$P^{(0)}_{A_1E}(eeee) = P^{(0)}_{EA_1}(eeee) = -\frac{1}{4\varepsilon_e}C_2^4$	$P^{(1)}_{A_1E}(eeee) = P^{(1)}_{EA_1}(eeee) = \frac{1}{9\varepsilon_e}C_2^2(2C_1^2 + C_2^2)$

that both Co(II) ions occupy perfect octahedral positions ($\Delta = \Delta' = 0$). Under this condition a single ion anisotropy is excluded.

6.3.2. *Pseudo-spin-1/2 Hamiltonian and exchange anisotropy in a Co(II) dimer*

To elucidate the main factors governing the magnetic anisotropy of the Co(II) dimer, let us analyse the parameters of the pseudo-spin-1/2 Hamiltonian acting within the ground Kramers doublet space. For the corner-shared bioctahedral cluster (D_{4h}) this Hamiltonian is axial

$$\begin{aligned}\hat{H}_{\text{eff}} = &-2J_{||}\hat{\tau}_Z^A\hat{\tau}_Z^B - 2J_{\perp}(\hat{\tau}_X^A\hat{\tau}_X^B + \hat{\tau}_Y^A\hat{\tau}_Y^B)\\ &+ g_{||}\beta\hat{\tau}_Z H_Z + g_{\perp}\beta(\hat{\tau}_X H_X + \hat{\tau}_Y H_Y) - \beta^2\Lambda_{||}H_Z^2 - \beta^2\Lambda_{\perp}(H_X^2 + H_Y^2),\end{aligned} \tag{6.18}$$

where $\hat{\tau}_Z = \hat{\tau}_Z^A + \hat{\tau}_Z^B$, etc. are the spin-1/2 operators defined on the basis of the Kramers doublet (see Section 4)

One has to find a relationship between the set of phenomenological parameters involved in Equation (6.18) and the microscopic parameters of the system ($Dq, B, \lambda, t_\sigma, t_\pi$). This problem admits an analytical solution when the SO coupling significantly exceeds the exchange interaction, and hence the perturbation theory is applicable. The difference between the procedure we use here and that applied in Section 2 is that now the perturbation operator $\hat{V}$ also contains the orbitally dependent exchange contributions, meanwhile the low-symmetry crystal field terms are excluded ($\Delta = \Delta' = 0$). In order to find the first-order pseudo-spin-1/2 Hamiltonian $\hat{H}^{(1)}_{\text{eff}}$, one has to calculate the matrices of one-site operators $\hat{\mathbf{s}}_j$, $\hat{\boldsymbol{l}}_j$, and $\hat{O}^j_{\Gamma\gamma}\hat{s}^j_{kq}$ involved in $\hat{V}$ within the basis $\Phi_j(1/2, 1/2)$,

Table 15. Correspondence between one-site operators $\hat{O}_{\Gamma\gamma}\hat{s}_{kq}$ and spin-1/2 operators.

One-site operators	Spin-1/2 operators	One-site operators	Spin-1/2 operators
$\hat{O}_{A_1}\hat{s}_{00}$	$\hat{\tau}_{00}$		
$\hat{O}_{T_1\alpha}\hat{s}_{00}$	$-(\mathrm{i}/3)(\hat{\tau}_{11}-\hat{\tau}_{1-1})$	$\hat{O}_{T_1\alpha}\hat{s}_{1\pm1}$	$\mp(5\mathrm{i}/12)\hat{\tau}_{00}$
$\hat{O}_{T_1\beta}\hat{s}_{00}$	$-(1/3)(\hat{\tau}_{11}+\hat{\tau}_{1-1})$	$\hat{O}_{T_1\beta}\hat{s}_{1\pm1}$	$(5/12)\hat{\tau}_{00}$
$\hat{O}_{T_1\gamma}\hat{s}_{00}$	$(\mathrm{i}\sqrt{2}/3)\hat{\tau}_{10}$	$\hat{O}_{T_1\gamma}\hat{s}_{10}$	$(5\mathrm{i}/6\sqrt{2})\hat{\tau}_{00}$
$\hat{O}_{A_1}\hat{s}_{10}$	$(5/3)\hat{\tau}_{10}$	$\hat{O}_{T_2\xi}\hat{s}_{10}$	$-(\mathrm{i}/6)(\hat{\tau}_{11}+\hat{\tau}_{1-1})$
$\hat{O}_{A_1}\hat{s}_{1\pm1}$	$(5/3)\hat{\tau}_{1\pm1}$	$\hat{O}_{T_2\xi}\hat{s}_{1\pm1}$	$(\mathrm{i}/6)\hat{\tau}_{10}$
$\hat{O}_{Eu}\hat{s}_{10}$	$-(1/3)\hat{\tau}_{10}$	$\hat{O}_{T_2\eta}\hat{s}_{10}$	$(1/6)(\hat{\tau}_{11}-\hat{\tau}_{1-1})$
$\hat{O}_{Eu}\hat{s}_{1\pm1}$	$(1/6)\hat{\tau}_{1\pm1}$	$\hat{O}_{T_2\eta}\hat{s}_{1\pm1}$	$\pm(1/6)\hat{\tau}_{10}$
$\hat{O}_{Ev}\hat{s}_{1\pm1}$	$(1/2\sqrt{3})\hat{\tau}_{1\mp1}$	$\hat{O}_{T_2\zeta}\hat{s}_{1\pm1}$	$\pm(\mathrm{i}/3\sqrt{2})\hat{\tau}_{1\mp1}$

$\Phi_j(1/2,-1/2)(j=A,B)$ and to express these matrices in terms of the spin-1/2 matrices. The results for spin and angular momentum operators are given by Equation (4.5). The results for $\hat{O}^j_{\Gamma\gamma}\hat{s}^j_{kq}$ are collected in Table 15 in which we use the operators τ_α in the cyclic basis: $\tau_{00}=\tau_z, \tau_{\pm1}=\mp(1/\sqrt{2})(\tau_x\pm i\tau_y)$. Then one can represent the first-order effective pseudo-spin-1/2 Hamiltonian $\hat{H}^{(1)}_{\mathrm{eff}}$ in the form of Equation (6.18), with the following parameters:

$$
\begin{aligned}
J^{(1)}_{||} &= -\frac{2t_\sigma^2}{81\varepsilon_{\mathrm{ex}}}\left(5C_1^2+2C_2^2\right)^2-\frac{t_\sigma t_\pi}{54\varepsilon_{\mathrm{ex}}}C_1^2C_2^2-\frac{t_\pi^2}{324\varepsilon_{\mathrm{ex}}}\left(100C_1^4+156C_1^2C_2^2+153C_2^4\right),\\
J^{(1)}_{\perp} &= -\frac{t_\sigma^2}{648\varepsilon_{\mathrm{ex}}}\left(20C_1^2+11C_2^2\right)^2-\frac{5t_\sigma t_\pi}{54\varepsilon_{\mathrm{ex}}}C_1^2C_2^2-\frac{t_\pi^2}{324\varepsilon_{\mathrm{ex}}}\left(44C_1^4+164C_1^2C_2^2+201C_2^4\right),\\
g^{(1)}_{||} &= g^{(1)}_{\perp}\equiv g_0=(1/3)(5g_e-2a\kappa),\quad \Lambda^{(1)}_{||}=\Lambda^{(1)}_{\perp}=0.
\end{aligned}
\tag{6.19}
$$

It is seen that the first-order perturbation procedure leads to an effective exchange interaction that is, in general, anisotropic. At the same time, within the first-order approximation, the *g*-factor proves to be isotropic and coincides with the *g*-factor for the Kramers doublet of the individual Co(II) ion in a perfect octahedral ligand field. The exchange anisotropy disappears only when both $C_2=0$ (strong crystal field limit) and $t_\pi=0$. In this limiting case one arrives at the isotropic pseudo-spin-1/2 Hamiltonian with $J^{(1)}_{||}=J^{(1)}_{\perp}\equiv J^{(1)}=(25/9)J$, where $J=-2t_\sigma^2/9\varepsilon_{\mathrm{ex}}$. In order to clarify this result, one can note that for $C_2=0$ $(B/Dq=0)$ and $t_\pi=0$ the initial kinetic exchange Hamiltonian defined by Equations (5.20) and (6.14), takes the simple HDVV form $\hat{H}_{\mathrm{ex}}=2J(9/4-\hat{\boldsymbol{s}}_A\hat{\boldsymbol{s}}_B)$, where $J=-2t_\sigma^2/9\varepsilon_{\mathrm{e}}$. This result has a clear physical meaning. In fact, by inspecting the electronic subshells, which participate in the transfer processes, one can see that in this limiting case the ground state of each Co(II) ion proves to be $\left|t_2^5(^2T_2)e^2(^3A_2),{}^4T_1\right\rangle$, so t_σ transfer connects (*via* excited states) the orbitally non-degenerate subshells $e^2(^3A_2)$, thus resulting in the isotropic HDVV interaction.

When $B/Dq\neq0$, the ground state also includes a contribution of the state $\left|t_2^4(^3T_1)e^3(^2E),{}^4T_1\right\rangle$ possessing the orbitally degenerate $e^3(^2E)$-subshell. This results in the anisotropic contributions to the Hamiltonian. In fact, when $B/Dq\neq0$ one gets $C_2\neq0$ and hence the anisotropic terms containing $\hat{O}^A_{Eu}\hat{O}^B_{Eu}$ and $\hat{O}^A_{A_1}\hat{O}^B_{Eu}+\hat{O}^A_{Eu}\hat{O}^B_{A_1}$ will appear along

with the isotropic one. These anisotropic terms become more pronounced when one passes from the strong cubic crystal field to the weak one. The $t_2 - t_2$ transfer ($t_\pi \neq 0$) also leads to the appearance of the anisotropic terms in the initial exchange Hamiltonian, and thus in the pseudo-spin-1/2 Hamiltonian. This anisotropy appears due to the contribution of the orbitally degenerate $t_2^5(^2T_2)$ subshells. In general, the anisotropy of the magnetic exchange is the result of the interplay of both named contributions, namely, the configuration mixing produced by the cubic crystal field and the transfer between t_2 orbitals.

In the first-order approximation the mixing of the ground states with the excited ones by the exchange interaction is neglected. For this reason, $\hat{H}_{\text{eff}}^{(1)}$ provides a satisfactory description of the magnetic properties only when the exchange splitting is much smaller than the SO one, but even in this case the description is not complete because $\hat{H}_{\text{eff}}^{(1)}$ does not include the TIP. One can significantly improve the results and extend the frameworks of their applicability by taking into account the term $\hat{H}_{\text{eff}}^{(2)}$.

Within this approximation, the anisotropy of g-factor can be described and the TIP contribution appears. The operator $\hat{H}_{\text{eff}}^{(2)}$ has been already deduced in Section 4.2.3 in the limit case of the isotropic magnetic exchange (second-order terms in Equations (4.16)–(4.18)). The expression for $\hat{H}_{\text{eff}}^{(2)}$ that takes into account orbitally dependent exchange contributions is too cumbersome to be useful in the subsequent analysis.

The above consideration was based on perturbation theory. At the same time, the concept of the effective pseudo spin-1/2 Hamiltonian is more general and remains applicable even in the case when the perturbation scheme fails. This is the case when the exchange interaction is comparable with the SO interaction, but the low-lying levels still arise from Kramers doublets. An analytical solution in this situation is impossible and the parameters should be found numerically. This can be done by comparing the eigenvalues of the pseudo-spin-1/2 Hamiltonian and three low-lying energy levels calculated with the initial microscopic Hamiltonian.

The parameters calculated in this way are shown in Figure 34 as the functions of B/Dq and in Figure 35 as the functions of t_π/t_σ. Figure 34a shows that the exchange interaction associated with t_σ-transfer is isotropic ($J_{||} = J_\perp$) in the strong crystal field limit ($B/Dq = 0$) and becomes anisotropic (with $J_{||} > J_\perp$) when $B/Dq \neq 0$. The same is true for g-factor in Figure 34b and TIP in Figure 34c. The first-order exchange parameters calculated with the aid of Equation (6.19) are also shown in Figure 34a. The difference between $J_{||}(J_\perp)$ and $J_{||}^{(1)}(J_\perp^{(1)})$ proves to be significant because the σ-type exchange interaction $t_\sigma^2/\varepsilon_e = 100\,\text{cm}^{-1}$ is not very small, and hence the exchange mixing of the Kramers doublets with the excited states cannot be neglected. Along with the exact g-factor, the first-order value g_0 is also shown in Figure 34b. In the case under consideration, g_0 coincides with the g-factor of the individual Co(II) ion. One can see that the exchange interaction dramatically changes g-factor from the value of about 4 (usual value for the individual Co(II) ion in isotropic case) to a value that is in the range 2–3, resulting at the same time in a small anisotropy of g when $B/Dq \neq 0$. The exact TIP parameters $\Lambda_{||}$ and $\Lambda_\perp$ in Figure 34c are shown together with the TIP parameter $\Lambda_0 = (20/\kappa a\lambda)(a\kappa - g_e)^2$ for the pair of non-interacting Co(II) ions occupying perfect octahedral positions. The exchange interaction accounts for the big difference between Λ_0 and the exact TIP parameters in Figure 34c.

Figure 35a shows the influence of π-transfer on the parameters $J_{||}$ and $J_\perp$ for the typical values $B = 970\,\text{cm}^{-1}$ and $Dq = 840\,\text{cm}^{-1}$ [100]. At $t_\pi = 0$, the effective exchange

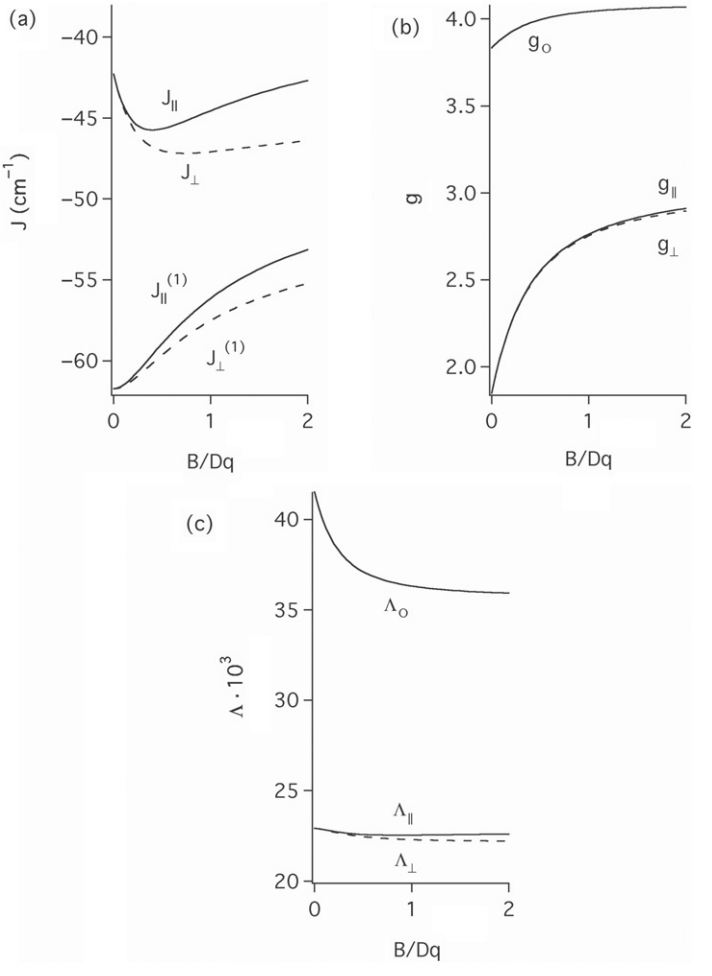

Figure 34. Influence of the ratio B/Dq on the parameters of the pseudo-spin-1/2 Hamiltonian, $t_\pi = 0$, $t_\sigma^2/\varepsilon_{ex} = 100\,cm^{-1}$, $\lambda = -180\,cm^{-1}$, $\kappa_c = 0.75$: (a) exchange parameters; (b) components of g-tensor and (c) the parameters of the TIP.

is anisotropic with $J_{||} > J_{\perp}$. This anisotropy results from the mixing of two $^4T_1$ states, as was discussed above. In addition, when $t_\pi \neq 0$, the anisotropy of the opposite sign appears due to the electron transfer between the degenerate subshells. These two contributions are in competition, so the increase of t_π can lead to the change of the sign of the anisotropy (Figure 35a). The same kind of behaviour takes place for g-factors (Figure 35b) and the parameters of the TIP (Figure 35c). Figure 35 also shows a significant deviation of the exact values of the effective parameters from their approximate values $J_{||}^{(1)}$, $J_{\perp}^{(1)}$, g_0 and Λ_0.

It is seen from Figures 34 and 35 that the inequalities $J_{||} > J_{||}^{(1)}$ and $J_{\perp} > J_{\perp}^{(1)}$ always hold. On the contrary, $g_{||}$, $g_{\perp} < g_0$ and $\Lambda_{||}$, $\Lambda_{\perp} < \Lambda_0$. For this reason, the first-order values $J_{||}^{(1)}, J_{\perp}^{(1)}$ can be regarded as the lower limits for the exchange parameters, while the

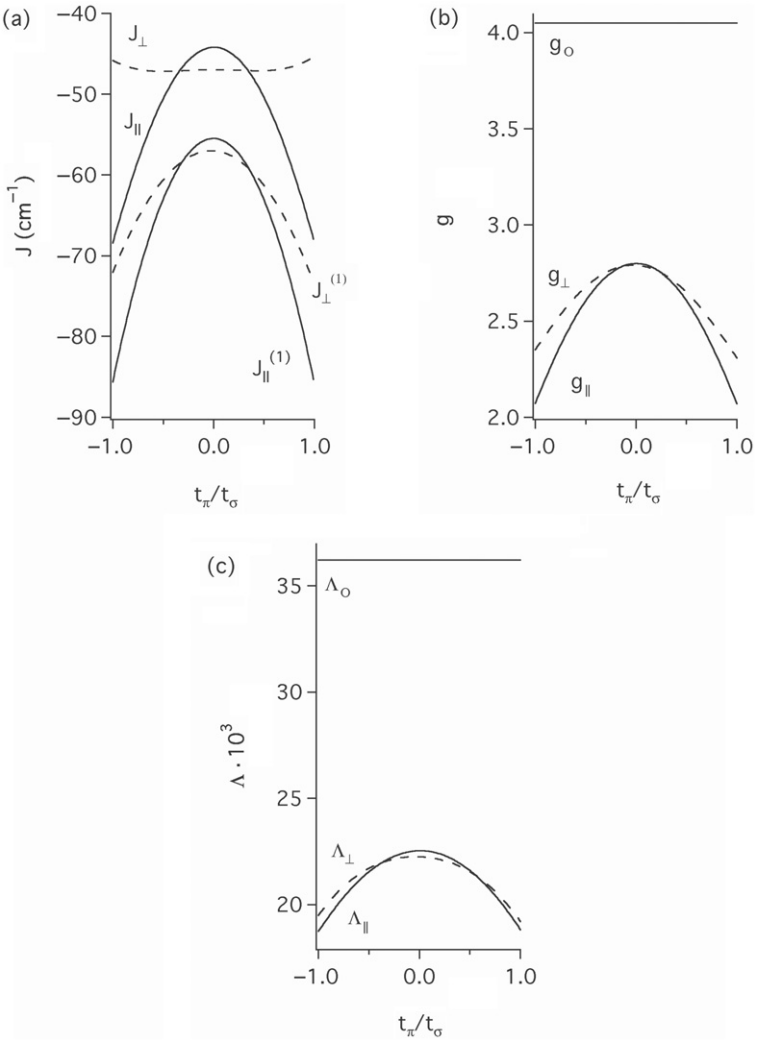

Figure 35. Combined effect of B/Dq and t_π/t_σ on the parameters of the pseudo-spin-1/2 Hamiltonian, $t_\sigma^2/\varepsilon_{ex} = 100\,cm^{-1}$, $B = 970\,cm^{-1}$, $Dq = 840\,cm^{-1}$, $\lambda = -180\,cm^{-1}$, $\kappa_c = 0.75$: (a) exchange parameters; (b) the components of g-tensor and (c) parameters of the TIP.

values g_0 and Λ_0 are the upper limits for the corresponding parameters. In the particular case of isotropic exchange, these statements simply follow from Equations (4.16)–(4.18) in which the condition $\Delta = \Delta' = 0$ is assumed.

Let us briefly summarise the main results described in this section. It was demonstrated that the electron transfer of t_2–t_2 type gives rise to the magnetic anisotropy independently of the strength of the cubic crystal field. On the contrary, the e–e transfer can produce the magnetic anisotropy only due to the fact that the ground state of the Co(II) ion represents a mixture of the cubic terms $^4T_1(t_2^5e^2)$ and $^4T_1(t_2^4e^3)$. In the limit of strong cubic field, when this mixture is negligible, the effect of the e–e transfer is fully isotropic. The outlined results

allow to formulate the criteria of applicability of the Lines model. First, the Lines model proves to be a good approximation if the cubic crystal field is strong enough and the parameters of t_2–t_2 transfer are small as compared to those for e–e transfer. Second, the Lines model can also be applicable for some specific relationships between the t_2–t_2 transfer and the strength of the cubic crystal field. In this case, the exchange anisotropy can become small as a result of the interplay of two competing contributions. These arguments are independent of the overall symmetry of the Co(II) pairs and could probably explain why the Lines theory is proved to be successful in many cases despite the fact of ignoring the anisotropic orbital contributions to the exchange.

6.3.3. *Cyanide-based single molecule magnets containing orbitally degenerate metal ions*

One of the most exciting developments of molecular magnetism in the last two decades is the discovery of metal clusters exhibiting magnetic bistability of an entirely molecular origin, compounds that are referred to as SMMs [1,2]. The majority of molecules exhibiting SMM behaviour incorporate oxide-based bridging ligands, which serve to mediate the exchange interaction between metal centres. In these systems the orbital angular momenta of the constituent metal ions are strongly quenched by the low-symmetry crystal fields, and therefore these systems can be termed spin clusters.

In the last 10 years, metal cyanide compounds have also attracted attention as promissing candidates for new cluster types for SMMs. A remarkable feature of this type of SMMs is that they contain the metal ions in a highly symmetric (octahedral or quasioctahedral) ligand surroundings. This can lead to the existence of unquenched orbital angular momentum in the ground crystal field terms of these ions. This new group of SMMs is exemplified by the metal-cyanide clusters $[Mn^{III}(CN)_6]_2[Mn^{II}(tmphen)_2]_3$ (tmphen = 3, 4, 7, 8-tetramethyl-1,10-phenanthroline) [30], $K[(5\text{-Brsalen})_2(H_2O)_2Mn(III)_2\text{-}Fe(III)(CN)_6]\cdot 2H_2O$ [31] and $[(Tp)_8(H_2O)_6Cu(II)_6Fe(III)_8(CN)_{24}]^{4+}$ [32], in which the low-spin Mn(III) and Fe(III) ions possess unquenched orbital angular momenta.

These systems are drastically different in several important aspects from the classical SMMs in which all the constituent metal ions are orbitally non-degenerate. First, in the presence of the axial crystal field acting on the low-spin Mn(III) and Fe(III) ions, their first-order orbital angular momenta gives rise to a significant single ion magnetic anisotropy, which cannot be derived from the conventional second-order ZFS Hamiltonian, as in the case of spin clusters. The role of the first-order single ion anisotropy in the formation of the magnetisation reversal barrier in the $[Mn^{III}(CN)_6]_2[Mn^{II}(tmphen)_2]_3$ cluster has been studied in detail in [115,116]. Second, as was pointed out in [135,136], the orbitally dependent contributions to the magnetic exchange in combination with the SO coupling are also able to create the magnetisation reversal barrier. Two comparatively simple model systems are considered in [135,136], namely the dimeric cluster Mn(III)–CN–Mn(II) shown in Figure 36 and the linear trimeric cluster Mn(II)–NC–Mn(III)–CN–Mn(II). These systems drew our attention because of the recently demonstrated ability of cyanide chemistry to obtain molecular linear clusters with orbitally degenerate ions such as the aformentioned SMMs reported in [31]. Hereafter we will briefly discuss how the exchange anisotropy can lead to the appearance of the magnetisation reversal barrier in the Mn(III)–CN–Mn(II) dimer.

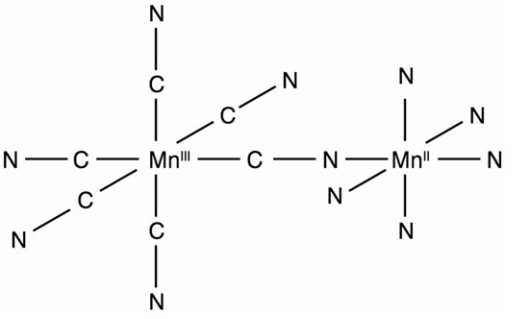

Figure 36. Structure of the Mn(III)–CN–Mn(II) dimer.

6.3.4. *Orbitally dependent superexchange in the Mn(III)–CN–Mn(II) pair*

In the Mn(III)–Mn(II) dimer, shown in Figure 36, the Mn(III) ion is in a strong cubic crystal field induced by six carbon atoms (ground state $^3T_1(t_2^4)$), while the Mn(II) ion is in a weak cubic crystal field produced by the nitrogen atoms (ground state $^6A_1(t_2^3e^2)$). The model in [135,136] includes the orbitally dependent superexchange mediated by the cyanide bridge, the SO coupling and the axial crystal field acting within the $^3T_1(t_2^4)$ state of the Mn(III) ion. Let us assign the indices A and B to the Mn(II) and Mn(III) ions, respectively. One can see that the $B \rightarrow A$ electron transfer leads to the CT states with very high excitation energies, and hence such transfer can be excluded from the consideration. There are two possibilities for the $A \rightarrow B$ electron transfer, namely, the transfer from the single occupied t_2 orbitals of the Mn(II) ion to the single occupied t_2 orbitals of the Mn(III) ion through the bonding π and antibonding π^* orbitals of the cyanide ion, and the transfer from the single occupied e orbitals of Mn(II) to the empty e orbitals of Mn(III) through the cyanide σ-orbitals (the hopping parameters corresponding to the $t_2 \rightarrow e$ transfer are expected to be negligible due to the orthogonality of t_2 and e orbitals). At the same time, recent density functional theory calculations of the exchange parameters in cyano-bridged species [163] demonstrated that the interaction through the cyanide σ-orbitals was significantly smaller compared to the interaction through the π and π^* orbitals (see also [164] and references therein). For this reason, in [135,136] only $t_2^A \rightarrow t_2^B$ transfer processes were taken into account in the exchange model. It is easy to see that the overlap between ξ-type t_2 orbitals of Mn(II) and Mn(III) through the π and π^* orbitals of cyanide bridge is strong, and the same overlap takes place between η orbitals. So there are two equivalent hopping parameters $t_{\xi\xi} = t_{\eta\eta} \equiv t$ associated to these overlaps (Figure 37), and the integral $t_{\zeta\zeta}$ can be omitted. Note that the $t_2^A \rightarrow t_2^B$ transfer cannot affect the e^2 subshell of the ion A ($^3A_2(e^2)$-state). At the same time, this transfer decreases the spin of the ion A by 1/2. The analysis of the Tanabe–Sugano diagrams [100] shows that the only appropriate state for the oxidised $t_2^2e^2$-configuration of the ion A is the state $^5T_2(t_2^2e^2)$ and the reduced t_2^5 configuration of the ion B gives rise to the only state $^2T_2(t_2^5)$. We thus arrive at the conclusion that the $t_2^A \rightarrow t_2^B$ transfer results in the only CT state $^5T_2(t_2^2e^2)_A - {}^2T_2(t_2^5)_B$. It is remarkable that the single-ion CT states are the 'pure' states, i.e. each of these states results only from the electronic configuration.

The orbital schemes for the $[\mathrm{Mn(II)}]_\mathrm{A}[\mathrm{Mn(III)}]_\mathrm{B}$ pair (ground state) and $[\mathrm{Mn(III)}]_\mathrm{A}[\mathrm{Mn(II)}]_\mathrm{B}$ pair (CT state), and the electron transfer process connecting these

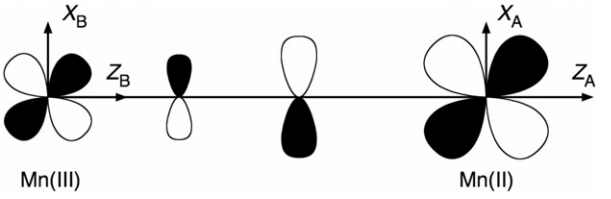

Figure 37. Scheme of overlap between t_2 orbitals of Mn(III) and Mn(II) ions through π orbitals of cyanide bridge.

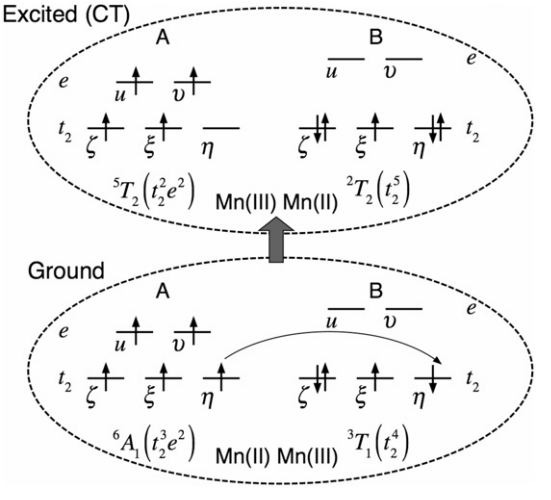

Figure 38. The kinetic exchange mechanism for the Mn(III)–CN–Mn(II) pair.

states are shown in Figure 38. It is to be noted that each orbital scheme depicts only one Slater determinant (microstate) of the many-electron open shell wave-function. For example, the only determinant $|\xi\,\bar{\eta}\,\zeta\,\bar{\zeta}|$ involved in the two-determinant wave-function $|^3T_1(t_2^4), \gamma, m_s = 0\rangle = (1/\sqrt{2})\big(|\bar{\xi}\eta\zeta\bar{\zeta}| + |\xi\bar{\eta}\zeta\bar{\zeta}|\big)$ of the low-spin Mn(III) ion is shown in Figure 38. On the contrary, the state $|^6A_2(t_2^3e^2), m_s = 5/2\rangle = |\xi\eta\zeta u\upsilon|$ is represented by the only microstate, so the corresponding orbital scheme in this case shows the full wave-function of the high-spin Mn(II) ion. The hopping electron does not change its spin projection and selects the initial and final microstates as exemplified in Figure 38.

Using the general formalism described in Section 5.1, one can find the following expression for the kinetic exchange Hamiltonian of the pair:

$$\hat{H}_{\mathrm{ex}}(A,B) = -(1/2)J(-5 + 2\hat{\boldsymbol{s}}_A\hat{\boldsymbol{s}}_B)\Big[2 + 3(\hat{l}_Z^B)^2\Big], \tag{6.20}$$

In Equation (6.20), the value

$$J = -t^2/(15\varepsilon_{A\to B}) \tag{6.21}$$

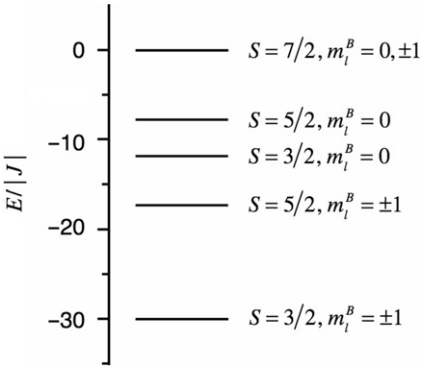

Figure 39. Energy pattern of the Mn(III)–CN–Mn(II) pair formed by the orbitally dependent magnetic exchange.

is the exchange parameter and $\varepsilon_{A\to B}$ is the excitation energy corresponding to the $A \to B$ transfer. This Hamiltonian has essentially non-Heisenberg form and includes both spin and orbital angular momenta operators (orbitally dependent exchange).

6.3.5. *Energy pattern of the Mn(III)–CN–Mn(II) dimer and barrier for the reversal of magnetisation*

The Hamiltonian, Equation (6.20), proves to be isotropic in the spin subspace and axially symmetric in the orbital subspace, so that S, M_S (total spin of the pair and its projection) and m_l^B are the good quantum numbers. The eigenvalues of $\hat{H}_{\rm ex}(A, B)$ are calculated as follows:

$$\begin{aligned} E(S, m_l^B = 0) &= -J[-63/4 + S(S+1)], \\ E(S, |m_l^B| = 1) &= -(5/2)J[-36/4 + S(S+1)]. \end{aligned} \tag{6.22}$$

The energy pattern of the Mn(III)–CN–Mn(II) pair formed by the magnetic exchange contains two superimposed groups of the energy levels with $m_l^B = 0$ and $|\, m_l^B| = 1$ (Figure 39). The total spin S of the pair assumes the values $S = 3/2$, $5/2$, $7/2$, and the energy levels within each group obey the Lande rule. The exchange splitting of both $m_l^B = 0$ and $|\, m_l^B| = 1$ multiplet proves to be antiferromagnetic ($S_{gr} = 3/2$). The conclusion about the antiferromagnetic exchange splitting in each group of the energy levels is in agreement with the underlying ideas of Anderson [84] and Goodenough and Kanamori [86] about the antiferromagnetic exchange coupling due to the electron hopping between the half-occupied orbitals.

Note that the Lande rule is not valid for the whole energy pattern, particularly, a non-monotonic alternation of the levels with $S = 3/2$ and $S = 5/2$ takes place. It is remarkable that the energy levels depend not only on the total spin quantum number S but also on $|\, m_l^B|$. This leads to the magnetic anisotropy of the system. In the magnetic field applied parallel to the C_4 axis of the bioctahedron, the orbital contribution to the Zeeman splitting of the ground level is significant (first-order effect) because the operator $-\kappa\beta\, \hat{l}_Z^B H_Z$ possesses the following non-vanishing matrix elements within the ground level

$$\left\langle S = 3/2,\ M_S,\ m_{lB} = \pm 1 \right| -\kappa\beta\, \hat{l}_Z^B H_Z \left| S = 3/2,\ M_S,\ m_{lB} = \pm 1 \right\rangle = \pm\kappa\,\beta\, H_Z. \tag{6.23}$$

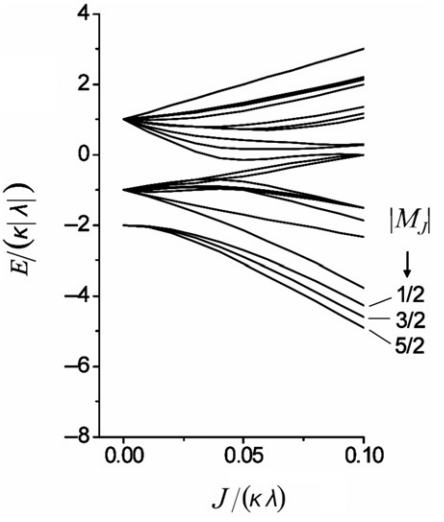

Figure 40. Combined effect of the exchange and the SO coupling on the energy levels of the Mn(III)–CN–Mn(II) pair.

On the contrary, the orbital contribution to the Zeeman splitting of the ground level in a perpendicular field is much smaller because it appears as a second-order effect due to the mixing of the ground level with the second excited level ($S = 3/2$, $m_l^B = 0$) by the operator $-\kappa\beta(\hat{l}_X^B H_X + \hat{l}_Y^B H_Y)$ (van Vleck paramagnetism). Therefore, as distinguished from the Heisenberg magnetic exchange, the orbitally dependent exchange interaction produces the strong magnetic anisotropy of the pair of ions.

Now, let us consider along with the exchange coupling in cyano-bridged Mn(II)–Mn(III) pair also the SO interaction, $-\kappa\lambda\hat{\boldsymbol{s}}_B\hat{\boldsymbol{l}}_B$, operating within the $^3T_1$ term of the Mn(III) ion. Figure 40 displays the combined effect of the orbitally dependent exchange and the SO coupling on the energy pattern of the Mn(III)–CN–Mn(II) pair. One can see that provided $J = 0$ (exchange interaction is excluded) the energy pattern of dimer consists of three levels $-2\kappa|\lambda|$, $-\kappa|\lambda|$ and $\kappa|\lambda|$, which correspond to $j_B = 0, 1$ and 2, respectively (j_B is the total angular momentum of the ion B). In the presence of exchange interaction ($J \neq 0$) the energies of the levels become dependent on $|M_J|$, where $M_J = m_s^A + m_s^B + m_l^B$ is the projection of the total angular momentum (m_s^A and m_s^B are the spin projections of the ions A and B). The energies of three low-lying levels with $M_J = \pm 5/2$, $M_J = \pm 3/2$ and $M_J = \pm 1/2$ monotonically increase with the decrease of $|M_J|$. We thus arrive at the conclusion that the orbitally-dependent exchange between Mn(III) and Mn(II) ions in combination with the SO coupling results in the formation of the barrier for the reversal of magnetisation. The magnitude of this barrier monotonically increases with the increase of the exchange interaction.

The above consideration deals with the case of perfect octahedral surrounding of the Mn(III) ion. In this case, the single-ion anisotropy is excluded and only exchange anisotropy is responsible for the existance of the magnetisation reversal barrier. A more general situation was also considered in [116], in which both the effect of single-ion

anisotropy caused by the axial crystal field and the effect of increasing the number of Mn ions in linear cyanide-based cluster were analysed. The inclusion of the negative axial crystal field acting on the Mn(III) ion was shown to result in a significant enhancement of the barrier height. Finally, it was demonstrated that the height of this barrier significantly increases when passing from dimer Mn(III)–CN–Mn(II) to trimer Mn(II)–NC–Mn(III)–CN–Mn(II). These results are relevant to the issue of a more rational design approach for the synthesis of cyano-based SMMs with higher blocking temperatures.

7. Conclusions and outlook

During several decades magnetochemistry of transition metal clusters was based on the HDVV model. This model played a decisive role in the discovery of the first exchange coupled system (dimeric cooper acetate) as well as in further identification and study of the new polynuclear compounds and magneto-structural correlations. The importance of anisotropic terms in the exchange Hamiltonian (mainly, single-ion anisotropy) has been understood at this early stage of magnetochemistry. These anisotropic interactions are crucially important, for example, for electron paramagnetic resonance (EPR), but, in general, they are rather small in HDVV systems. At the same time, the interest to the anisotropic interactions was progressively growing from the beginning of 90th due to the discovery of the molecular nanomagnets (SMMs and SCMs) and the understanding of the vitally important role of the magnetic anisotropy in the formation of the barrier for the reversal of magnetisation. Although many efforts have been made to control the anisotropy barrier in these systems, this task remains of current interest and requires new approaches.

One of the promising ways of increasing the magnetic anisotropy in SMMs is to go beyond HDVV systems and to focus on the magnetic clusters composed of orbitally degenerate metal ions that have unquenched orbital angular momenta. Although seven decades ago van Vleck pointed out the restrictions of the HDVV model, the problem of orbital degeneracy has not been attacked till the 1960s. That time marked a new stage in the study of the exchange interaction in orbitally degenerate systems that has primarily been focused on the solid state physics and led to the derivation of the orbitally dependent Hamiltonian and discovery of orbital ordering in JT crystals [121,123]. At the same time, one of the main effects produced by the orbitally dependent exchange, namely, strong magnetic anisotropy, has not been understood to full extent at that time and has not been explored in molecular magnetism. It should also be mentioned that only particular cases in the whole problem of degeneracy have been treated (some particular electronic configurations, high symmetry, etc.) and the exchange Hamiltonian has not been derived in general form that would take into account all details relevant to molecular magnetism, e.g. overall symmetry, crystal fields, orbital structure, transfer pathways versus geometry, etc. Looking back, one can see that the systematic studies of the orbitally degenerate ions have not been undertaken until recently and the earlier theoretical approaches had to be improved to serve as a theoretical background for the study of degenerate systems. From this point of view, the new recently developed approaches discussed in this review represent a step forward in the theoretical description of this class of systems.

The aim of this article was to demonstrate, in an accessible way, how the orbital degeneracy affects the exchange interaction and energy pattern of polymetallic molecular

systems. The main emphasis was put on the conceptual aspects and, from this point of view, the systems discussed in this review are mainly chosen to illustrate the approaches and methodology rather than to give a systematic description of the particular kinds of systems (the last is partly filled up by references). We have given a general consideration of the effective orbitally dependent Hamiltonian that is expected to become a powerful tool in molecular magnetism. One can mention at least two reasons for this optimistic expectation: (1) we have presented an universal procedure that allows to deduce the Hamiltonian for a given pair of metal ions with given electronic configurations and overall symmetry of the pair, so that the deduced Hamiltonian is general and adapted to arbitrary geometry and electronic configurations of the constituent ions; (2) we have given a simple and rather general receipt that allows to treat this Hamiltonian. The procedure is based on the ITO approach and can be easily realised on the basis of the well-designed MAGPACK software [165] that allows to directly evaluate the thermodynamic characteristics of the named systems and (3) the proposed approach is microscopic in its nature so that the parameters of the Hamiltonian are explicitly expressed in terms of the key parameters of the individual metal ions, like orbital populations, crystal field parameters, etc., and in this way analyse the physical origin of different kinds of exchange contributions. This kind of microscopic approach has clear advantages as compared with the alternative approaches adopted in the molecular magnetism. In fact, although the *ab initio* calculations give accurate numerical results, they, in some sense, mask the information about internal parameters and interactions. Alternatively, the phenomenological Hamiltonian, solely based on the symmetry arguments, leads to the overparametrisation due to a large number of unknown semiempirical parameters.

As one could see from the above consideration, the degeneracy represents a complicated many-side problem. Even taking into account all advantages provided by the general approach to the problem of the orbitally dependent exchange, one faces a challenge in the full description of complex degenerate systems. For this reason, sometimes it could be more suitable to use a simplified model based on the use of isotropic exchange Hamiltonian (Lines model and its generalisations). In this model, the anisotropy is solely a result of a combined action of a low-symmetry crystal field and SO interaction. Of course, the limits of applicability of this approximation can be found only on the basis of the more general orbitally dependent approach, as was discussed in this review for the particular case of Co(II) ions. Both the model of the orbitally dependent exchange and isotropic exchange model can be reduced to different, more particular microscopic and phenomenological models. Different models reviewed in this article and the interrelations between them are schematically shown in Figure 41. In the limit of strong SO coupling and axial crystal fields acting on metal ions, both isotropic exchange model and more sophisticated consideration, based on the orbitally-dependent exchange Hamiltonian lead to a pseudo-spin-1/2 Hamiltonian for the interacting Kramers doublet ions (Figure 41). Of course, both the initial orbitally dependent exchange Hamiltonian and the pseudo-spin-1/2 Hamiltonian deduced on the microscopic background satisfy all generally required symmetry properties like invariance under the point group operations and time reversal. Nevertheless, the microscopic nature of this Hamiltonians assumes definite interrelation between the involved parameters. On the contrary, in phenomenological effective Hamiltonians deduced on the base of the symmetry conditions, the parameters

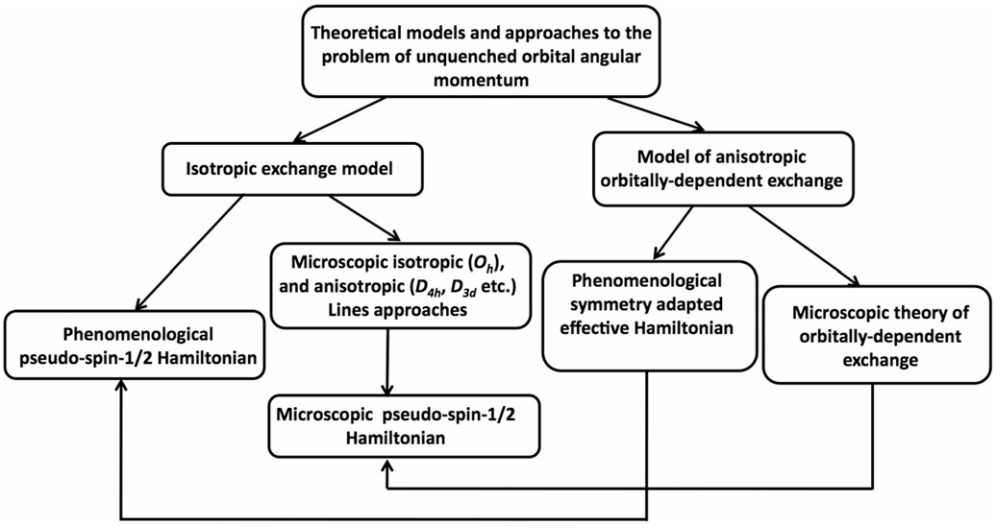

Figure 41. Models and approaches used for the theoretical descriptions of the orbitally degenerate systems.

remain independent from the symmetry point of view. These phenomenological versions of the approaches are also listed in Figure 41 because they are frequently used in molecular magnetism and, especially, in EPR and INS studies.

To summarise the contents of the present review article, the following key topics are to be mentioned:

(1) The orbital magnetic contributions manifest themselves both in the local factors and in the inter-centre magnetic interaction. First, we have discussed the model that neglects the influence of the orbital angular momenta on the exchange interaction (Lines model). It was elucidated how the single-ion anisotropy affects the parameters of the effective pseudo-spin-1/2 Hamiltonian for the low-lying Kramers doublets. Special attention was paid on systems based on the clusters of Co(II) ions, which are in the focus of the many studies in molecular magnetism.

(2) We have considered in detail the orbitally dependent contributions to the exchange interaction that is probably the most important (at least conceptually) part of this review. We have presented a rigorous mathematical procedure of the derivation of the kinetic exchange Hamiltonian for a pair of coordinated orbitally degenerate transition metal ions. The Hamiltonian is expressed in terms of the orbital matrices (irreducible tensors of the local point group) and spin operators. The microscopic background of the theory allowed us to find the interrelations between the parameters of the Hamiltonian and the internal parameters of the system including all relevant transfer integrals and fundamental intracenter interactions, like crystal field and Racah parameters for the constituent metal ions in their ground, oxidised and reduced configurations. The developed formalism accompanied by the use of the efficient ITO technique in the spherical group made it possible to describe all relevant interactions (exchange, low-symmetry crystal fields, SO coupling, etc.)

within the unified computational scheme. It was shown that the orbitally dependent exchange leads to an anomalously strong magnetic anisotropy that can be considered as a main manifestation of the unquenched orbital angular momentum. The language of the angular momenta and ITOs of R_3 group proved to be useful not only in the design of the computational procedure but also in a qualitative discussion of the magnetic anisotropy.

(3) Several characteristic examples are given with the aim to illustrate how the described technique can be applied and how the results can be analysed. The magnetic properties of the binuclear face-shared unit $[Ti_2Cl_9]^{3-}$ in $Cs_3Ti_2Cl_9$ have been discussed with a special emphasis on the experimentally observed magnetic anisotropy. A general outlook on the non-trivial symmetry properties of the exchange Hamiltonian was given. It was shown how the magnetic anisotropy associated with the orbitally dependent exchange is governed by the different kinds of the electron transfer processes.

(4) The major electronic factors controlling the magnetic anisotropy in Co(II) pairs have been discussed. The degree of the exchange anisotropy was shown to depend on the strength of the cubic crystal field and on the relative efficiency of two kinds of the electron transfer pathways between unfilled d-shells (e–e and t_2–t_2) contributing to the kinetic exchange. In the case of strong SO interaction, the effective Hamiltonian was projected onto the subspace of low-lying Kramers doublets and, similarly a pseudo-spin-1/2 Hamiltonian was derived. Unlike the commonly accepted phenomenological approaches based merely on the symmetry arguments, the proposed procedure is grounded on the microscopic consideration and hence allows to establish the interrelation between idem parameters of the system and the parameters of the pseudo-spin-1/2 Hamiltonian.

(5) In the consideration of the cyanide-bridged Mn(III)–Mn(II) pair, it was demonstrated that under some conditions the orbitally dependent exchange is able to produce the energy pattern that can be associated with the barrier for the reversal of magnetisation. This result seems to be instructive in the controlled design of new cyano-based SMMs with high-blocking temperatures.

The size of this article did not allow us to discuss several important questions related to the degeneracy. First, we did not address the problem of JTE that is an essential part of the theory of the systems exhibiting orbital degeneracy (see books by Englman [166], Bersuker and Polinger [167] and Bersuker [168]). The JTE in magnetic clusters requires special consideration that is expected to be a perspective part of the work on the exchange systems containing degenerate ions. Nevertheless, some decisive conclusions can be made on the basis of a simple qualitative consideration addressing to the basic concepts of the JTE. According to the JT theorem, the symmetric atomic configuration leading to the electronic degeneracy proves to be unstable. In the adiabatic limit of a strong JT coupling, the distortions of the ligand surroundings can be considered as stable so that the electronic degeneracy is removed and the ground states of the constituent ions are the orbital singlets (see a comprehensive discussion in [167,168]). In this case, the magnetic interaction can be treated again within the HDVV Hamiltonian that is valid if the ground singlet is well isolated from the excited levels in each stable low symmetry JT configuration. This can be considered as the effect of the JT reduction of the orbitally dependent exchange accompanied by the restoration of the HDVV exchange. In more general terms, this can be

referred to as the reduction of the orbital angular momentum in JT systems (Ham effect) [166–168].

Strong JT coupling is observed in the family of famous SMMs represented by the *Mn*12-acetate [1,2]. This system is composed of a tetrahedral core of oxygen-coordinated Mn(IV) ions, which are surrounded by a ring of eight Mn(III) ions with oxo and acetate coordination. The Mn(III) coordination environment is subjected to a strong JT distortion [169–171] so that the orbital degeneracy is removed. Antiferromagnetic HDVV interactions between the Mn(IV) and Mn(III) ions lead to an $S = 10$ ground state. The distortions are correlated within the molecule to give structure with the specific axes of local anisotropic contributions. As it was demonstrated in [172], the situation of strong JTE resulting in the static distortion occurs in a ferromagnetically coupled Mn_{19} aggregate with a record $S = 83/2$ ground spin state. This shows that the JT-based 'cooperativity' at the molecular level is a quite common (at least for Mn oxides) phenomenon. On the contrary, in a series of cyano-bridged complexes the orbitally dependent exchange probably dominates. In the intermediate cases of comparable JT coupling and orbitally dependent exchange interaction the adiabatic approximation fails, and one faces a dynamical JT situation that is a challenging problem of molecular magnetism. In general, the JTE and orbitally dependent exchange in molecular clusters are competitive just like in solids where JT coupling results in the structural ordering [121–123], whereas the orbitally dependent exchange results in the orbital ordering. Therefore, the magnetic clusters that are intermediate between microscopic and bulk systems can serve as models for the study of the cooperative phenomena and, in particular, of a complicated interplay between different types of electronic and structural phases in solids. This issue seems to be a perspective topic for the future in-depth studies in magnetism.

As far as the orbital degeneracy is concerned, one should mention that even in spin-systems the ground state of the system entire can be orbitally degenerate (or 'accidentally' degenerate in terms of spin coupling scheme) [14,15]. These systems prove to be spin frustrated that results in a series of interesting physical consequences [173–178]. The problem of frustration in the presence of unquenched orbital angular momenta seems to be an intriguing question for the further studies in this area.

In the present article we did not discuss the problem of orbitally dependent double exchange in mixed-valence clusters composed of metal ions whose ground crystal field terms in one or both oxidation degrees possess unquenched orbital angular momentum. The theory of the orbitally dependent double exchange was developed in [179,180]. In particular, it was demonstrated that under some conditions the double exchange interaction can lead to a strong magnetic anisotropy. As an example of such a system, the fully-delocalised Fe(II)Fe(III) face-shared bioctahedral dimer $[L_2Fe_2(\mu\text{-}OH)_3](ClO_4)_2 \cdot 2CH_3OH \cdot 2H_2O$ (L is the terminal tridentate ligand) synthesised and characterised by Wieghardt's group [181,182] can be mentioned. A more comprehensive study of the double exchange in degenerate systems seems to be an actual forthcoming problem of molecular magnetism.

Among the systems in which orbital effects seem to be important, the compounds exhibiting the so-called 'giant negative magnetisation' are to be mentioned. These are mainly the Fe(II)Fe(III) compounds with organic cations in which in small magnetic fields of roughly 100 Oe the magnetisation points along the field direction just below the ferrimagnetic transition of about 45 K but it changes sign below the compensation

temperature of about 28 K (see [183,184] and referances therein). It has been demonstrated by Fishman and Reboredo [185–187] that the magnetic compensation effect in the Fe(II)Fe(III) bimetallic oxalates with the honeycomb structure arises due to the presence of the unquenched orbital angular momentum of the Fe(II) ion in a strongly trigonally distorted surrounding. In [185–187], the superexchange interaction between Fe(II) and Fe(III) centres through the oxalate bridge was assumed to be isotropic. The role of the orbitally dependent exchange contributions in the magnetic compensation effect remains an open question.

In this article, we did not review rapidly developing field of the *ab initio* calculations of the exchange and JT vibronic parameters that represent an inevitable part of the problem. In this respect, a series of the papers of Atanasov *et al*. should be specially mentioned. In [188] (see also references therein and [189–191]), a combined ligand field and density functional theory (DFT) analysis of the magnetic anisotropy and JTE in oligonuclear complexes based on the Fe^{III}–CN–M^{II} exchange coupled pairs is performed.

In this review we only focused on the clusters of 3d-ions and did not discuss the systems that include 4d, 5d and 4f-ions. Besides the difference in the hierarchy of the key interactions (magnetic exchange, crystal fields and SO coupling) that should be carefully taken into account, the main ideas underlying the theoretical treatment of such systems are quite similar to those established for the 3d-systems. Therefore the described approaches can be (with some modifications) used for the description of such systems as well (see, e.g. [192–195]).

It was demonstrated that the unquenched orbital angular momentum can be responsible for the SMM behaviour of magnetic clusters, but the detailed discussion of SMMs and SCMs composed of orbitally degenerate metal ions remained out of the scope of this review. It is worth to note in this context that, at present, numerous SMMs and SCMs containing orbitally degenerate 3d, 4f, 4d and 5d ions have been reported [30–32,196–205]. The theoretical description of the orbital effects in SMMs and SCMs can be found in [115,116,135,206–212]. It is notable in this context that the understanding of the role of the orbitally dependent exchange as a source of strong magnetic anisotropy is expected to broaden horizons for the controlled search for the new SMMs with higher blocking temperatures. In fact, in the SMMs reported until now the blocking temperatures do not exceed a few Kelvin, which are too low for the application of these systems as data-storage units. Therefore, the design of new SMMs with higher blocking temperatures and thus with higher magnetisation reversal barriers represent an important goal in the field of molecular magnetism. The magnetisation reversal barrier for the spin-cluster with the integer ground state spin S is given by the well-known expression $\Delta_b = |D_S|S^2$, where $D_S < 0$ is the effective molecular ZFS parameter for the ground S-state. This expression shows that the barrier can be increased either by the increase of the anisotropy parameter $|D_S|$ or by the increase of S. Particularly, the increase of S seemed to be a promising way to design the SMMs with high-blocking temperatures. However, as has been recently demonstrated by Waldmann [213], the parameter D_S proves to be proportional to S^{-2} and hence the barrier Δ_b does not rise with the increase of S. Probably, for this conceptually important reason, the numerous attempts to increase S by the synthesis of big spin-clusters with high values of the ground state spin [72,214,215] did not yet produce better SMMs. As distinguished from the spin-clusters in which the magnitude of the barrier depends mainly on the relatively small ZFS of the ground spin-state, the barrier in the systems

comprising transition metal ions with unquenched orbital angular momenta can be essentially larger. At the same time, more knowledge is required about the relaxation processes in degenerate systems that are undoubtedly faster than in spin systems and, moreover, have specific features due to the involvement of the orbital states directly coupled to phonons. In any case, the design of new SMMs based on orbitally degenerate ions seems to be a promising route to reach higher magnetic barrier and to enchance the blocking temperature.

Acknowledgements

B. Tsukerblat gratefully acknowledges financial support from the Israel Science Foundation (grant no. 168/09). J.M. Clemente-Juan and E. Coronado thank Spanish MICINN (CSD2007-00010-consolider-ingenio in Molecular Nanoscience, MAT2007-61584, CTQ-2008-06720 and CTQ-2005-09385), Generalitat Valenciana (PROMETEO/2008/128) and the EU (MolSpinQIP project) for financial support. We also thank the people who during many years have been collaborating with us in molecular magnetism. Their names appear in this review article.

References

[1] D. Gatteschi, R. Sessoli, and R. J. Villain, *Molecular Nanomagnets* (Oxford University Press, Oxford, 2006).
[2] (a) E. Coronado and K. R. Dunbar, *Inorg. Chem.* **48**(8), (2009), Special issue on Molecular Magnetism, Eds. K. R. Dunbar and E. Coronado; (b) E. Coronado and K. R. Dunbar, Inorg. Chem. **48**, 3293 (2009).
[3] (a) D. Gatteschi and R. Sessoli, Angew. Chem. Int. Ed. **42**, 268 (2003); (b) D. Gatteschi and R. Sessoli, J. Mag. Mag. Mat. **272**, 1030 (2004).
[4] A. Bencini and D. Gatteschi, *Electron Paramagnetic Resonance of Exchange Coupled Systems* (Springer, Berlin, 1990).
[5] O. Kahn, *Molecular Magnetism* (VCH, New York, 1993).
[6] O. Waldmann, Coord. Chem. Rev. **249**, 2550 (2005).
[7] R. Willett, D. Gatteschi, O. Kahn (Eds). *Magneto-structural Correlation in Exchange Coupled Systems*, NATO ASI Series C140; Kluwer: Dordrecht, 1985.
[8] J. Miller and A. Epstein, MRS Bull. **25**, 21 (2000).
[9] G. Christou, D. Gatteschi, D. N. Hendrickson, and R. Sessoli, MRS Bull. **25**, 66 (2000).
[10] R. Sessoli, H.-L. Tsai, A. R. Schake, S. Wang, J. B. Vincent, K. Folting, D. Gatteschi, G. Christou, and D. N. Hendrickson, J. Am. Chem. Soc. **115**, 1804 (1993).
[11] R. Sessoli, D. Gatteschi, A. Caneschi, and M. A. Novak, Nature **365**, 141 (1993).
[12] J. M. Clemente-Juan and E. Coronado, Coord. Chem. Rev. **193**, 361 (1999).
[13] M. Verdaguer, A. Bleuzen, J. Vaissermann, M. Seuileman, C. Desplanches, A. Scuiller, C. Train, G. Gelly, C. Lomenech, I. V. P. Rosenman, C. Cartier, and F. Villian, Coord. Chem. Rev. **190**, 1023 (1999).
[14] (a) B. S. Tsukerblat and M. I. Belinsky, *Magnetochemistry and Radiospectroscopy of Exchange Clusters* (Pub. Stiintsa (Acad. Sci. Moldova), Kishinev, 1983); (b) B. S. Tsukerblat, *Group Theory in Chemistry and Spectroscopy* (Dover, Mineola, NY, 2006).
[15] B. S. Tsukerblat, M. I. Belinskii, and V. E. Fainzilberg, in *Soviet Science Review B*, edited by M. E. Vol'pin (Harwood Academic Publisher, New York, 1987), Vol. 9, pp. 337–481.
[16] J. J. Borras-Almenar, J. M. Clemente-Juan, E. Coronado, A. V. Palii, B. S. Tsukerblat, in: *Magnetoscience From Molecules to Materials*, eds. J. Miller, M. Drillon, Willey-VCH, 2001, pp. 155–210.

[17] V. Ya. Mitrofanov, A. E. Nikiforov, and V. I. Cherepanov, *Spectroscopy of Exchange-Coupled Complexes in Ionic Crystals* (Nauka, Moskow, 1985).
[18] E. Coronado, R. Georges, and B. S. Tsukerblat, in *Localized and Itinerant Molecular Magnetism: From Molecular Assemblies to the Devices,* NATO ASI Series, edited by E. Coronado, P. Delhaes, D. Gatteschi, and J. Miller (Kluwer Academic Publishers, 1996), pp. 65–84.
[19] J. M. Clemente, R. Georges, A. V. Palii, and B. S. Tsukerblat, in *Localized and Itinerant Molecular Magnetism: From Molecular Assemblies to the Devices,* NATO ASI Series, edited by E. Coronado, P. Delhaes, D. Gatteschi, and J. Miller (Kluwer Academic Publishers, 1996), pp. 85–104.
[20] R. Bŏca, *Theoretical Foundations of Molecular Magnetism* (Amsterdam, Elsevier, 1999).
[21] G. Christou, D. Gatteschi, D. N. Hendrickson, and R. Sessoli, MRS Bull. **25**, 66 (2000).
[22] R. Sessoli, H.-L. Tsai, A. R. Schake, S. Wang, J. B. Vincent, K. Folting, D. Gatteschi, G. Christou, and D. N. Hendrickson, J. Am. Chem. Soc. **115**, 1804 (1993).
[23] R. Sessoli, D. Gatteschi, A. Caneschi, and M. A. Novak, Nature **365**, 141 (1993).
[24] G. J. Eppley, H. L. Tsai, N. de Vries, G. Christou, and D. N. Hendrickson, J. Am. Chem. Soc. **117**, 301 (1995).
[25] S. M. J. Aubin, Z. Sun, I., A. Guzei, A. L. Rheingold, G. Christou, and D. N. Hendrickson, Chem. Commun. **22**, 2239 (1997).
[26] M. R. Cheesman, V., S. Oganesyan, R. Sessoli, D. Gatteschi, and A. J. Thomson, Chem. Commun. **17**, 1677 (1997).
[27] S. L. Castro, Z. Sun, C. M. Grant, J. C. Bollinger, D. N. Hendrickson, and G. Christou, J. Am. Chem. Soc. **120**, 2365 (1998).
[28] J. C. Goodwin, R. Sessoli, D. Gatteschi, W. Wernsdorfer, A. K. Powell, S. L. Heath, and A. L. Barra, J. Chem. Soc., Dalton Trans. **24**, 4902 (2000).
[29] C. Boskovic, E. K. Brechin, W. E. Strteib, K. Folting, J. C. Bollinger, D. N. Hendrickson, and G. Christou, J. Am. Chem. Soc. **124**, 3725 (2002).
[30] C. P. Berlinguette, D. Vaughn, C. Cañada-Vilalta, J.-R. Galán-Mascarós, and K. R. Dunbar, Angew. Chem. Int. Ed. **42**, 1523 (2003).
[31] H. J. Choi, J. J. Sokol, and J. R. Long, Inor. Chem. **43**, 1606 (2004).
[32] S. Wang, J. L. Zuo, H. C. Zhou, H. J. Choi, Y. Ke, and J. R. Long, Angew. Chem. Int. Ed. **43**, 5940 (2004).
[33] J. S. Miller, Polyhedron **28**, 1596 (2009).
[34] J. S. Miller, Inorg. Chem. **39**, 4392 (2000).
[35] J. M. Manriquez, G. T. Yee, R. S. Mclean, A. J. Epstein, and J. S. Miller, Science **252**, 1415 (1991).
[36] W. R. Entley and G. S. Girolami, Science **268**, 397 (1995).
[37] T. Mallah, S. Thiebaut, M. Verdaguer, and P. Veillet, Science **262**, 1554 (1993).
[38] S. Ferlay, T. Mallah, R. Ouahes, P. Veillet, and M. Verdaguer, Nature **378**, 701 (1995).
[39] T. Mallah, S. Thiebaut, M. Verdaguer, and P. Veillet, Science **262**, 1554 (1993).
[40] V. Gadet, T. Mallah, I. Castro, M. Verdaguer, and P. Veillet, J. Am. Chem. Soc **114**, 9213 (1992).
[41] D. A. Shultz, R. K. Kumar, S. Bin-Salamon, and M.L. Kirk, Polyhedron **24**, 2876 (2005).
[42] (a) E. Coronado, J. R. Galán-Mascarós, C. J. Gómez-García, and V. Laukhin, Nature **408**, 447 (2000); (b) E. Coronado and P. Day, Chem. Rev. **104**, 5419 (2004); (c) J. Camarero and E. Coronado, J. Mater. Chem. **19**, 1678 (2009).
[43] S. Farley, T. Mallah, R. Ouhaes, P. Veillet, and M. Verdaguer, Nature **378**, 701 (1995).
[44] P. Gütlich, A. Hauser, and H. Spiering, Angew. Chem. **106**, 2109 (1994).
[45] P. Gütlich, A. Hauser, and H. Spiering, Angew. Chem. Int. Ed. Engl. **2024**, 33 (1994).
[46] P. Gütlich, Y. Garcia, and H. A. Goodwin, Chem. Soc. Rev. **29**, 419 (2000).
[47] O. Sato, T. Iyoda, A. Fujishima, and K. Hashimoto, Science **271**, 49 (1996).

[48] O. Sato, T. Iyoda, A. Fujishima, and K. Hashimoto, Science **272**, 704 (1996).
[49] M. Verdaguer, Science **272**, 698 (1996).
[50] A. Dei, Angew. Chem. Int. Ed. **44**, 1160 (2005).
[51] Y. Arimoto, Shin-ichi Ohkoshi, Z. Jin Zhong, H. Seino, Y. Mizobe, and K. Hashimoto, J. Am. Chem. Soc. **125**, 9240 (2003).
[52] F. Palacio and J. S. Miller, Nature **408**, 421 (2000).
[53] M. Tamura, Y. Nakagawa, D. Shiomi, Y. Nozawa, M. Hosokoshi, M. Ishikawa, M. Takahashi, and M. Kinoshita, Chem. Phys. Lett. **186**, 401 (1991).
[54] F. Palacio, G. Antorrena, M. Castro, M. Brunel, J. M. Rawson, J. M. Smith, J. N. B. N. Bricklebank, J. Novoa, and C. Ritter, Phys. Rev. Lett. **79**, 2336 (1997).
[55] I. Fujita, Y. Yeki, T. Takui, T. Kinoshita, K. Itoh, F. Miko, Y. Sawaki, H. Iwamura, A. Izuoka, and T. Sugawara, J. Am. Chem. Soc. **112**, 4074 (1990).
[56] T. Ishida and H. Iwamura, J. Am. Chem. Soc. **113**, 4238 (1991).
[57] A. Rajca, S. Utamapanya, and S. Thayumanavan, J. Am. Chem. Soc. **114**, 1884 (1992).
[58] N. Nakamura, K. Inoue, and H. Iwamura, Angew. Chem. Int. Ed. Engl. **32**, 873 (1993).
[59] N. Ventosa, D. Ruiz, C. Rovira, and J. Veciana, Mol. Cryst. Liq. Cryst. **232**, 333 (1993).
[60] G. Blondin and J. J. Girerd, Chem. Rev. **90**, 1359 (1989).
[61] G. Christou, Acc. Chem. Res. **22**, 328 (1989).
[62] S. J. Lippard, Angew. Chem. Int. Ed. Engl. **30**, 34 (1991).
[63] K. L. Taft, G. C. Papaefthymiou, and S. J. Lippard, Inorg. Chem. **33**, 1510 (1994).
[64] M. Leuenberger and D. Loss, Nature **410**, 789 (2001).
[65] D. P. DiVincenzo, Fortschr. Phys. **48**, 771 (2000).
[66] W. Wersndorfer, Nat. Mater. **6**, 174 (2007).
[67] (a) J. Lehmann, A. Gaita-Arino, E. Coronado, and D. Loss, Nature Nanotechnol. **2**, 312 (2007); (b) J. Lehmann, A. Gaita-Ariño, E. Coronado, and D. Loss, J. Mater. Chem. **19**, 1672 (2009).
[68] F. Troiani, A. Ghirri, M. Affronte, S. Carretta, P. Santini, G. Amoretti, S. Piligkos, G. Timco, and R. E. P. Winpenny, Phys. Rev. Lett. **94**, 207208 (2005).
[69] M. Affronte, F. Troiani, A. Ghirri, S. Carretta, P. Santini, V. Corradini, R. Schuecker, C. Muryn, G. Timco, and R. E. Winpenny, Dalton Trans. **23**, 2810 (2006).
[70] M. Affronte, F. Troiani, A. Ghirri, A. Candini, M. Evangelisti, V. Corradini, S. Carretta, P. Santini, G. Amoretti, F. Tuna, G. Timco, and R. E. Winpenny, J. Phys. D: Appl. Phys **40**, 2999 (2007).
[71] S. Bertaina, S. Gambarelli, T. Mitra, B. Tsukerblat, A. Müller, and B. Barbara, Nature **453**, 20 (2008).
[72] P. C. E. Stamp, Nature **453**, 167 (2008).
[73] R. E. P. Winpenny, Angew. Chem. Int. Ed. **47**, 2 (2008).
[74] D. Stepanenko, M. Trif, and D. Loss, Inorg. Chim. Acta **361**, 3740 (2008).
[75] A. Ardavan, O. Rival, J. J. L. Morton, S. Blundell, A. M. Tyryshkin, G. A. Timco, and E. P. Winpenny, Phys. Rev. Lett. **98**, 057201 (2007).
[76] F. K. Larsen, E. J. L. McInnes, H. El Mkami, J. Overgaard, S. Piligkos, G. Rajaraman, E. Rentschler, A. A. Smith, G. M. Smith, V. Boote, M. Jennings, G. A. Timco, and R. E. P. Winpenny, Angew. Chem. Int. Ed. **42**, 101 (2003).
[77] A. Morello, P. C. E. Stamp, and I. S. Tupitsyn, Phys. Rev. Lett. **97**, 207206 (2006).
[78] S. B. Braun-Sand and O. Wiest, J. Phys. Chem. A **107**, 285 (2003).
[79] V. V. Dobrovitski, M. I. Katsnelson, and B. N. Harmon, Phys. Rev. Lett. **84**, 3458 (2000).
[80] G. A. Timco, S. Carretta, F. Troiani, F. Tuna, R. J. Pritchard, C. A. Muryn, E. J. L. McInnes, A. Ghirri, A. Candini, P. Santini, G. Amoretti, M. Affronte, and R. E. P. Winpenny, Nature Nanotechnol. **4**, 173 (2009).
[81] G. Mitrikas, Y. Sanakis, C. P. Raptopoulou, G. Kordas, and G. Papavassiliou, Phys. Chem. Chem. Phys. **10**, 743 (2008).

[82] C. Schlegel, J. van Slageren, M. Manoli, E. K. Brechin, and M. Dressel, Phys. Rev. Lett. **101**, 147203 (2008).
[83] J. H . van Vleck, *The Theory of Electric and Magnetic Susceptibilities* (Oxford University Press, London, 1932).
[84] P. W. Anderson, Phys. Rev. **115**, 2 (1959).
[85] P. W. Anderson, in *Solid State Physics*, edited by F. Seitz and D. Turnbull (Academic Press, New York, 1963), Vol. 14, p. 99.
[86] J. B. Goodenough, *Magnetism and Chemical Bond* (Wiley Interscience, New York, 1963).
[87] J. M. Clemente, A. V. Palii, B. S. Tsukerblat, and G. Georges, in *Localized and Itinerant Molecular Magnetism: From Molecular Assemblies to the Devices,* NATO ASI Series, edited by E. Coronado, P. Delhaès, D. Gatteschi, and J. S. Miller (Kluwer Academic, Dordrecht, 1996), Vol. E-321, pp. 85–104; 26 id. E. Coronado, B. S. Tsukerblat, R. Georges, pp. 65–84.
[88] H. M. McConell, Proc R. A. Welch Foundation Chem. Res. **11**, 144 (1967).
[89] C. Kollmar and O. Kahn, J. Am. Chem. Soc. **113**, 7987 (1991).
[90] H. Weihe and H. U. Güdel, Chem. Phys. Lett. **261**, 123 (1996).
[91] J. J. Borrás-Almenar, J. M. Clemente-Juan, E. Coronado, A. V. Palii, and B. S. Tsukerblat, J. Phys. Chem. A **102**, 200 (1998).
[92] J. J. Borrás-Almenar, J. M. Clemente-Juan, E. Coronado, A. V. Palii, and B. S. Tsukerblat, Phys. Lett. A **238**, 164 (1998).
[93] J. J. Borrás-Almenar, J. M. Clemente-Juan, E. Coronado, A. V. Palii, and B. S. Tsukerblat, Chem. Phys. **274**, 131 (2001).
[94] J. J. Borrás-Almenar, J. M. Clemente-Juan, E. Coronado, A. V. Palii, and B. S. Tsukerblat, Chem. Phys. **274**, 145 (2001).
[95] R. Boča, Coord. Chem. Rev. **248**, 757 (2004).
[96] R. Bŏca, Coord. Chem. Rev. **173**, 167 (1998).
[97] I. and E. Dzyaloshinsky, Phys. Chem. **4**, 241 (1958).
[98] T. Moriya, Phys. Rev. **117**, 635 (1960).
[99] T. Moriya, Phys. Rev. **120**, 91 (1960).
[100] S. Sugano, Y. Tanabe, and H. Kamimura, *Multiplets of Transition-metal Ions in Crystals* (Academic Press, New York, London, 1970).
[101] A. Abragam and B. Bleaney, *Electron Paramagnetic Resonance of Transition Ions* (Clarendon, Oxford, England, 1970).
[102] J. H. Van vleck, Revista de Matemática y Fisica Teórica **14**, 189 (1962).
[103] P. M. Levy, in: *Magnetic Oxides* (D. J. Craik, Ed.), John Wiley, p. 181, 1975.
[104] M. E. Lines, J. Chem. Phys. **55**, 2977 (1971).
[105] A. P. Ginsberg, Inorg. Chim. Acta Rev. **5**, 45 (1971).
[106] E. Coronado, M. Drillon, P. R. Nugteren, L. J. de Jongh, and D. Beltran, J. Am. Chem. Soc. **110**, 3907 (1988).
[107] J. M. Clemente, H. Andres, M. Aebersold, J. J. Borrás-Almenar, E. Coronado, H. U. Güdel, H. Büttner, and C. Kearly, Inorg. Chem. **36**, 2244 (1997).
[108] H. Andres, M. Aebersold, H. U. Güdel, J. M. Clemente, E. Coronado, H. Büttner, C. Kearly, and M. Zolliker, Chem. Phys. Lett. **289**, 224 (1998).
[109] H. Andres, J. M. Clemente-Juan, M. Aebersold, H. U. Güdel, E. Coronado, H. Büttner, C. Kearly, J. Melero, and R. Burriel, J. Am. Chem. Soc. **121**, 10028 (1999).
[110] H. Andres, J. M. Clemente-Juan, R. Basler, M. Aebersold, H. U. Güdel, J. J. Borrás-Almenar, A. Gaita, E. Coronado, H. Büttner, and S. Janssen, Inorg. Chem. **40**, 1943 (2001).
[111] J. M. Clemente-Juan, E. Coronado, A. Gaita-Ariño, C. Giménez-Saiz, G. Chaboussant, H.-U. Güdel, R. Burriel, and H. Mutka, Eur. J. Chem. **8**, 5701 (2002).
[112] J. M. Clemente-Juan, E. Coronado, A. Gaita-Ariño, C. Giménez-Saiz, H.-U. Güdel, A. Sieber, R. Bircher, and H. Mutka, Inorg. Chem. **44**, 3389 (2005).

[113] B. S. Tsukerblat, A. V. Palii, V. Yu. Mirovitskii, S. M. Ostrovsky, K. Turta, T. Jovmir, S. Shova, J. Bartolome, M. Evangelisti, and G. Filoti, J. Chem. Phys. **115**, 9528 (2001).
[114] A. V. Palii, B. S. Tsukerblat, E. Coronado, J. M. Clemente-Juan, and J. J. Borrás-Almenar, Inorg. Chem. **42**, 2455 (2003).
[115] A. V. Palii, S. M. Ostrovsky, S. I. Klokishner, B. S. Tsukerblat, C. P. Berlinguette, K. R. Dunbar, and J. R. Galán-Mascarós, J. Am. Chem. Soc. **126**, 16860 (2004).
[116] B. S. Tsukerblat, A. V. Palii, S. M. Ostrovsky, S. V. Kunitsky, S. I. Klokishner, and K. R. Dunbar, J. Chem. Theory Comput. **1**, 668 (2005).
[117] P. M. Levy, Phys. Rev. **135**, 155 (1964).
[118] P. M. Levy, Phys. Rev., A **177**, 509 (1969).
[119] M. V. Eremin, V. N. Kalinenkov, and Y. V. Rakitin, Phys. Status Solidi B **89**, 503 (1978).
[120] M. V. Eremin, V. N. Kalinenkov, and Y. V. Rakitin, Phys. Status Solidi B **90**, 123 (1978).
[121] D. I. Khomskii and K. I. Kugel, Sov. Phys. Usp. **136**, 231 (1982).
[122] K. I. Kugel and D. I. Khomskii, Zhurnal Eksp. Teor. Fiz. **64**, 1429 (1973).
[123] M. D. Kaplan and B. G. Vekhter, *Cooperative Phenomena in Jahn-Teller Crystals* (Plenum, New York, 1995).
[124] M. Drillon and R. Georges, Phys. Rev. B **24**, 1278 (1981).
[125] M. Drillon and R. Georges, Phys. Rev. B **26**, 3882 (1982).
[126] B. Leuenberger and H. U. Güdel, Mol. Phys. **51**, 1 (1984).
[127] A. Ceulemans, G. A. Heylen, L. F. Chibotaru, T. L. Maes, K. Pierloot, C. Ribbing, and L. G. Vanquickenborne, Inorg. Chim. Acta **251**, 15 (1996).
[128] A. Ceulemans, L. F. Chibotaru, G. A. Heylen, and K. Pierloot, Mol. Phys. **97**, 1197 (1999).
[129] A. Ceulemans, L. F. Chibotaru, G. A. Heylen, K. Pierloot, and L. G. Vanquickenborne, Chem. Rev. **100**, 787 (2000).
[130] J. J. Borrás-Almenar, J. M. Clemente-Juan, E. Coronado, A. V. Palii, and B. S. Tsukerblat, J. Chem. Phys. **114**, 1148 (2001).
[131] J. J. Borrás-Almenar, J. M. Clemente-Juan, E. Coronado, A. V. Palii, and B. S. Tsukerblat, J. Sol. State. Chem. **159**, 268 (2001).
[132] J. J. Borras-Almenar, E. Coronado, J. M. Clemente-Juan, A. V. Palii, and B. S. Tsukerblat, Polyhedron **22**, 2521 (2003).
[133] A. V. Palii, B. S. Tsukerblat, E. Coronado, J. M. Clemente-Juan, and J. J. Borrás-Almenar, J. Chem. Phys. **118**, 5566 (2003).
[134] A. V. Palii, B. S. Tsukerblat, E. Coronado, J. M. Clemente-Juan, and J. J. Borrás-Almenar, Polyhedron **22**, 2537 (2003).
[135] A.V. Palii, Proceedings of the 3rd International Conference on Mathematical Modeling and Computer Simulation of Materials Technologies, 3 (2004) 95.
[136] A. V. Palii, S. M. Ostrovsky, S. I. Klokishner, B. S. Tsukerblat, and K. R. Dunbar, Chem. Phys. Chem. **7**, 871 (2006).
[137] F. Lloret, M. Julve, J. Cano, R. Ruiz-Garcia, and E. Pardo, Inorg. Chim. Acta **361**, 343 (2008).
[138] V. Calvo-Perez, S. Ostrovsky, A. Vega, J. Pelikan, E. Spodine, and W. Haase, Inorg. Chem. **45**, 644 (2006).
[139] S. M. Ostrovsky, K. Falk, J. Pelikan, D. A. Brown, Z. Tomkowicz, and W. Haase, Inorg. Chem. **45**, 688 (2006).
[140] A. K. Sharma, F. Lloret, and R. Mukherjee, Inorg. Chem. **46**, 5128 (2007).
[141] D. A. Varshalovich, A. N. Moskalev, V., and K. Khersonskii, *Quantum Theory of Angular Momentum* (World Scientific, Singapore, 1988).
[142] J. J. Borras-Almenar, J. M. Clemente, E. Coronado, and B. S. Tsukerblat, Inorg. Chem. **38**, 6081 (1999).
[143] R. L. Carlin, *Magnetochemistry* (Springer, Berlin, 1986).
[144] A. V. Palii, Phys. Lett. A **365**, 116 (2007).

[145] A. V. Palii, O. S. Reu, S. M. Ostrovsky, S. I. Klokishner, B. S. Tsukerblat, Z.-M. Sun, J.-G. Mao, A. V. Prosvirin, H.-H. Zhao, and K. R. Dunbar, J. Am. Chem. Soc. **130**, 14729 (2008).
[146] A. V. Palii, S. M. Ostrovsky, S. I. Klokishner, O. S. Reu, Z.-M. Sun, A. V. Prosvirin, H.-H. Zhao, J.-G. Mao, and K. R. Dunbar, J. Phys. Chem., A **110**, 14003 (2006).
[147] B. R. Judd, *Second Quantization and Atomic Spectroscopy* (The Johns Hopkins Press, Baltimore, 1967).
[148] E. Clementi and C. Roetti, At. Data Nucl. Data Tables **14**, 177 (1974).
[149] J. E. Huheey, E. A. Keiter, and R. L. Keiter, *Inorganic Chemistry* (Harper Collins College, New York, 1993).
[150] J. S. Griffith, *The Irreducible Tensor Method for Molecular Symmetry Groups* (Prentice-Hall, New York, 1962).
[151] T. Damhus, Mol. Phys. **50**, 497 (1983).
[152] L. B. Silver, *Irreducible tensor methods* (Academic Press, New York, 1976).
[153] L. F. Feiner and A. M. Oleś, Physica B **259**, 796 (1999).
[154] R. Saillant and R. A. D. Wentworth, Inorg. Chem. **7**, 1606 (1968).
[155] B. Briat, O. Kahn, I. Morgenstern-Badarau, and J. C. Rivoal, Inorg. Chem. **20**, 4193 (1981).
[156] G. J. Wessel and J. J. W. Ijdo, Acta Crystallogr. **10**, 466 (1957).
[157] B. Leuenberger, H. U. Güdel, and A. Furrer, Chem. Phys. Lett. **126**, 255 (1986).
[158] O. Kahn, Mol. Phys. **31**, 957 (1976).
[159] L. Chen, F. A. Cotton, K. R. Dunbar, X. Feng, R. A. Heintz, and C. Uzelmeir, Inorg. Chem. **35**, 7358 (1996).
[160] K. Fink, C. Wang, and V. Staemmler, Inorg. Chem. **38**, 3847 (1999).
[161] A. V. Palii, B. S. Tsukerblat, E. Coronado, J. M. Clemente-Juan, and J. J. Borrás-Almenar, J. Chem. Phys. **118**, 5566 (2003).
[162] A. V. Palii, B. S. Tsukerblat, E. Coronado, J. M. Clemente-Juan, and J. J. Borrás-Almenar, Polyhedron **22**, 2537 (2003).
[163] M. Nishino, Y. Yoshioka, and K. Yamaguchi, Chem. Phys. Lett. **297**, 51 (1998).
[164] H. Weihe and H. U. Güdel, Comments Inorg. Chem. **22** (1–2), 75 (2000).
[165] J. J. Borrás-Almenar, J. M. Clemente-Juan, E. Coronado, and B. S. Tsukerblat, J. Comput. Chem. **22**, 985 (2001).
[166] R. Englman, *The Jahn–Teller Effect in Molecules and Crystals* (Wiley, London, 1972).
[167] I., B. Bersuker, and V. Z. Polinger, *Vibronic Interactions in Molecules and Crystals* (Springer-Verlag, Berlin, 1989).
[168] I.B. Bersuker, *The Jahn-Teller Effect*, (Cambridge University Press, Cambridge, 2006).
[169] A. Sieber, R. Bircher, O. Waldmann, G. Carver, G. Chaboussant, H. Mutka, and H.-U. Güdel, Angew. Chem. Int. Ed. **44**, 4239 (2005).
[170] J . van Slageren, S. Dengler, J. Gómez-Segura, D. Ruiz-Molina, and M. Dressel, Inorg. Chim. Acta **361**, 3714 (2008).
[171] M. Soler, W. Wernsdorfer, Z. Sun, D. Ruiz, J. C. Huffman, D. N. Hendrickson, and G. Christou, Polyhedron **22**, 1783 (2003).
[172] A. M. Ako, I. J. Hewitt, V. Mereacre, R. Clérac, W. Wernsdorfer, C. E. Anson, and A. K. Powell, Angew. Chem. Int. Ed. **45**, 4926 (2006).
[173] J. Schnack, J. Low Temp. Phys. **142**, 279 (2006).
[174] J. Schnack, C. R. Chim. **10**, 15 (2007).
[175] R. Schnalle and J. Schnack, Phys.Rev. B **79**, 104419 (2009).
[176] R. Schnalle and J. Schnack, Polyhedron **28**, 1620 (2009).
[177] M. I. Belinsky, Inorg. Chem. **47**, 3521 (2008).
[178] M. I. Belinsky, Inorg. Chem. **47**, 3532 (2008).
[179] J. J. Borras-Almenar, J. M. Clemente-Juan, E. Coronado, A. V. Palii, and B. S. Tsukerblat, Chem. Phys. **254**, 275 (2000).

[180] A. V. Palii, Phys. Lett. A **295**, 147 (2002).
[181] S. Drücke, P. Chaudhuri, K. Pohl, K. Wieghardt, X.-Q. Ding, E. Bill, A. Sawaryn, A. X. Trautwein, H. Winkler, and S. J. Gurman, J. Chem. Soc., Chem. Commun. **59**, (1989).
[182] X.-Q. Ding, E. L. Bominaar, E. Bill, H. Winkler, A. X. Trautwein, S. Drücke, P. Chaudhuri, and K. Wieghardt, J. Chem. Phys. **92**, 178 (1990).
[183] E. Coronado, J. R. Galán-Mascarós, C. J. Gómez-García, and J. M. Martínez-Agudo, Adv. Mater. **11**, 558 (1999).
[184] G. Tang, Y. He, F. Liang, S. Li, and Y. Huang, Physica B **392**, 337 (2007).
[185] R. S. Fishman and F. A. Reboredo, Phys. Rev. Lett. **99**, 217203 (2007).
[186] R. S. Fishman and F. A. Reboredo, Phys. Rev. B **77**, 144421 (2008).
[187] P. Reis, R. S. Fishman, F. A. Reboredo, and J. Moreno, Phys. Rev. B **77**, 174433 (2008).
[188] M. Atanasov, P. Comba, and C. A. Daul, Inorg. Chem. **47**, 2449 (2008).
[189] M. Atanasov, P. Comba, and C. A. Daul, J. Phys. Chem. A **110**, 13332 (2006).
[190] M. Atanasov, C. Busche, P. Comba, F. El Hallak, B. Martin, G. Rajaraman, G. Rajaraman, J . van Slageren, and H. Wadepohl, Inorg. Chem. **47**, 8112 (2008).
[191] M. Atanasov, P. Comba, C. A. Daul, and A. Hauser, J. Phys. Chem. A **111**, 9145 (2007).
[192] V. S. Mironov, J. Phys.: Condens. Matter **8**, 10551 (1996).
[193] V. S. Mironov, L. F. Chibotaru, and A. Ceulemans, Phys. Rev. B **67**, 014424 (2003).
[194] V. S. Mironov, L. F. Chibotaru, and A. Ceulemans, J. Am. Chem. Soc. **125**, 9750 (2003).
[195] A. V. Palii, B. S. Tsukerblat, J. M. Clemente-Juan, and E. Coronado, Inorg. Chem. **44**, 3984 (2005).
[196] N. Ishikawa, M. Sugita, T. Ishikawa, S. Koshihara, and Y. Kaizu, J. Am. Chem. Soc. **125**, 8694 (2003).
[197] N. Ishikawa, M. Sugita, T. Ishikawa, S. Koshihara, and Y. Kaizu, J. Phys. Chem. B **108**, 11265 (2004).
[198] N. Ishikawa, M. Sugita, and W. Wernsdorfer, J. Am. Chem. Soc. **127**, 3650 (2005).
[199] N. Ishikawa, M. Sugita, and W. Wernsdorfer, Angew. Chem. Int. Ed. **44**, 2931 (2005).
[200] M. A. AlDamen, J. M. Clemente-Juan, E. Coronado, C. Martí-Gastaldo, and A. Gaita-Ariño, J. Am. Chem. Soc. **130**, 8874 (2008).
[201] M. A. AlDamen, S. Cardona, J. M. Clemente-Juan, A. Gaita-Ariño, E. Coronado, F. Luis, C. Martí-Gastaldo, and O. Montero, Inorg. Chem. **48**, 3467 (2009).
[202] J. Tang, I. Hewitt, N. T. Madhu, G. Chastanet, W. Wernsdorfer, C. E. Anson, C. Benelli, R. Sessoli, and A. K. Powell, Angew. Chem. Int. Ed. **45**, 1729 (2006).
[203] E. J. Schelter, A. V. Prosvirin, W. M. Reiff, and K. R. Dunbar, Angew. Chem. Int. Ed. **43**, 4912 (2004).
[204] S. Osa, T. Kido, N. Matsumoto, N. Re, A. Pochaba, and J. Mrozinski, J. Am. Chem. Soc. **126**, 420 (2004).
[205] Z.-M. Sun, A. V. Prosvirin, H.-H. Zhao, J.-G. Mao, and K.R. Dunbar, J. Appl. Phys. **97**, 10B305 (2005).
[206] J. Luzon, K. Bernot, J. J. Hewitt, C. E. Anson, A. K. Powell, and R. Sessoli, Phys. Rev. Lett. **100**, 247205 (2008).
[207] L.F. Chibotaru, L. Ungur, and A. Soncini, Angew. Chem., Int. Ed. **47**, 4126 (2008).
[208] A. V. Palii, S. M. Ostrovsky, S. I. Klokishner, B. S. Tsukerblat, E. J. Schelter, A. V. Prosvirin, and K. R. Dunbar, Inorg. Chim. Acta **360**, 3915 (2007).
[209] V. and S. Mironov, Doklady Phys. Chem. **415**, 199 (2007).
[210] A. V. Palii, S. M. Ostrovsky, S. I. Klokishner, O. S. Reu, Z.-M. Sun, A. V. Prosvirin, H.-H. Zhao, J.-G. Mao, and K. R. Dunbar, J. Phys. Chem. A **110**, 14003 (2006).
[211] A. V. Palii, O. S. Reu, S. M. Ostrovsky, S. I. Klokishner, B. S. Tsukerblat, Z.-M. Sun, J.-G. Mao, A. V. Prosvirin, H.-H. Zhao, and K. R. Dunbar, J. Am. Chem. Soc. **130**, 14729 (2008).

[212] S. I. Klokishner, S. M. Ostrovsky, O. S. Reu, A. V. Palii, P. L. W. Tregenna-Piggott, T. Brock-Nannestad, J. Bendix, and H. Mutka, J. Phys. Chem. C **20**, 8573 (2009).
[213] O. Waldmann, Inorg. Chem. **46**, 10035 (2007).
[214] D. M. Low, L. F. Jones, A. Bell, E. K. Brechin, T. Mallah, E. Riviére, S. J. Teat, and E. J. L. McInnes, Angew. Chem., Int. Ed. **42**, 3781 (2003).
[215] M. Murugesu, M. Habrych, W. Wernsdorfer, K. A. Abboud, and G. Christou, J. Am. Chem. Soc. **126**, 4766 (2004).